Summer 8-12-2014

The Spectrochemical Characterization of Novel Vis-NIR Fluorescence Dyes and Developing a Laser Induced Fluorescence Capillary Zone Electrophoresis (LIF-CZE) Technique to Study Alkanesulfonate Monooxygenase

Garfield Beckford

THE SPECTROCHEMICAL CHARACTERIZATION OF NOVEL VIS-NIR FLUORESCENCE DYES AND DEVELOPING A LASER INDUCED FLUORESCENCE CAPILLARY ZONE ELECTROPHORESIS (LIF-CZE) TECHNIQUE TO STUDY ALKANESULFONATE MONOOXYGENASE

by

GARFIELD KENROY BECKFORD

Under the Direction of Gabor Patonay

ABSTRACT

A new Laser Induced Fluorescence Capillary Zone Electrophoresis (LIF-CZE) bioassay to detect and study the catalytic activity of the sulfur assimilating enzyme commonly found in *E*. coli species; alkanesulfonate monooxygenase *(EC 1.14.14.5)* is described for the first time. This technique enables the possibility for direct injection onto a capillary for detection without the need for pre-concentration of sample and with minimal sample preparative steps prior to analysis.

In this bioassay, a group of Fischer based cyanine dyes and two Oxazine (Nile red) derivatives were designed for further optimization as key Vis-NIR fluorescent substrate. In developing this technique, the test dyes were first assessed for their photophysical properties, based on four criteria; (1) photostable (2) solvatochromism (3) binding affinity towards both the monooxygenase active site and serum albumin and (4) chemical stability in strong electric field

strength. Applying key dye characterization procedures including; molar absorptivity determination, quantum yield determination, photostability, solvatochromism and protein interaction studies it was determined that the Fischer indolium cyanine dyes were most suitable for the method development. The data revealed that under the test conditions, reduced flavin, the oxidative monooxygenase catalytically specifically converts the alkylsulfonate substituted cyanine dyes to the corresponding aldehyde.

This new bioassay has proven to be quick, portable, sensitive, reliable and the exhibit the possibility of 'on-the-spot' detection; advantages not readily realized with other commonly applied techniques such as PCR, SPR, ELISA and GC used to study bacterial sulfur assimilation processes. In addition, recent literature results proposed by other research groups developing similar techniques showed strong reliance on GC analyses. Those assays involve the use of low molecular weight straight chain non-emissive alkanesulfonate substrates. Once enzyme catalysis occurs the aldehyde is formed becomes rather volatile and requires complex and tedious headspace sampling for GC analyses. This feature limits the *in vitro* applicability and eliminated the possibility *in vivo* development. Our goal is to further develop, optimize and present this CZE based bioassay as a suitable alternative to the current trends in the field while creating a more robust and sensitive *in vitro* monooxygenase detection method with the possibilities of *in vivo* application.

INDEX WORDS: Human Serum Albumin (HSA), Steric specificity, Solvatochromism, Near-infrared laser induced fluorescence (NIR-LIF) spectroscopy, J-aggregation (Bathochromic) and H-aggregation (Hypsochromic), Riboflavin mononucleotide, Alkanesulfonate monooxygenase.

THE SPECTROCHEMICAL CHARACTERIZATION OF NOVEL VIS-NIR FLUORESCENCE DYES AND DEVELOPING A LASER INDUCED FLUORESCENCE CAPILLARY ZONE ELECTROPHORESIS (LIF-CZE) TECHNIQUE TO STUDY ALKANESULFONATE MONOOXYGENASE

by

GARFIELD KENROY BECKFORD

A Dissertation Submitted in Partial Fulfillment of the Requirements for the Degree of

Doctor of Philosophy

in the College of Arts and Sciences

Georgia State University

2014

THE SPECTROCHEMICAL CHARACTERIZATION OF NOVEL VIS-NIR FLUORESCENCE DYES AND DEVELOPING A LASER INDUCED FLUORESCENCE CAPILLARY ZONE ELECTROPHORESIS (LIF-CZE) TECHNIQUE TO STUDY ALKANESULFONATE MONOOXYGENASE

by

GARFIELD KENROY BECKFORD

Committee Chair: Gabor Patonay

Committee: Maged Henary

Gangli Wang

Electronic Version Approved:

Office of Graduate Studies

College of Arts and Sciences

Georgia State University

August 2014

DEDICATION

This dissertation is dedicated to my loving mother and father (deceased), to my wonderful wife Shirlene and my two great kids; Jewelle and Justin.

ACKNOWLEDGEMENTS

I am deeply grateful to my advisor Dr. Gabor Patonay for the guidance, encouragement and mentorship he provided me towards fulfilling this great task of completing my Doctoral degree and becoming a Bioanalytical Chemist. Throughout these years of my research there were many individuals who have not only encouraged and motivated me but have made a profound impact assisting me in making this dream a reality. Most importantly I am grateful to my Parents; Agnes Maud and Lambert George Beckford (deceased). For their incessant prayers and words of encouragement I am extremely thankful. Also, I must truly thank my wife Dr. Shirlene Jackson Beckford and my two young kids; Jewelle Jessica Beckford and Justin Jackson Beckford for their unconditional love and selfless support throughout the years. I also like to express my gratitude to Mr. Neville and Mrs. Francine Walker for their kind accommodation when my wife and I first entered the United States for our graduate studies.

Beyond my academic achievements, there are many other professors that have also contributed significantly to my personal development at the Georgia State University and for this I am extremely grateful to Dr. Maged Henary for assisting me tremendously with my research, and for reassuring me at times when I became doubtful. In addition, a great thank you to Drs. Keith Pascoe, Shahab Shamsi and Dabney Dixon for their kinds words of encouragement. Also, I am deeply indebted to the lab mates of joint Patonay-Henary research groups, especially Gala Chapmen. Your friendliness and team work has been inspiring over the years. You all are the most loving lab mates I could ever ask for. To all my other family members, friends and associates who have assisted and encouraged me in the academic pursuit, I will be forever grateful.

TABLE OF CONTENTS

LIST OF TABLES

LIST OF FIGURES

LIST OF SCHEMES

1 APPLICATION OF FLUORESCENT DYES IN BIOANALYTICAL SCIENCE

1.1 Introduction

The ultraviolet (UV) to (Vis) band of the electromagnetic spectra have been utilized in bioanalytical spectroscopy for many decades in both academia and industry. Unlike other regions of the spectrum, increase popularity of this band as an analytical tool is in part be attributed to the abundant availability of relatively inexpensive instrumentation and the numerous favorable spectral properties exhibited by molecule that are considered UV-Vis active.

In the last century there is a paradigm shift in bioanalytical spectroscopy which culminates with greater utilization of the near-infrared (NIR) range, and the of NIR-absorbing chromophores have become more valuable in classical optophysics and molecular spectroscopy to includes clinical applications such as *in vitro* and *in vivo* [1-7] bioanalyses. One key advantage of utilizing the NIR region, is the much reduced background interference from the complex matrix, and reduced light scattering and shifting of the Raman line further from the spectral region of interest [8, 9] . The part of the NIR region where most NIR fluorophores are available (i.e., the 700-1200 nm range) has several advantages for bioanalytical chemists and affords very low detection limits due to the high molar absorptivity of NIR fluorophores.

Multiphoton excitation (MPE) techniques are also becoming increasingly important through the development of cheaper and more intense pulsed laser sources in the NIR-region. The low-background and small excitation volumes attainable with MPE facilitates sensitive measurements in samples with a volume below femto liter, thus, making it a suitable detection method in capillary electrophoresis and nanoparticle-based bio-affinity assays.

The use of fluorescent dyes for optical spectroscopy has attracted considerable new interests in quantitative and qualitative bioanalytical science. Whereas common separation techniques such as gel electrophoresis (GE), capillary electrophoresis (CE) and high-performance liquid chromatography (HPLC) as well as gene probe and immunoassays relied on detection in the visible region of the spectrum, scientists are now taking full advantage of mid red and infrared regions because of the comparative optical advantages. As such, new near infrared (NIR) probes are being rapidly developed for this reason. The application of these fluorescent molecules continues to demonstrate a plethora of photophysical properties making them unique for bioanalyses[8-14].

Traditional fluorescent probes, for example, rhodamines and fluoresceins, absorb and emit in the ultraviolet or visible (300 – 700 nm) region of the spectrum. With the development of new excitation sources, and in particular light emitting diodes (LEDs) and diode lasers, optical spectroscopy in the short range near infrared (700 – 900 nm) and near-infrared (900 – 2000 nm) regions have proven more advantageous and profitable. Optical light sources and detectors in this spectral window become continuously cheaper through large scale use in the telecommunication industry and opto-digital recording. Among the benefits of using the NIR band, is the inherent reduced Rayleigh and Raman light scattering, which is $1/\lambda^4$ dependence on wavelength along with the diminished auto-fluorescence of biological tissues, making biomedical applications in particular, very attractive [2, 15, 16]. Also, the near-infrared region is favorable in fiber optic sensing because of the reduced light intensity loss associated with quartz fibres at higher wavelengths. A comparative list of these benefits is illustrated in Table 1.1.

Table 1.1 Comparison of noise levels in the NIR and visible regions [9]

Source of Noise	Visible region	NIR region
Detector	High	Low
Scatter (Rayleigh/Raman)	Greater at lower wavelengths (scattering is $^1/_4$ dependent on λ)	Reduced
Autofluorescence	Most biomolecules exhibit fluorescence	Reduced

The application of new NIR sensors in the detection of key biomarkers continue to advance in part because of an increasing scope of clinical application and the need for better micro-environmental monitoring. Interestingly, most commercially available fluorescent dyes self-aggregate in aqueous solutions resulting from π-stacking of the planar π-electron conjugation systems giving rise to both H-(hypsochromic) and J-(bathochromic) aggregation. Self- aggregation depends primarily on solvent polarity but may also be affected by temperature, pH, dye concentration and ionic strength [2]. Besides the aggregation properties of conventional fluorescent, they also suffer from low photostability, poor quantum efficiency, low Stoke shifts and severe quenching of the fluorescence of cyanine dyes in biopolymer conjugates, e. g. quenching of Cy5 and Cy7 dye variants on conjugation [17, 18]. Visible and near infrared fluorescent dyes are relatively stable in the solid state, however, they are susceptible to photochemical degradation which may result in photobleaching. Given the propensity to self-aggregate and photooxidize, the application of fluorescent dyes in solution is rather limited, thus, many new analogs are being developed with enhanced solubility and reduced photo-sensitivity and a host of other favourable photophysical properties.

In this chapter we explored the most common classes of fluorescent dyes applied in modern bioanalytical science for detection purposes. We have included dyes that exhibit the most suitable combination of both photophysical and chemical properties useful for simplified method developments. These include rhodamine, coumarin, oxazine and cyanine and derivatives. As a requirement for their application in bioanalytical method development, we have also describes their unique optical properties and their usefulness as prime candidates in creating this novel enzyme based bioanalytical detection protocol.

1.2 Types of Ultra-Violet /Visible Fluorescent Dyes available for bioanalyses

1.2.1 Rhodamines

Rhodamines are among the most commonly used dyes in complex bioassays. These fluorescent molecules belonging to a family of 3,6-di(substituted-amino)-9-benzoate derivatives of xanthenes, these optical fluorophores are commonly used as fluorescent probes in trace metal analyses [17] and are also widely utilized for biomedical research, for example; labeling of biological compounds, such as antibodies or DNA [19] and as fluorescent tracers in histochemical studies [20-25]. Among these green dyes, Rhodamine Green has been known to exhibit the highest emission efficiency and the longest sustained fluorescence even after cellular internalization [26]. Rhodamines can be derivatized with either an isothiocyanato group *e.g*. tetramethylrhodamine isothiocyanate or an *N*-hydroxysuccinimidyl (NHS) ester functionality *e.g.* 5-carboxytetramethylrhodamine succinimidyl ester for covalent labelling at the amino group of proteins or amino-functionalized nucleotides. As hydrophobic compounds, rhodamines and their derivatives usually display poor water solubility, a prerequisite of effective conjugation reactions involving biologically relevant macromolecules (proteins, nucleic acids, carbohydrates). Also, the suitability

of rhodamines as fluorescent probes may be further limited by poor solubility in aqueous solutions which enhances aggregation and dimerization reactions [27, 28]. It remains unclear, if unique chemical properties among individual rhodamine core family members affect photophysical propertiess critical to *in vivo* optical imaging or other *in vivo* bioanalytical assay. One noted parameter is the preservation fluorescence intensity in low pH and polar environments, similar to that of the endolysosome. In addition, the persistence of fluorescence intensity after cellular internalization; and sufficient signal-to-noise ratios of fluorophore-targeted enzyme species to elucidate key biological processes cannot be over-emphasized.

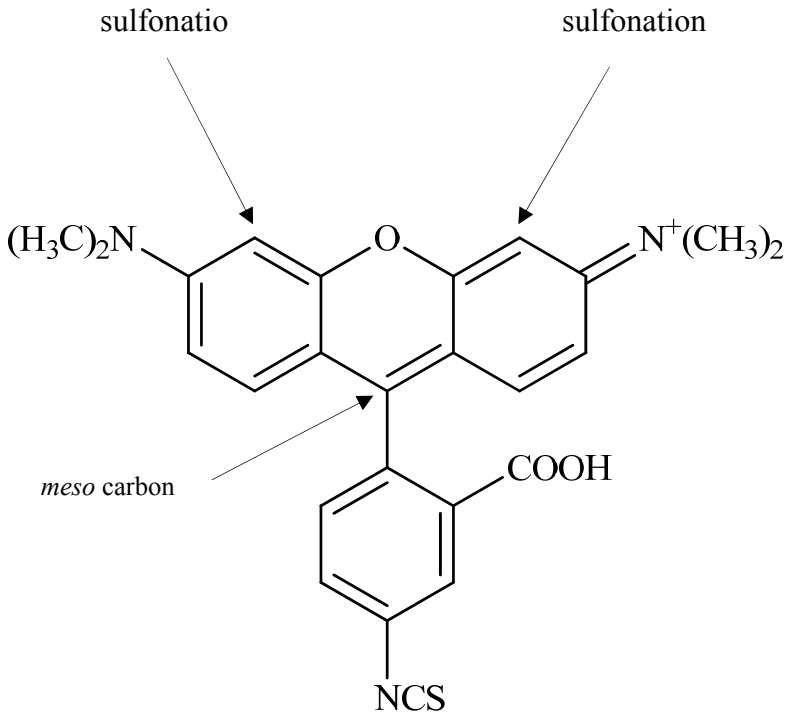

Figure 1.1 Structure of isothiocyanato-functionalized fluorescein.

To overcome some of the common photophysical limitations associated with the utility of rhodamine as a fluorescence probe, such as of aggregation and unspecific absorption, a simple and efficient method is used to increase the water solubility these molecules. Recent studies have reported the successful synthesis of water soluble sulfonated rhodamine 6G with a rigidized xanthenes fragments. Besides reducing aggregate formation, sulfonation of the probes proved quite useful in inhibiting fluorescence quenching associated with conjugation, enhances the photostability and pH sensitivity [19]. In addition, the advantageous spectral characteristics displayed with sulfonation of the rhodamine molecules, further spectral tunability can be achieved with variation at the c-*meso* substituent [29, 30]. There are only a few discussed synthetic routes that yield novel rhodamine-derivatives with ideal spectral properties suitable for the development of different biomolecular assays. Wu *et al*. demonstrated the preparation of new rhodamine analogs by modification of the 2-carboxylate group to yield; fluorescein, rosamine, Tokyo green, Pennsylvania green [30].

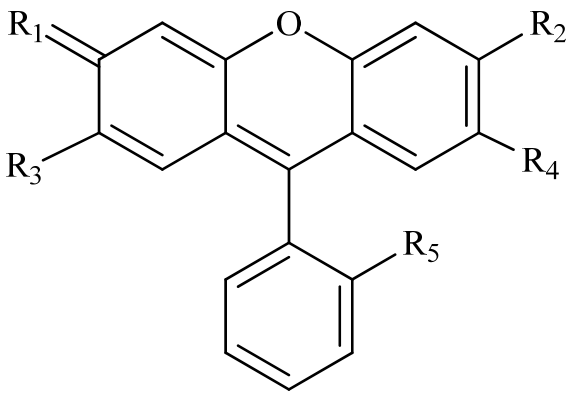

Figure 1.2 General structure of rhodamine derivatives.

The bioanalytical application of rhodamines in studying key biological processes require optical probes that permit *in vivo* identification of specific targeted molecules. Optimal utility of these fluorescent probes *in vivo* and for further *in vivo* development relies upon many different factors key among them are; probe fluorescence intensity and probe stability in harsh subcellular environments. As such it is always imperative to design the best suitable molecules.

Table 1.2 Sustituted rhodamine derivatives [29, 30].

R^1	R^2	R^3	R^4	R^5	Compound
$N^+(CH_3)_2$	$N(CH_3)_2$	H	H	CH	Rhodamine
$N^+(CH_3)_2$	$N(CH_3)_2$	H	H	H	Rosamine
O	OH	H	H	CH	Fluorescein
O	OH	F	F	CH_3	Pennsylvania Green
O	OH	H	H	CH	Tokyo Green

1.2.2 Coumarins

Another unique class of dyes that have found commonplace in modern spectroscopic detection of biomolecules and complex biochemical processes are the Coumarins. This is a group of low molecular weight fluorescent dyes with maximum absorbance in the 320 – 530 nm region of the spectrum. Like most fluorescent compounds previously discussed, coumarins exhibit strong fluorescent intensity in the ultraviolet/visible range, thus making them applicable in laser active media, optical brighteners, and light-emitting diodes [31]. Coumarins are synthesized as heterocyclic aromatic molecules derived from cinnamic acid via ortho-hydroxylation synthetic pathway. Derivatization of the molecular structure results in unique photophysical behavior and may further induce photosensitizer properties [32]. Unlike most fluorescent dyes, coumarins and its derivatives are produced naturally in plants as essential oils thus, further enabling their pharmaceutical suitability. Bryantseva *et al* studied the fluorescent characteristics of coumarin photosensitizers using furocoumarins; a class of derivatized coumarins that absorb in the 320 – 400 nm

spectral range. Intersystem crossing in the order of ~ 10^{10} to 10^{11} sec^{-1} was reported, which confirms the applicability of the substituted dyes as prime photosensitizers [32].

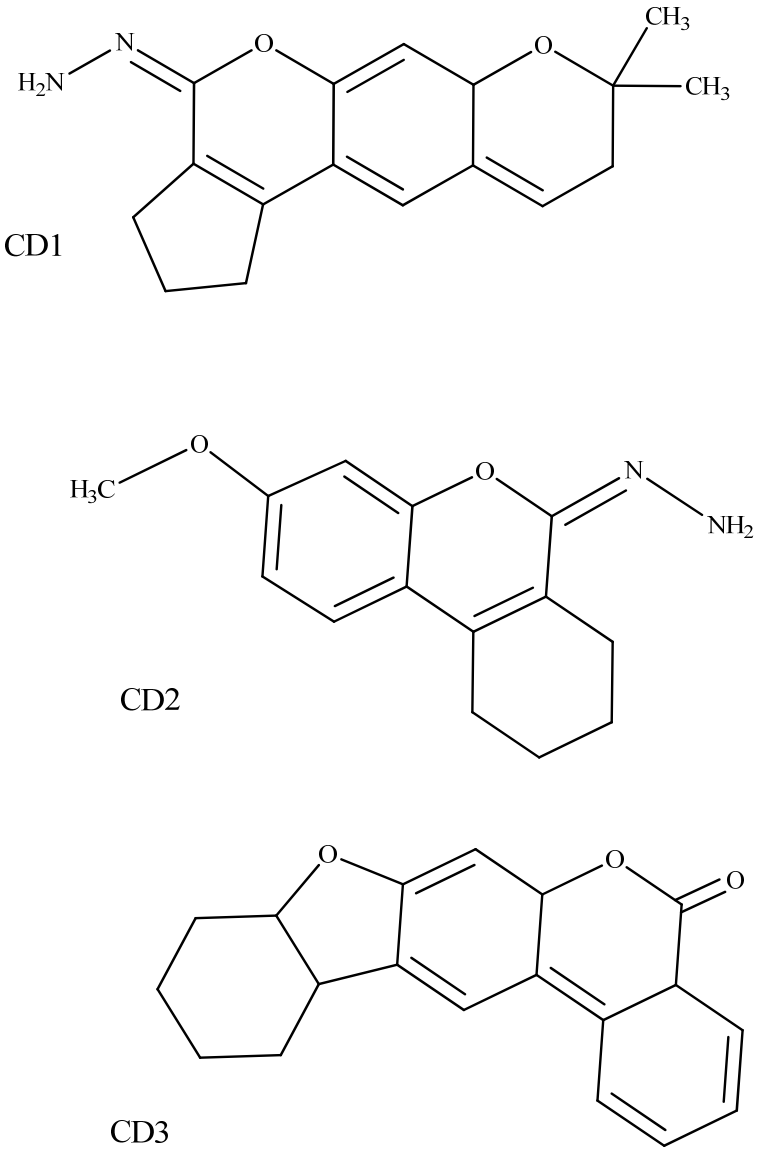

Figure 1.3 Substituted Coumarin dyes characterized by Bryantseva *et al.*[32]

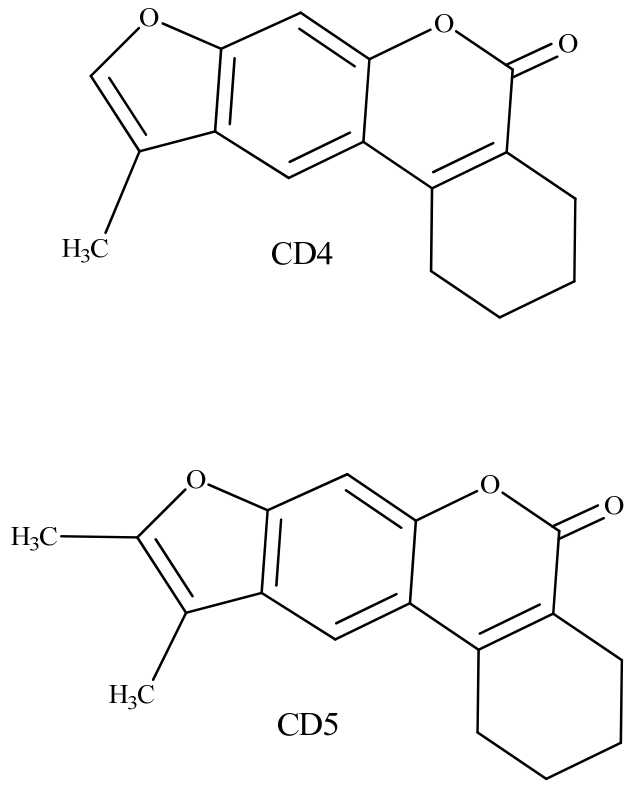

Figure 1.4 Substituted Coumarin dyes characterized by Bryantseva *et al.*[32]

Also, new sequential biosynthetic oxidation and alkylation reactions of coumarins (to form furanocoumarins) that are reported, enable the molecules to act as bifunctional photoreagents, capable of conjugating double stranded DNA by cross linking both strands [31 33-36].

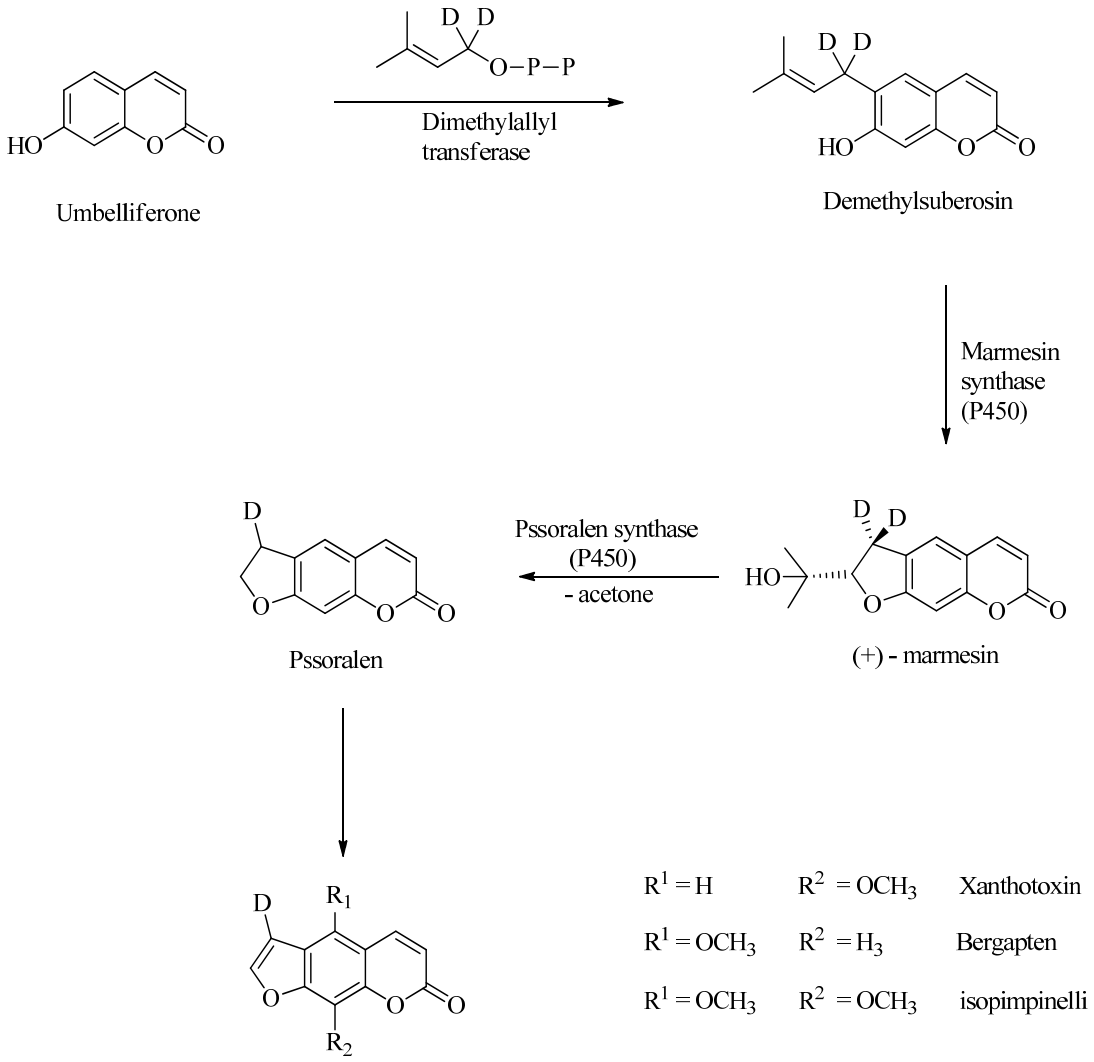

Scheme 1.1 Biosynthetic pathway reported by Stanjek *et al.*[34] towards the formation of furanocoumarins: xanthotoxin, bergapten and isopimpinelli from umbelliferone (a coumarin compound).

1.2.3 Oxazines

Oxazine refers to another family of dyes that are known for their unique photophysical properties and are considered to be strongly fluorescent in the 480 – 600 nm band of the spectrum. Oxazines are characterized by heterocyclic systems containing one oxygen and one nitrogen atom. Oxazines form numerous types of derivatives whereby, common isomers are formed depending on the relative position of the heteroatoms and relative position of the double bonds in the tricyclic aromatic moiety. This unique structural property gives rise to the Benzoazine subfamily of compounds, chief among them are the; Nile Red (9-diethylamino-5H-benzo[α]phenoxazine-5-one) and Nile blue dyes. The Benzoxazine derivatives contain an oxazine ring a heterocyclic six-membered ring system with the nitrogen and oxygen atoms directly incorporated into the central six membered ring [37-40].

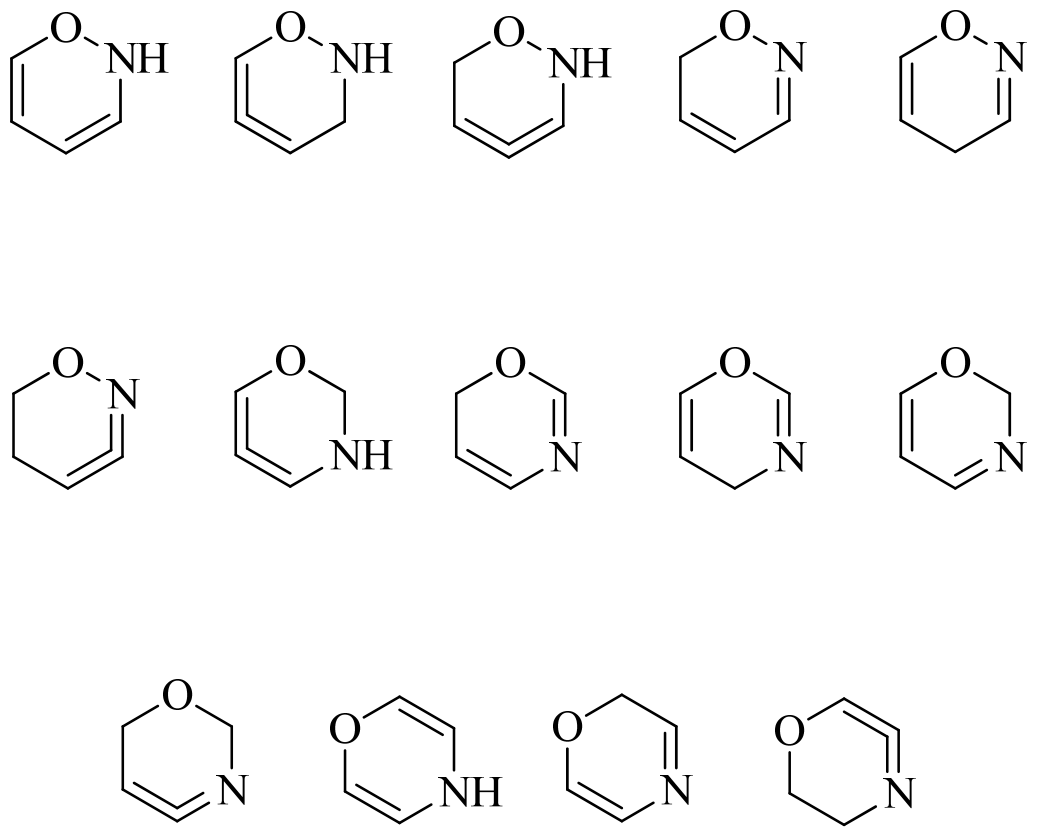

Figure 1.5 Fourteen possible isomers of the general oxazine structure [41, 42].

Within the last few decades, benzoxazine derivatives have become more popular in applications such as polymers, resins, and cross-linking agents owning to favorable thermal and chemical resistance, electrical properties and most, design flexibility. Despite their wide opto-physical and opto-electronic applications,

Nile Red has been extensive used as an ideal probe for lipids detection due to the fact that it exhibits high affinity, specificity and sensitivity hydrophobicity of lipids. In the interaction of Nile Red with structural lipids such as the eukaryotic cell walls, there is a characteristic shift in

the emission band from red to yellow for polar and non-polar lipids respectively. Thus is used as a intracellular stain [43-46]. For this reason, Nile Red has been widely utilized in investigating lipid storage diseases and lipogenesis [43-45]. However, because of selective and non-uniform uptake across cell walls, a quantitative ratio of red and yellow emissions has been very challenging for tissue imaging and other bioanalytical applications. As such, reported quantitative data is quite limited and most evaluations are performed in flow cytometry as oppose to other spectroscopic techniques such as absorbance and emission similar to other fluorescent dyes. Flow cytometric analysis provides a single cumulative value for the entire cell which can be ambiguous about the nature and localization of intracellular lipids, as many different organelles; ER, Golgi, mitochondria, lipid droplets, etc., thus producing strong red emission with poor contrast [44, 45]. This demonstrates that, Nile Red bioanalytical techniques are very limited in fluorescence microscopy studies. Nonetheless, they may still be qualitative but provide only little quantitative data.

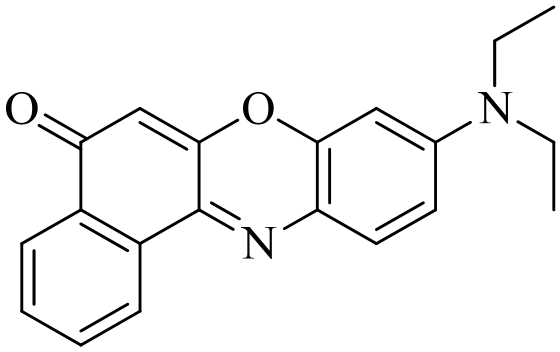

Figure 1.6 Structure of Nile Red

1.3 Near Infrared (NIR) Fluorescent Dyes available for Bioanalyses

1.3.1 Cyanine Dyes

Among the large variety of commercially available fluorescent probes used in biomolecular detection, Cyanine dyes are among the most highly recognized partly because of their intense absorption in the Vis-NIR region. These chromophores typically comprise two heterocyclic rings that are bound together by a polymethine linker; each heterocyclic ring system incorporates one or more nitrogen atoms as shown in the general structure of figure 1.6 [47, 48].

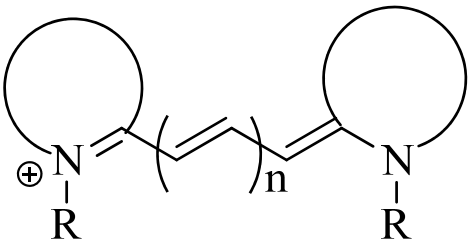

Figure 1.7 General structure of a Cyanine dye

Variation in the length of the polymethine linker affects photophysical properties on these NIR compounds. Their common names denote the number of methine groups in the polyene chain [49, 50]. The incorporation of an additional vinylene group in the polymethine linker, typically results in a red wavelength shifts of up to 100 nm in the absorbance maxima [17].

Cyanine dyes are commonly classified by the heterocyclic moiety at the end of the polymethine chains, for example, oxonol, merocyanine and so forth. These fluorescent molecules are also categorized based on the polymethine chain itself and can be denoted by the number of methane groups incorporated into the linker; mono-, tri-, penta-, heptamethine, etc. The two heteroaromatic moieties linked to the polyene consist of imidazole, pyridine, pyrrole, quinoline, thiazole, etc. Among the various classes of probes, heptamethinme along with trimethine (often referred to as Carbocyanine) dyes have been studied extensively for various applications in bio-science, optoelectronic, environmental assays and other broad areas of science.

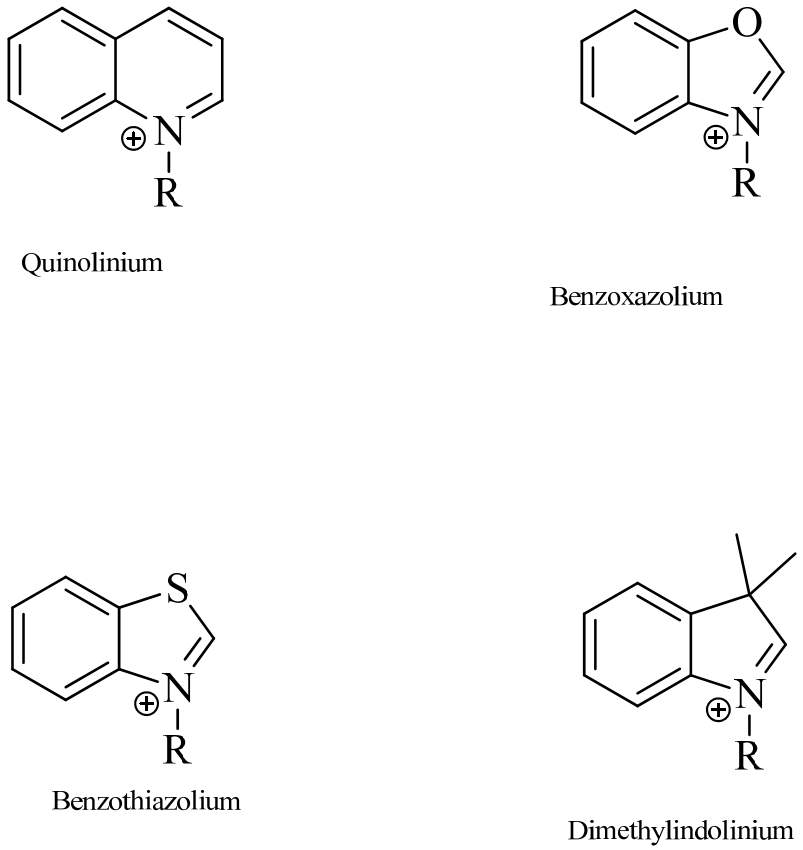

Figure 1.8 Four common heterocyclic moieties used in preparation of cyanine dyes.

Generally, due to the intrinsic auto-fluorescence in the ultraviolet or visible region, tissue imaging and other dye based bioanalytical assays are rather problematic and is characterized by low signal-to-noise ratio. This limitation is most often times overcome by applying cyanine dyes which are inherently known for their strong NIR absorbance and emission; outside the optical band of most if not all naturally occurring biomolecules. In addition, unlike most other common-

ly encountered fluorescent dyes, during dye synthesis, unreacted starting materials and degradation products are normally UV active. This helps to simplify dye purification because of the great spectral separation (as demonstrated in Scheme 1.2) thus making the process possible with techniques such as capillary electrophoresis and liquid chromatography using NIR detection. Despite these unique advantages, these fluorescent molecules are still susceptible to factors such as low solubility, photobleaching and dye aggregation which limits their bioanalytical potential, thus the need for ongoing research to identified more suitable probes.

Carbocyanine dyes are popular in the development of digital data processing, optical communication, molecular labeling, light harvesting and drug delivery agents. In a more recent study, Ma *et al* [62] investigated the application of NIR cyanine dyes in the development of Organic Light-emitting Diode (OLED) for use in optical communication and information processing. The optical properties of a fluorescence conjugate of poly(*N*-vinylcarbazole) (PVK) doped with the commercial NIR cyanine dye, 2-[2-[2-Chloro-3-[2-(1,3-dihydro-1,1,3-trimethyl-2Hbenzo[e]-indol2ylidene)ethylidene]-1-cyclohexen-1-yl]-ethenyl]-1,1,3-trimethyl-1H-benzo[e]-indolium-4-methylbenzenesulfonate (ADS830AT) was studied by spin-casting techniques [63]. In this work the investigator developed an OLED of improved electroluminescence (EL) efficiency and reduced overlap from ultraviolet emission.

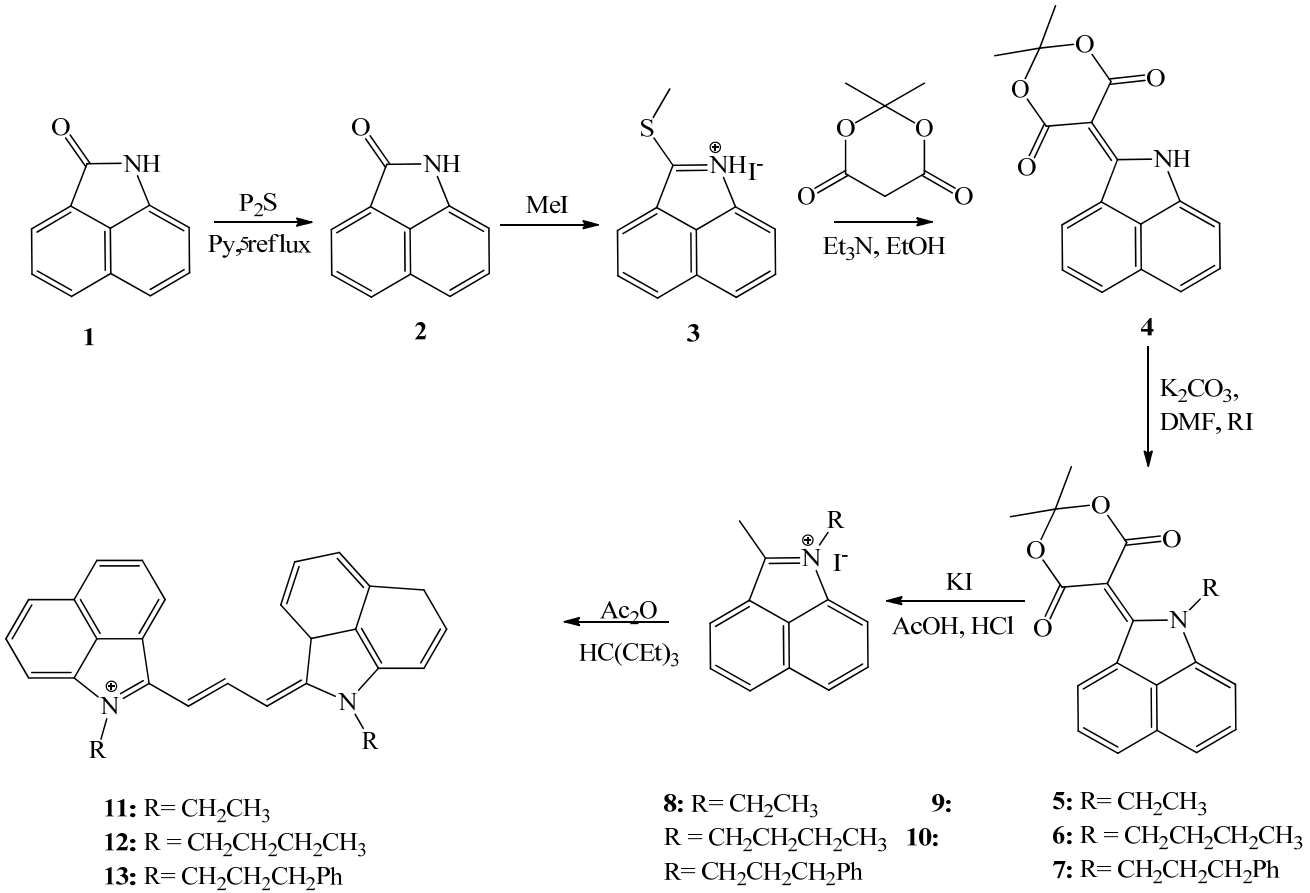

Scheme 1.2 General synthetic pathway of Trimethine (carbocyanine) dyes

Most of the Vis-NIR emissive materials reported in literature are ionic cyanine dyes with limited practical applications due to low electroluminescence efficiency. During the studies Ma discovered that in addition to improved electroluminescence efficiency, a single emission layer PVK device doped OLED emits pure monochromatic NIR radiation at 890 nm and displayed stable spectral properties with forward bias voltages. Further advancements around the NIR region of the spectrum led to the fabrication of other optoelectronic cyanine analogues. New acidochromic molecules were synthesized and studied. Alonso and coworkers developed novel heptamethincyanine dyes that have proven useful in the fabrication of inexpensive communication components [51]. The rapid technological growth in the telecommunication field propelled an increased demand for new and less expensive optochemical sensors. This resulted in the proliferation of chromoionophoric embedded plasticide Polyvinyl Chloride (PVC) optodes capable of detecting the optical transduction signal generated by chemical reactions. Whereas classic acid-base indicators with absorption maxima in the visible region of the spectrum are suitable as potential chromoionophores, their applicability as plasticide PVC optodes is limited by spectral interferences. Only few classes of molecules fluoresce in the NIR region thus, enabling reduced spectral interferences and enhanced sensitivity. Puyol *et al* further characterized three types of chromoionophores (Figure 1.8): nortricarbocyanine dyes (**3**), norindosquarocyanine dyes (**5**) and norindocrococyanine dyes (**7**) based on an acid-base equilibrium with an aim to optimize the spectral characteristics by lowering the pK_a values [52] .

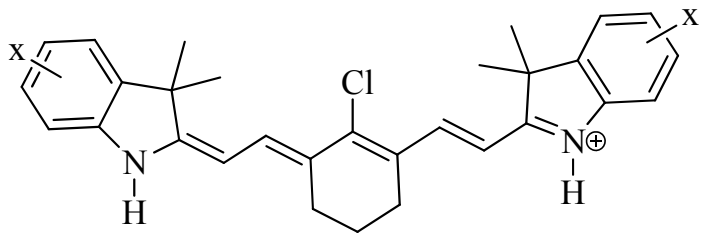

(3)

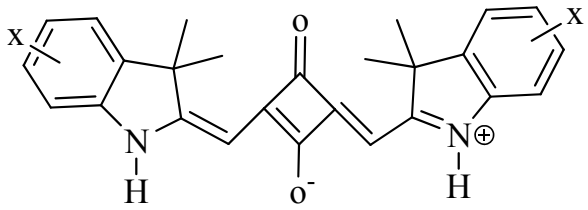

(5)

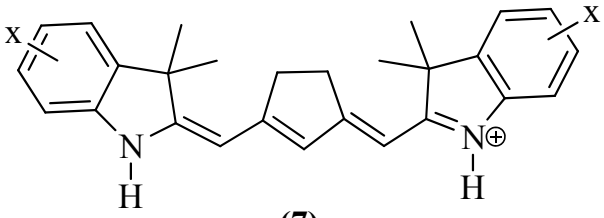

(7)

Figure 1.9 Norcyanine dyes prepared by Puyol *et al*. for use as pH chromoionophores [53, 54].

This work highlights the effects of acid-base equilibrium on the optochemical properties of newly synthesized cyanine dyes. New trends in PVC optodes are geared towards widening the scope of chromoionophore applications by miniaturization of chemical analytical platforms, with a subsequent reduction in the size and complexity of optical systems. Laser diodes emitting at 670 and 780 nm are most suited for this purpose because of the high molar absorptivities of the dyes used with them, the high intensity of the laser diodes and low overall cost [52-54]. It was demonstrated that the improved spectral characteristic and subsequent chromoionophore suitability in optochemical sensing of cyanine dyes, depend primarily on the conjugated chromophoric system and the nature of the polymethine side chain. Nortricarbocyanine dyes commonly consist of longer polymethine chains than its norindosquarocyanine and norindocyanine counterparts thereby, displaying favorable absorption characteristics for longer wavelength in the NIR region of the spectrum. Besides, the ability to induce ring formation of the side chain further enhances spectral stability thus greater potential for optochemical fabrication and chemical sensing capabilities [53, 54]. Similar to the approach used by Puyol, Qian *et al*. characterized the spectral behavior of two groups (one symmetrical and the other asymmetrical) of novel NIR cyanine dyes[53, 54] (shown in figure 1.9) as fluorescent pH sensors by monitoring the pK_a value of the molecules. The studies indicated strong fluorescence enhancement as well as distinct bathochrmoic shifts of the absorption peaks from 525 to 570 nm as a result of the protonation of two of the symmetrical NIR fluorescence analogues. Also, R group substitution at the C-3 position of the indole ring resulted in distinct spectral changes to the emission maxima and the quantum efficiency of these cyanine dyes (see table 1.3). However, such favorable spectral changes could not be explained through mere proton deprotonation or resonance effect within the molecule. It was reported that pH sensitivity is attributed to changes from photo-induced electron transfer (PET) to in-

tramolecular charge transfer (ICT) mechanisms, thus the compound can be fabricated into a pH sensor of high pK_a [53, 55]. Zhang *et al*. also prepared a modified analogue to a novel fluorescent molecule for improved spectral properties as a fluorescent pH indicator [56].

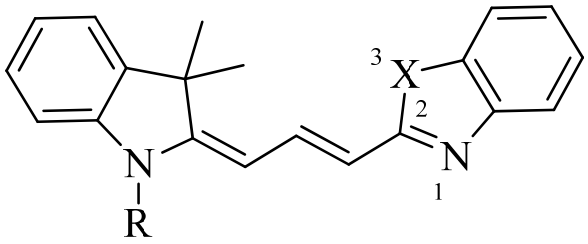

Ia	**R = $(CH_2)_5COOH$**	**X = $C(CH_3)_2$**
Ib	**R = $(CH_2)_5COOH$**	**X = CH_2**
IIa	**R = $(CH_3)_5SO_3^-$**	**X = $C(CH_3)_2$**
IIb	**R = $(CH_3)_5SO_3^-$**	**X = CH_2**

Figure 1.10 Structure of asymmetrical cyanine dyes prepared by Xu et al. [55, 57] to study pH sensitivity.

Table 1.3 Spectral characteristics of novel cyanine dyes bearing different R groups at the C-3 position indoleum ring, developed by Xu *et al.* [55, 57]

	Cyanine dyes			
	Ia	**IIa**	**Ib**	**IIb**
Methanol				
λ_{max}	550.3	549.5	493.9	495.4
$\lambda_{EM\ max}$	553.0	554.5	496.3	500.3
$\lambda_{EM\ max}$	569.4	571.4	528.0	525.1
Δ_S	16.4	15.9	34.1	24.80
Φ	0.129	0.164	0.005	0.003
Water				
λ_{max}	540.3	540.3	490.4	489.5
$\lambda_{EM\ max}$	546.7	547.5	494.1	494.1
$\lambda_{EM\ max}$	566.6	567.2	516.1	521.6
Δ_S	19.9	19.7	22.0	27.50
Φ	0.060	0.060	0.007	0.004

As reported by Achilefu *et al*. [56], norcarbocyanines dyes such as indocyanine green and cypate conjugates are easily prepared as target-specific pH indicators, through substitution on the indole-ring for conjugation of the free carbonyl groups in biomolecules [51, 56].

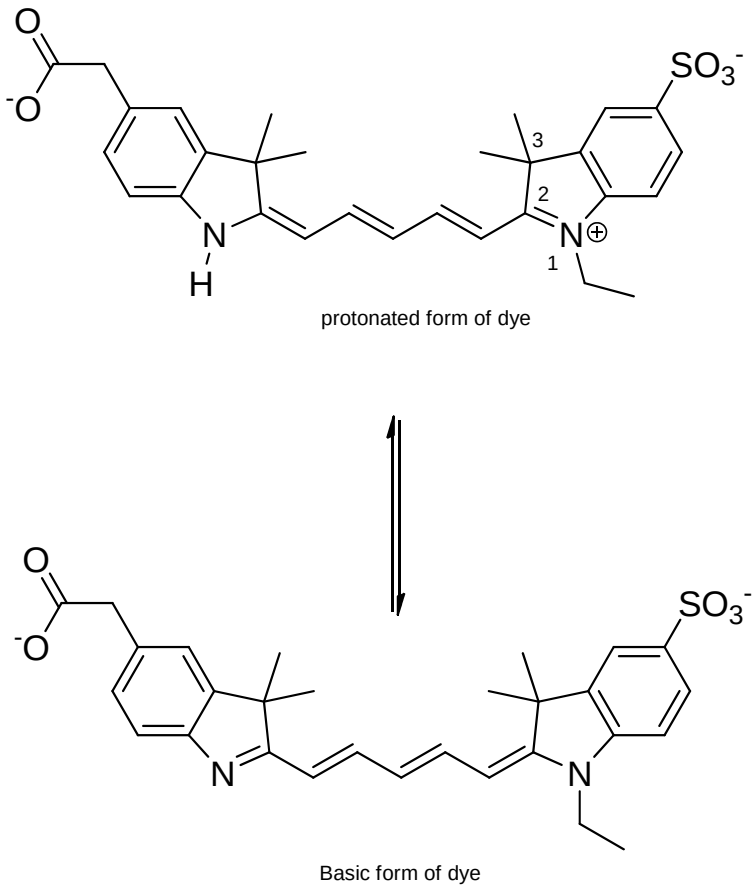

Scheme 1.3 The NIR cyanine base-form pH sensitive fluorescence probe decribed by Puyol *et al.* [53, 54, 58]

1.3.2 Recent trends in the application of Vis-NIR fluorophores

In recent years, the development of new sensors for the detection of key biomarkers continued to advance primarily because of an increasing scope of clinical application and the need for better microenvironmental monitoring. For example, redox-active dinuclear ruthenium conjugates are functionalized with cyanine dyes for clinical monitoring of important bio-chemical substances such as glucose or hydrogen peroxide under physiological conditions. Xun *et al*. have successfully synthesized various redox-active conjugates of ruthenium-1,2-dicarbonylhydrazide, these complexes display intense absorbance in the NIR region of the spectrum when present in the mixed-valence state as Ru^{2+} and Ru^{3+} due to the oxidative potential of hydrogen peroxide or any strong available biological oxidant. Glucose oxidation to hydrogen peroxide provided a suitable oxidative pathway for the formation of the ruthenium mixed-valence complexes and as such creates the ideal platform for the fabrication of the glucose NIR optical sensors [59, 60]. The combination of simplicity in design and low electrical interferences further propelled the development of redox based NIR optical sensors.

Research has shown that synthesized mono-substituted vis-NIR cyanine dyes are suitable for use as transducers in distributed fiber-optic ammonia sensors [61, 62]. While most commercially available Vis-NIR fluorescent molecules display diminished optical properties and are less suitable for sensing chemically and biologically important substances such as ammonia. Šimon *et al*. [63] reported a cyanine dye displaying ammonia-induced absorption peak at 620 - 680 nm. These newly developed fluorescence probes are been designed for the near to mid-infrared regions with diminished light scattering interference and background autofluorescence [50, 64]. The application of these dyes has even been extended to incorporate the fabrication of optical fiber sensors util-

ized in evaluating the decomposition of heavy hydrocarbons in transformer oil. The application of NIR dyes to detect slight changes in refractive indices incorporates the partial discharge of gaseous hydrocarbons such as methane, ethane, propane and butane resulting from chemical disturbances in liquid hydrocarbons, for example, transformer fluids. This technique involves evanescent field absorption (EFA) measurements with NIR optical sensors coupled-spectrometer, for enhanced performance. Although the intensity of the C-H, N-H or O-H bond vibration is reduced by as much as a factor of 100 in the NIR as oppose to the corresponding ground modes at higher wavelength, such as, the mid infrared region (MIR), the former is preferred for its advantage of enhanced spectral purity and improved signal-to-noise ratio [46]. Furthermore, hydrocarbon sensing by EFA-MIR techniques requires the use of silver halides fibers which, because they are sensitive to chemical attacks, suffer from UV degradation and high transmission loss, making them less attractive for optical fiber development. As a result, the NIR fabricated devices are more applicable for both their mechanical and optical properties, hence are more suitable for practical sensing applications [63, 65-67].

The field of near infrared spectroscopy has undergone an unprecedented surge in the application of NIR fluorophores specifically in the areas of optoelectronics and optochromic technology. More researchers are taking advantage of improved sensitivity resulting from lower background autofluorescence and reduced light scattering for deep tissue *in vivo* imaging. Typical examples of NIR cyanine dyes reported in literature include indocyanine green (ICG) and the IRDye78 [67]. Chen *et al* discussed the non-invasive imaging and quantification of $\alpha_v\beta_3$-positive integrin level in the blood. $\alpha_v\beta_3$ integrin is believed to be responsible for the regulation of tumor growth and metastasis as well as angiogenesis. Increased blood level of this target molecule is a

key factor in the evaluation of the aggressiveness of the disease [68]. In this work, the researchers outlined the integrin receptor specificity of the newly synthesized peptide-dye conjugate arginine-glycine-aspartic acid (RGD)-Cy5.5 as a contrast agent *in vitro*, *in vivo*, and *ex vivo* imaging [68]. An intravenous injection of a 3 nano-molar dose of the fluorescent probes resulted in an instantaneous whole-body imagery of an athymic nude mice specimen. However, after 4 hrs post injection the U87MG tumor could be distinctly differentiated from the background tissue. Whereas the uptake and decomposition of the fluorescent probe was rapid in healthy tissue, it was rather slow in affected tissue. *ex vivo* evaluations were also performed and results revealed improved sensitivity, achieving enhanced emission intensity and tissue contrast. This fluorescence probe is ideal for intraoperative NIR imaging due to its superb tissue contrasting capabilities and overall low toxicity. ICG-polyamine (polyethylamine, PEI) (IR820-PEI) is also a prime NIR dye conjugate developed specifically for *in vivo* NIR fluorescence imaging with improved photostability and reduced aggregation formation. With a large stoke shift of 115 nm in aqueous solution, this NIR fluorophore displayed strong binding affinity for DNA. Coupled to the low molecular weight and relatively high quantum efficiency of ICG, this newly synthesized conjugated NIR fluorescent dye facilitates improved deep tissue imagery for the evaluation of liver function and non-invasive angiography in ophthalmology [68]. Similar results are achieved with *in vitro* optical NIR imaging studies using novel carbocyanine-glucosamine conjugates. In addition to improved quantum efficiency and decreased aggregation tendencies in polar environments, NIR dye-glucosamine conjugates exhibit low toxicity and moderate to low pH response at physiological pH range. Owing to improved solubility in aqueous solutions and increased quantum yields, conjugation results in enhanced cellular uptake and a concomitant intracellular NIR fluorescence enhancement in breast epithelial cell lines [69]. NIR fluorescence monitoring of glu-

cosamine levels has also enabled *in vivo* assessment of lysosomal proteins and provided a viable option for the evaluation of cancer and metastasis in their early stages [70]. Similar approaches have being attempted in order to study lysosomal target cells using near infrared dyes. This is achieved primarily by binding a self-quenching targeting moiety which is subsequently internalized into the lysosomal target cells. The application of this self-quenched avidin-rhodamine X conjugate (Av-ROX), facilitates the *in vivo* targeting as well as NIR imaging differentiation of the aberrant tumor cells and the healthy background tissue. While intracellular degradation within the lysosomes leads to dequenching and subsequent fluorescence reactivation within the target cells, virtually no effect is observed within the surrounding tissue [71, 72]. Besides achieving high fluorescence signal-to-noise ratios for the targeted tumor cells, this technique allows improved molecular imaging.

Near Infrared dyes have found application for *in vivo* molecular imaging of cellular events in early aortic valve disease. NIR dyes are used to visualize endothelial cells, macrophages, proteolysis and osteogenesis in the aortic valve of hypercholesterolemic apolipoprotein E-deficient mice. Early detection of aortic valve diseases such as macrophage activation, osteogenesis and protein intramolecular degradation can be achieved by utilizing NIR molecular imaging [73] also, it is reported that NIR molecular imaging visualization of valvular cell functions *in vivo* may identify therapeutic targets in early atheriosclerosis diagnosis.

A free-radical precipitation polymerization method was used to prepare thermally responsive poly(*N*-isopropylacrylamide-co-acrylamide) (P(NIPA-co-AAm)) nanohydro-drels which can later be evaluated by *in vivo* NIR fluorescence imaging on healthy and S180 tumor infected

denuded mice specimens. Fluorescent imaging studies may be performed by evaluating the overall fluorescence intensity of an entrapped novel Near infrared dye NIRD-12 into P(NIPA-co-AAm) nanohydrogels on both sets of specimens, which may or may not be exposed to controlled hyperthermic treatment. The researchers have reported passive and non-specific thermally targeted behavior. In reality, the thermal responsive fluorescence-tagged nanohydrogels are only accumulated in at higher temperatures in both healthy or tumor affected tissue. Whereas in other research experiments the affected cells are differentiated by the NIR fluorescence, in the current experiments these results were not fully observed. Nonetheless, the thermal response of P(NIPA-co-AAm) nanohydrogels regardless of health status provided a viable option as a thermal carrier of drugs, especially for tumor diagnosis. In addition to the key thermal response of the P(NIPA-co-AAm) nanohydrogels, NIR dye conjugate is indicated by a distinct bathochromic shift at the absorption maxima. This is further characterized by enhanced photostability resulting from the entrapment of the fluorescent probe within the nanohydrogel polymer [59, 60]. The technique improves molecular imaging and enables extending the overall time available for *in vivo* monitoring of dynamic process of dye-loaded nanohydrgel polymers.

1.3.3 Squaraines

Squaraines are a class of dyes that are well known for their intense fluorescence in the near infrared region of the spectrum. These NIR molecules exhibit significant triplet quantum yields and are characterized by their unique aromatic four membered ring system derived from squaric acid [74-78]. Recently, a number of squarylium-derivatives are being developed for application as such as chemosensors [79], *in vivo* imaging [80] photovoltaics and low-cost, large-area solar cells [81]. Unlike most of the other commonly encountered fluorophores, squaraines applicability is

limited by the high electron deficient four membered ring which inherently undergoes nucleophilic attacks [76]. As a result Xue *et al*. have proposed a new synthetic pathway for the preparation of a pair of triptycene-based tetralactan macrocycles which can protect the squaraine molecules from polar solvents by formation of a dye-macrocycle complex [77]. Furthermore, there is currently a vast number of commercially available squaraine-derived rotaxanes that have been developed for improved protection from nucleophilic attacks and enhanced spectral characteristics such as reduced aggregate formation [82]. Most often, the rotaxanes analogues exhibited the same excellent photophysical properties as the precursor squaraines, as well as improved spectral properties as a result of the encapsulating macrocyclization [77].

A common spectral improvement to the rotaxanes, is the retardation of photo-bleaching tendencies of the molecules. In fact, Arunkumar *et al* reported the preservation of the color of the rotaxane molecule in aqueous solution after several weeks as oppose to the squarylium precurcor which undergoes photobleacing within 48 hours at similar experimental conditions. In addition, incorporation of the encapsulating macrocycle results in diminished adsorption band broadening by inhibiting interchromophoric interactions both in solution and in the solid state [82]. The spectral versatility of squaraines dyes make them quite unique as fluorescent probes and near infrared labels for biomedical applications [83, 84]. Terpetschnig *et al*. described a novel *N*-succinimidyl ester-derivatized indolium squaraine dyes which displayed strong conjugation affinity for Human Serum Albumin (HSA) [7, 74, 85-87]. Conjugation of the water-soluble NIR fluorophore yielded five-fold improved quantum efficiency and enhanced fluorescence lifetime [9, 82-84]. In addition to the common “methylene base” synthetic pathway involving squaric acid or its derivatives, a novel synthetic route for mono-substituted squarines by reacting with malononitrile, cyano- and ni-

troacetic esters, barbituric acid, and 1,3-indanedione was proposed [94]. Interestingly, these mono-substituted squaraine dyes are in a similar spectral range of the more popularly known Cy5 and Cy5.5 NIR fluorescent dyes and are even considered more stable in aqueous solutions with molar coefficients in excess of 265,000 M^{-1} cm^{-1} [86, 88].

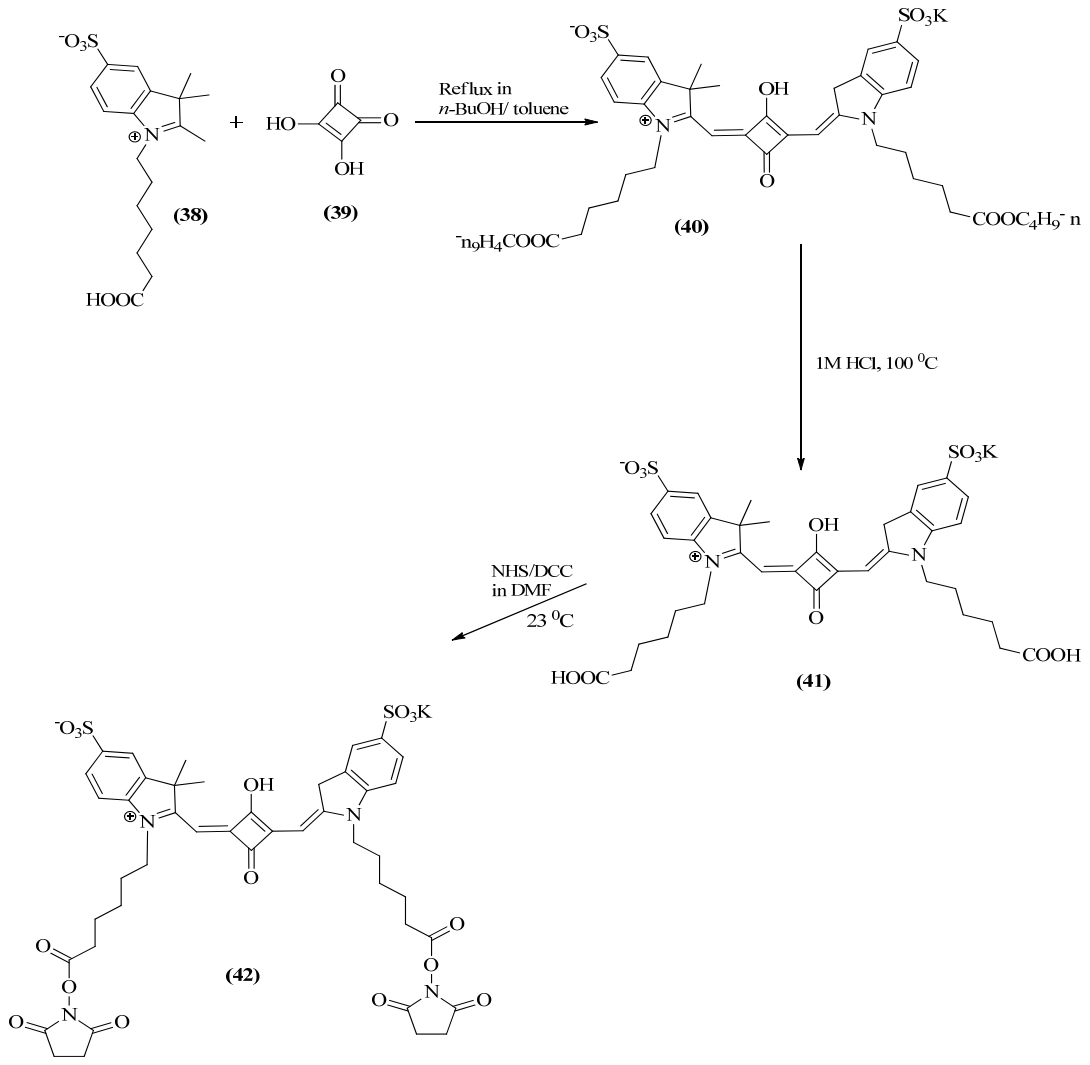

Scheme 1.4 Synthetic route to Sq635 squaraine dye 42 containing *N*-succinimidyl ester moieties. The Sq635 is utilized in fluorescence resonance energy transfer (FRET) immunoassay by Terpetschnig and co-workers [7, 9, 85, 87, 89].

1.3.4 Phthalocyanines and naphthalocyanines

Similar to the squaraines, phthalocyanines (Pcs) and naphthalocyanins (Npcs) dyes are versatile planar fluorophoes exhibiting strong fluorescent intensity in the near infrared band and have become commonplace in modern emissive spectroscopy. Pcs and Npcs have been recently attracting enormous popularity for their use in the fabrication of molecular devices such as electrochromic displays [90], light-emitting diodes [91], gas sensors [91-93] and photodynamic therapy agents [94]. While phthalocyanines exhibit the natural tendency to self-aggregate owing to the large aromatic π-system [95, 96] as a result of coplanar Pc ring association, the general spectral characteristics are easily "fine-tuned" by a central metals and peripheral substitution at the rings [92, 97]. Thus, these NIR fluorophores usually prepared as metal-free or metal-complexed conjugates. Generally, the peripheral substituents are used to modulate the hydrophobic character of these compounds making them more or less soluble in polar solvents. Consequently, the octa-substituted Pcs usually exhibit reduced solubility in comparison to the tetra-substituted counterparts. In addition to modifying the solubility and hydrophobic behavior, peripheral substitution to these compounds yields a diverse range of functionalities enabling greater applicability. For example, the electrochemical and spectroelectrochemical behaviours of Copper-Pc complexes have been investigated in relation to the position of tetra-substituted phenylthio groups in the alpha and beta positions [98]. Despite the many achievements made in the use of Pcs and Npcs within the last few decades there is limited literature evidence to show that these dyes are being optimized routine biological applications, let alone enzyme catalysis primarily as substrates.

1.3.5 Rotaxanes

Rotaxanes belong to a unique class of supramolecular fluorescent compounds comprising macrocyclic and dumbbell shaped components[78, 99]. These molecules also consist of a ring and a threadlike component incorporating two recognition sites (stations). Within the last decade there has been tremendous progress in the development of new synthetic pathways of these interlocked molecules. In recent work Michaels *et al.* have proposed the synthesis of novel conjugated poly-rotaxane compounds by an aqueous Suzuki polymerization pathway, using hydrophobic binding to promote threading of cyclodextrin units [100]. In this study new cyclodextrin-encapsulated fluorescent compounds were fabricated with conjugated polymer cores based on poly(*para*-phenylene), polyfluorene and poly(diphenylene-vinylene), threaded through 0.9-1.6 cyclodextrins per repeat units. Besides improved overall quantum efficiency these conjugated fluorescent rotaxanes molecules exhibit enhanced chemical stability attracting widespread interest for opto-electronic applications [100]. Recently, there have been increased interests in insulated π-conjugated systems with high stability, high solubility and improved quantum efficiency due to the isolation of the π- π conjugated systems from the external environment and reduced π- π interactions among the conjugates [2, 3, 9, 13, 64, 101-106].

Among the most notable characteristics of the rotaxanes is their photo switching capability [107-112]. The photo-physical properties of the bi-stable rotaxane molecules are attributed to molecular movements stimulated by external stimuli and are controlled by the two recognition sites as a shuttling process which may alter the ring position [89, 107-109, 113-130]. Most of the rotaxane-based molecular switches reported in literature involve mechanical movement of a “ring” component between the two “thread” components induced by pH [128], electrical potential [115, 131],

chemical interactions [114, 125, 127, 129] or photochemical stimuli [124]. However, new research is focused on developing alternative switching principles such as photo-induced charge transfer interactions of a tetracationic ring with a photoactive electron donor. This subsequently reduces conformational changes to the rotaxane supramolecules and maintain overall molecular structure [89]. This principle of switching involves a rapid photo-induced electron transfer cascade, which last only a few seconds with the rotaxanes being in their tropylium state. It is believed that the irradiation of the arylcycloheptatrienes molecules **2** (λ_{max} = 285 nm) and **4** (λ_{max} = 285 nm) shown in scheme 5, results in a single step photoreaction to form the respective acridinium salts; **3** (λ_{max} = 435 nm) and **5** (λ_{max} = 559 nm). Whereas the conventional chemical or pH triggered shuttling processes often lead to undesired side reactions, photo-switching eliminates the formation of waste products, enabling these bi-stable rotaxanes to serve as archetype molecules for nanoscale photo-electronic systems[119, 126]. Nonetheless, although the use of fluorescence detection in sensors is widely explored, there are still only a few fluorescence triggered rotaxane photo-switches [124, 130] reported in the literature.

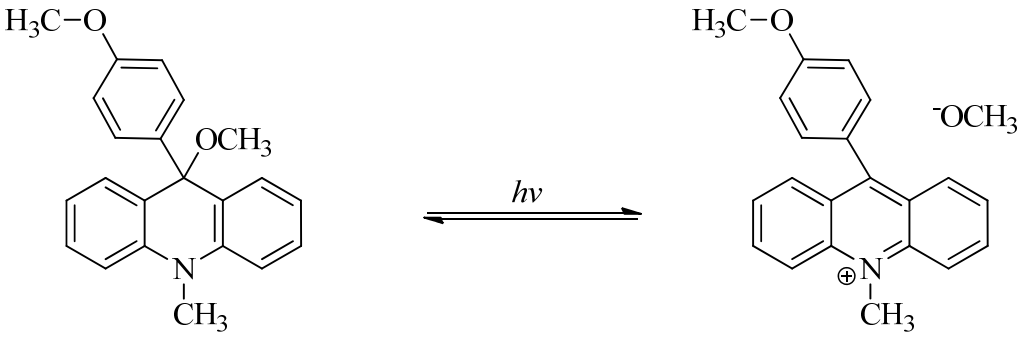

2

λ_{max} 285 nm and 330

3

λ_{max} 543

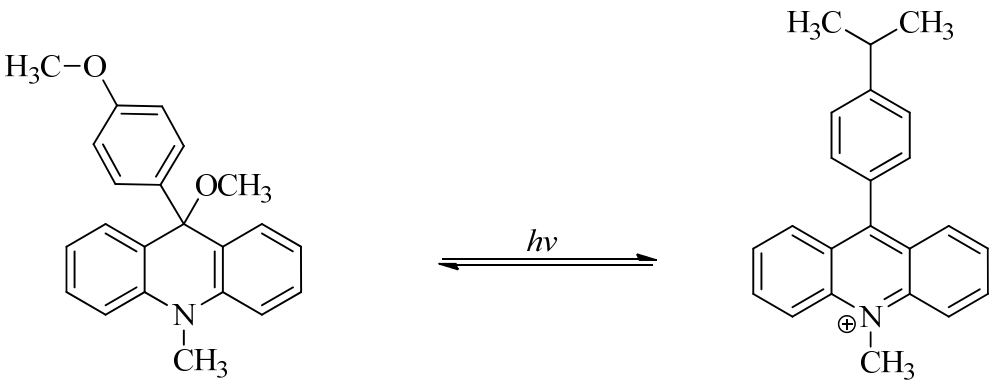

4

λ_{max} 285 nm and 330

5

λ_{max} 559

Scheme 1.5 Two types of photo switches in rotaxanes that were developed by Abraham and co-workers [89, 113].

While we discussed several different classes of dyes, herein we report on the development of this new bioassay primarily with two of the classes; Nile red and trimethine (carbocyanine) derivatives. To develop the technique, the dyes were first evaluated based on four fundamental parameters for their unique spectral characteristics as relates the method development. These parameters include; (1) dyes photostable, (2) solvatochromic properties in varied solvent media, (3) dye binding affinity for the hydrophobic binding domains of the serum albumin along with the active site of the monooxygenase and (4) chemical stability against the silanol coated polyacrylamide capillary and strong electric field strengths during CE separation. Once each dye was successfully screened, the Fischer indolium chromophore bearing the butyl sulfonate group or the most suitable compound was selected for the purpose of further developing the test method. Each of the four test parameter encompasses an array of both chemical and physical dye characterizations protocols.

Like any conventional standardized dye based detection technique, the photostability of the test dyes is of utmost importance. Photostability provide useful information on the repeatability of the test results. Most dye compounds are known to photofade with time and potentially affect the repeatability and precision of the bioassay. Thus it is imperative that the dyes use for this detection technique be photostable and are less susceptible to photofading when exposed to moderate light intensity over a considerable period of time. Any undesirable change in emission of the test dyes could eventually potentially affect the overall detection signal which could result in the loss of the quantitative capabilities of the technique.

As a requirement for the test method, the dyes are designed to exhibit favorable solvatochromism properties in different solvent media. One distinguished feature of this novel bioassay is the fact that the proposed test dyes display specific photophysical properties in the original form but exhibit new photophysical behavior subsequent to enzyme catalysis. In move applicable dye based detection techniques that involve structural modifications, the test dyes are usually emissive pre- and post dye modification. This feature is often times considered less attractive as it could subsequently limit detection at lower concentrations, if the change in emission is not rather excessive. Fortunately, for this new technique, the test dyes are designed in a manner to reduce this pre-post emission limitation. Structural changes to our newly synthesized dyes are expected to result in the virtual loss of emission owing to enzyme catalysis. The importance of this phenomenon is that the dye molecules are rather emissive in one form but are non-emissive in another. This clear contrast in emission signal is paramount is designing this new technique capable of distinguishing and detecting ultra dilute test samples; a key advantage of the technique.

In additional to the advantageous solvatochromism properties of the test dyes, it is expected that changes to the dye structure will also be confirmed by through interaction with various dye binding biomolecules. As determined in our preliminary analyses, trimethine dyes interact differently with complex proteins based on their hydrophobic properties. As the dye molecules are altered at the heterocyclic moiety their binding properties are significantly affected based on the specific molecular structure and electronic environments. Modification to the indolium side chains is also important to dye-biomolecule interaction. For this purpose, we have proposed that varying chromophore and the sulfonated side chains will alter photophysical prop-

erties of the dye compounds and could affect catalysis, thus confirming enzyme activity but more importantly assist in selecting the most suitable structure for method development. As an extension, investigating the changes to hydrophobic nature of the dyes as it relates to their binding tendencies with different biomolecules is important in understanding the complex catalytic activity between the monooxygenase and the fluorescent substrate. Also, because our previous analyses illustrate linear binding relationships between biomolecules and hydrophobic dye ligands, any post catalysis data acquired from these binding studies can serve as a platform for method quantitation. Therefore with these initial dye characterization analyses prior to enzyme catalysis and electrophoretic detection, the best dye suitable class of dye can be determined for further optimization and subsequent method development. These initial analyses provides to the opportunity to choose the most suitable chromophore and assess the necessary dye modification to achieve the best detection of monooxygenase catalysis.

Once the dyes are fully characterized and the most suitable candidate is further optimized, the application of this novel CE enzyme based bioanalytical technique promises superior analytical advantages in comparison to commonly used assays. The technique is proposed to be quick, portable, sensitive, reliable and the exhibit the possibility of ‘on-the-spot’ detection; advantages not readily realized with other commonly applied techniques used to study bacterial sulfur assimilation processes such as PCR, SPR, ELISA and GC. In addition, recent literature results proposed by other research groups developing similar techniques showed strong reliance on GC analyses. Those assays primarily involve the use of straight chain non-emissive alkane sulfonate substituted substrates with less than eight carbons. Once enzyme catalysis occurs and the aldehyde is formed, the product becomes rather volatile and requires complex and tedious

headspace sampling for GC analyses. This feature limits the *in vitro* applicability and eliminated the possibility *in vivo* development. Our goal is to further develop, optimize and present this CZE based bioassay as a suitable alternative to the current trends in the field while creating a more robust and sensitive *in vitro* monooxygenase detection method with the possibilities of *in vivo* application.

1.4 Summary

Traditional fluorescence probes such as the rhodamines and fluoresceins have been around for decades and have been used extensively in various bioanalytical related research. More recently these dyes have become popular in other non-traditional applications like optical recording, fiber optic technology, communication and laser development. Despite the many strides made, there are many challenges in the practical application of fluorescent dyes and dye technology in general. Most commercially available dyes are known to absorb and emit in the visible to ultraviolet band and are also susceptible to strong light scattering tendencies. In addition, despite these compounds typically exhibiting high fluorescence, they are easily photobleached when exposed to strong visible light over extended periods of time. For these reasons recent research trends are more towards developing new fluorescent dyes that are more photo stable and exhibit photo activity higher up in the NIR region of the spectrum. Key among these new compounds are cyanine dyes which are most often times active in the visible to NIR band. Cyanine dyes have become commonplace in numerous forms of bioanalytical applications including DNA sequencing, protein labeling and enzyme catalysis studies. However, like their ultraviolet predecessor, cyanine dyes are known to display low solubility in biologically relevant reagents. Nonetheless, cyanine dyes have proven comparatively superior for their improved

photophysical properties such as high molar absorptivity and high quantum efficiency. Besides, the wide range of options available to the alter the structural design of cyanine dyes to satisfy specific scientific needs have rendered them even more useful as fluorescence probes key in the development of new bioanalytical technique to study new and existing enzyme catalysis mechanisms with strong possibilities for further *in vivo* method development.

1.5 References

1. G. Patonay, G. Beckford, L. Strekowski, M. Henary, J. S. Kim and S. Crow, 2009.
2. G. Patonay, J. S. Kim, R. Kodagahally and L. Strekowski, *Applied Spectroscopy*, 2005, **59**, 682-690.
3. G. Patonay, J. Salon, J. Sowell and L. Strekowski, *Molecules*, 2004, **9**, 40-49.
4. S. K. Patra and M. K. Pai, *European Journal of Biochemistry*, 1997, **246**, 658-664.
5. L. Patrick, *Alternative Medicine Review*, 2006, **11**, 2-22.
6. L. Patrick, *Alternative Medicine Review*, 2006, **11**, 114-127.
7. L. Patsenker, A. Tatarets, O. Kolosovaa, O. Obukhova, Y. Povrozin, I. Fedyunyayeva, I. Yermolenko and E. Terpetschnig, Fluorescence Methods and Applications: Spectroscopy Imaging and Probes: Annals of New York Academy of Science, 2008.
8. R. P. Haugland, Eugene, OR : Molecular Probes, 7th edn., 1999, p. 1 computer optical disc : ill. (some color) ; 4 3/4 in.
9. T. G. G. Vo-Dinh, [Cambridge], 2003.
10. J. R. Lakowicz, *Probe design and chemical sensing*, Plenum Press, New York, 1994.

11. H. Szmacinski, J. R. Lakowicz and M. L. Johnson, in *Numerical Computer Methods, Pt B*, 1994, vol. 240, pp. 723-748.

12. W. Rettig, *Applied fluorescence in chemistry, biology, and medicine*, New York, Berlin, 1999.

13. J. Sowell, J. C. Mason, L. Strekowski and G. Patonay, *Electrophoresis*, 2001, **22**, 2512-2517.

14. A. C. McGinnis, S. Devanathan, G. Patonay and S. A. Crow, *Acs Symposium Series*, 1992, **509**, 229-241.

15. P. K. Bachmann, H. Hummel, T. Justel, J. Merikhi, C. R. Ronda and V. Weiler, *Journal of Nanophotonics*, 2008, **2**.

16. G. Beckford, E. Owens, M. Henary and G. Patonay, *Talanta*, 2012, **92**, 45-52.

17. J. K. Jin, J. Z. Sun, Y. Q. Dong, H. P. Xu, W. Z. Yuan and B. Z. Tang, *Journal of Luminescence*, 2009, **129**, 19-23.

18. Y. Z. Zhang, J. F. Xiang, Y. L. Tang, G. Z. Xu and W. P. Yan, *Dyes and Pigments*, 2008, **76**, 88-93.

19. M. P. Shandura, Y. M. Poronik and Y. P. Kovtun, *Dyes and Pigments*, 2007, **73**, 25-30.

20. S. J. Rembish and M. A. Trush, *Free Radical Biology and Medicine*, 1994, **17**, 117-126.

21. S. J. Rembish, Y. L. Yang and M. A. Trush, *Research Communications in Molecular Pathology and Pharmacology*, 1994, **85**, 115-129.

22. M. Poot, Y. Z. Zhang, J. A. Kramer, K. S. Wells, L. Jones, D. K. Hanzel, A. G. Lugade, V. L. Singer and R. P. Haughland, *Journal of Histochemistry & Cytochemistry*, 1996, **44**, 1363-1372.

23. J. Sakanoue, K. Ichikawa, Y. Nomura and M. Tamura, *Journal of Biochemistry*, 1997, **121**, 29-37.

24. A. J. Pereira, B. Dalby, R. J. Stewart, S. J. Doxsey and L. S. B. Goldstein, *Journal of Cell Biology*, 1997, **136**, 1081-1090.

25. M. A. Trush, L. E. Twerdok, S. J. Rembish, H. Zhu and Y. B. Li, *Environmental Health Perspectives*, 1996, **104**, 1227-1234.

26. H. N. Kim, M. H. Lee, H. J. Kim, J. S. Kim and J. Yoon, *Chemical Society Reviews*, 2008, **37**, 1465-1472.

27. C. Eggeling, J. Widengren, R. Rigler and C. A. M. Seidel, *Analytical Chemistry*, 1998, **70**, 2651-2659.

28. A. Romieu, D. Brossard, M. Hamon, H. Outaabout, C. Portal and P. Y. Renard, *Bioconjugate Chemistry*, 2008, **19**, 279-289.

29. J. Folling, V. Belov, R. Kunetsky, R. Medda, A. Schonle, A. Egner, C. Eggeling, M. Bossi and S. W. Hell, *Angewandte Chemie-International Edition*, 2007, **46**, 6266-6270.

30. L. X. Wu and K. Burgess, *Journal of Organic Chemistry*, 2008, **73**, 8711-8718.

31. I. G. Antropova, A. A. Fenin and A. A. Revina, *High Energy Chemistry*, 2007, **41**, 61-64.

32. N. Bryantseva, I. Sokolova, A. Tsyrenzhapova, N. Selivanov, V. Khilya and Y. Garazd, *Journal of Applied Spectroscopy*, 2008, **75**, 700-705.

33. M. I. Dobrikov, *Uspekhi Khimii*, 1999, **68**, 1062-1079.

34. V. Stanjek, J. Piel and W. Boland, *Phytochemistry*, 1999, **50**, 1141-1145.

35. L. Bissonnette, J. T. Arnason and M. L. Smith, *Phytochemical Analysis*, 2008, **19**, 342-347.

36. M. L. Smith, P. Gregory, N. F. A. Bafi-Yeboa and J. T. Arnason, *Photochemistry and Photobiology*, 2004, **79**, 506-509.

37. A. Grofcsik, M. Kubinyi, A. Ruzsinszky, T. Veszpremi and W. J. Jones, *Journal of Molecular Structure*, 2000, **555**, 15-19.

38. K. Milanchian, H. Tajalli, A. G. Gilani and M. S. Zakerhamidi, *Optical Materials*, 2009, **32**, 12-17.

39. R. J. Nieckarz, J. Oomens, G. Berden, P. Sagulenko and R. Zenobi, *Physical Chemistry Chemical Physics*, 2013, **15**, 5049-5056.

40. Y. Prostota, J. Berthet, S. Delbaere and P. J. Coelho, *Dyes and Pigments*, 2013, **96**, 569-573.

41. T. Naqvi, K. K. Kapoor and R. L. Sharma, *Indian Journal of Chemistry Section B-Organic Chemistry Including Medicinal Chemistry*, 2010, **49**, 1282-1289.

42. M. Tomasulo, S. Sortino and F. M. Raymo, *Journal of Photochemistry and Photobiology a-Chemistry*, 2008, **200**, 44-49.

43. S. D. Fowler and P. Greenspan, *Journal of Histochemistry and Cytochemistry*, 1985, **33**, 833-836.

44. P. Greenspan and S. D. Fowler, *Journal of Lipid Research*, 1985, **26**, 781-789.

45. P. Greenspan, E. P. Mayer and S. D. Fowler, *Journal of Cell Biology*, 1985, **100**, 965-974.

46. S. Martin and R. G. Parton, *Nature Reviews Molecular Cell Biology*, 2006, **7**, 373-378.

47. R. R. Gupta, *Springer*, 2008, **14**, 248.

48. V. K. Gupta and L. R. Gowda, *Journal of Molecular Structure*, 2008, **891**, 456-462.

49. L. Strekowski, *Heterocyclic polymethine dyes : synthesis, properties and applications*, Springer, Berlin, 2008.

50. L. Strekowski and B. Wilson, *Mutation Research-Fundamental and Molecular Mechanisms of Mutagenesis*, 2007, **623**, 3-13.

51. Y. Xuan, G. Qian, Z. Y. Wang and D. G. Ma, *Thin Solid Films*, 2008, **516**, 7891-7893.

52. C. Encinas, S. Miltsov, E. Otazo, L. Rivera, M. Puyol and J. Alonso, *Dyes and Pigments*, 2006, **71**, 28-36.

53. M. Puyol, C. Encinas, L. Rivera, S. Mijtsov and J. Alonso, *Dyes and Pigments*, 2007, **73**, 383-389.

54. M. Puyol, C. Encinas, L. Rivera, S. Miltsov and J. Alonso, *Sensors and Actuators B-Chemical*, 2007, **122**, 53-59.

55. Y. F. Xu, Y. Liu and X. H. Qian, *Journal of Photochemistry and Photobiology a-Chemistry*, 2007, **190**, 1-8.

56. S. D. Xun, G. LeClair, J. D. Zhang, X. Chen, J. P. Gao and Z. Y. Wang, *Organic Letters*, 2006, **8**, 1697-1700.

57. Y. Q. Xu, Z. Y. Li, A. Malkovskiy, S. G. Sun and Y. Pang, *Journal of Physical Chemistry B*, **114**, 8574-8580.

58. S. J. Xu, Y. Luo, R. Graeser, A. Warnecke, F. Kratz, P. Hauff, K. Licha and R. Haag, *Bioorganic & Medicinal Chemistry Letters*, 2009, **19**, 1030-1034.

59. X. H. Zhang, Y. S. Yao, C. Li, W. B. Wang, X. X. Cheng, X. S. Wang and B. W. Zhang, *Chinese Journal of Chemistry*, 2008, **26**, 929-934.

60. Y. Z. Zhang, Q. F. Yang, H. Y. Du, Y. L. Tang, G. Z. Xu and W. P. Yan, *Chinese Journal of Chemistry*, 2008, **26**, 397-401.

61. C. Malins, M. Landl, P. Simon and B. D. MacCraith, *Sensors and Actuators B-Chemical*, 1998, **51**, 359-367.

62. E. Scorsone, S. Christie, K. C. Persaud, P. Simon and F. Kvasnik, *Sensors and Actuators B-Chemical*, 2003, 37-45.

63. P. Simon, M. Landl, M. Breza and F. Kvasnik, Sensors and Actuators B-chemical, 2003.

64. L. Tarazi, N. Narayanan, J. Sowell, G. Patonay and L. Strekowski, *Spectrochimica Acta Part a-Molecular and Biomolecular Spectroscopy*, 2002, **58**, 257-264.

65. P. A. S. Jorge, P. Caldas, J. Da Silva, C. C. Rosa, A. G. Oliva, J. L. Santos and F. Farahi, *Fiber and Integrated Optics*, 2005, **24**, 201-225.

66. M. Benounis, T. Aka-Ngnui, N. Jaffrezic and J. P. Dutasta, *Sensors and Actuators a-Physical*, 2008, **141**, 76-83.

67. M. Benounis, N. Jaffrezic-Renault, J. P. Dutasta, K. Cherif and A. Abdelghani, 2005.

68. J. Klohs, A. Wunder and K. Licha, *Basic Research in Cardiology*, 2008, **103**, 144-151.

69. C. Li, T. R. Greenwood, Z. M. Bhujwalla and K. Glunde, *Organic Letters*, 2006, **8**, 3623-3626.

70. K. Glunde, C. A. Foss, T. Takagi, F. Wildes and Z. M. Bhujwalla, *Bioconjugate Chemistry*, 2005, **16**, 843-851.

71. Y. Hama, Y. Urano, Y. Koyama, M. Bernardo, P. L. Choyke and H. Kobayashi, *Bioconjugate Chemistry*, 2006, **17**, 1426-1431.

72. Y. Hama, Y. Urano, Y. Koyama, M. Kamiya, M. Bernardo, R. S. Paik, I. S. Shin, C. H. Paik, P. L. Choyke and H. Kobayashi, *Cancer Research*, 2007, **67**, 2791-2799.

73. E. Aikawa, M. Nahrendorf, D. Sosnovik, V. M. Lok, F. A. Jaffer, M. Aikawa and R. Weissleder, *Circulation*, 2007, **115**, 377-386.

74. E. G. Matveeva, E. A. Terpetschnig, M. Stevens, L. Patsenker, O. S. Kolosova, Z. Gryczynski and I. Gryczynski, *Dyes and Pigments*, 2009, **80**, 41-46.

75. M. Z. Wang, H. Xie, J. Q. Zhu, M. G. Xie, T. K. Li and Y. Li, *Journal of Materials Science*, 2007, **42**, 7678-7683.

76. J. V. Ros-Lis, B. Garcia, D. Jimenez, R. Martinez-Manez, F. Sancenon, J. Soto, F. Gonzalvo and M. C. Valldecabres, *Journal of the American Chemical Society*, 2004, **126**, 4064-4065.

77. M. Xue and C. F. Chen, *Chemical Communications*, 2008, 6128-6130.

78. J. J. Gassensmith, L. Barr, J. M. Baumes, A. Paek, A. Nguyen and B. D. Smith, *Organic Letters*, 2008, **10**, 3343-3346.

79. S. Sreejith, K. P. Divya and A. Ajayaghosh, *Angewandte Chemie-International Edition*, 2008, **47**, 7883-7887.

80. D. G. Devi, T. R. Cibin, D. Ramaiah and A. Abraham, *Journal of Photochemistry and Photobiology B-Biology*, 2008, **92**, 153-159.

81. P. Ravirajan, S. A. Haque, J. R. Durrant, D. D. C. Bradley and J. Nelson, *Advanced Functional Materials*, 2005, **15**, 609-618.

82. E. Arunkumar, C. C. Forbes and B. D. Smith, *European Journal of Organic Chemistry*, 2005, 4051-4059.

83. K. D. Volkova, V. B. Kovalska, M. Y. Losytskyy, A. Bento, L. V. Reis, P. F. Santos, P. Almeida and S. M. Yarmoluk, *Journal of Fluorescence*, 2008, **18**, 877-882.

84. K. D. Volkova, V. B. Kovalska, G. M. Segers-Nolten, G. Veldhuis, V. Subramaniam and S. M. Yarmoluk, *Biotechnic & Histochemistry*, 2009, **84**, 55-61.

85. B. Oswald, F. Lehmann, L. Simon, E. Terpetschnig and O. S. Wolfbeis, *Analytical Biochemistry*, 2000, **280**, 272-277.

86. A. L. Tatarets, I. A. Fedyunyaeva, E. Terpetschnig and L. D. Patsenker, *Dyes and Pigments*, 2005, **64**, 125-134.

87. E. Terpetschnig, H. Szmacinski, A. Ozinskas and J. R. Lakowicz, *Analytical Biochemistry*, 1994, **217**, 197-204.

88. A. L. Tatarets, I. A. Fedyunyayeva, T. S. Dyubko, Y. A. Povrozin, A. O. Doroshenko, E. A. Temetschnig and L. D. Patsenker, *Analytica Chimica Acta*, 2006, **570**, 214-223.

89. W. Abraham, K. Buck, M. Orda-Zgadzaj, S. Schmidt-Schaffer and U. W. Grummt, *Chemical Communications*, 2007, 3094-3096.

90. M. Juricek, P. H. J. Kouwer, J. Rehak, J. Sly and A. E. Rowan, *Journal of Organic Chemistry*, 2009, **74**, 21-25.

91. R. Wang, W. Liu, Y. Chen, J. L. Zuo and X. Z. You, *Dyes and Pigments*, 2009, **81**, 40-44.

92. T. V. Basova, I. V. Jushina, A. G. Gurek, D. Atilla and V. Ahsen, *Dyes and Pigments*, 2009, **80**, 67-72.

93. F. Hacivelioglu, M. Durmus, S. Yesilot, A. G. Gurek, A. Kilic and V. Ahsen, *Dyes and Pigments*, 2008, **79**, 14-23.

94. Y. Y. Hu, G. Q. Lai, Y. J. Shen and Y. F. Li, *Dyes and Pigments*, 2005, **66**, 49-53.

95. S. Bayar, H. A. Dincer and E. Gonca, *Dyes and Pigments*, 2009, **80**, 156-162.

96. A. G. Martynov, O. V. Zubareva, Y. G. Gorbunova, S. G. Sakharov and A. Y. Tsivadze, *Inorganica Chimica Acta*, 2009, **362**, 11-18.

97. P. Zimcik, M. Miletin, V. Novakova, K. Kopecky and Z. Dvorakova, *Dyes and Pigments*, 2009, **81**, 35-39.

98. M. Villano, V. Amendola, G. Sandona, M. P. Donzello, C. Ercolani and M. Meneghetti, *Journal of Physical Chemistry B*, 2006, **110**, 24354-24360.

99. A. Farcas, N. Jarroux, P. Guegan, A. Fifere, M. Pinteala and V. Harabagiu, *Journal of Applied Polymer Science*, 2008, **110**, 2384-2392.

100. J. J. Michels, M. J. O'Connell, P. N. Taylor, J. S. Wilson, F. Cacialli and H. L. Anderson, *Chemistry-a European Journal*, 2003, **9**, 6167-6176.

101. F. Meadows, N. Narayanan and G. Patonay, *Talanta*, 2000, **50**, 1149-1155.

102. L. Tarazi, N. Narayanan and G. Patonay, *Microchemical Journal*, 2000, **64**, 247-256.

103. J. Sowell, K. A. Agnew-Heard, J. C. Mason, C. Mama, L. Strekowski and G. Patonay, *Journal of Chromatography B*, 2001, **755**, 91-99.

104. L. Tarazi, H. Choi, J. C. Mason, J. Sowell, L. Strekowski and G. Patonay, *Microchemical Journal*, 2002, **72**, 55-62.

105. C. M. Yang, O. Shimelis, X. J. Zhou, G. D. Li, C. Bayle, M. Nertz, H. Lee, L. Strekowski, G. Patonay, F. Couderc and R. W. Giese, Conference Proceedings, 2002.

106. Y. C. B.A.Armitage, M.P. Dobhal , M.Henary, N. James,B. J edrzejewska, J.Kabatc, J. Kim, M.Mojzych, H. Nakazumi, B. Jedrzejewska, J.Kabatc, J. Kim, M.Mojzych, H. Nakazumi J. Paczkowski, R.K. Pandey, G. Patonay, V.Z. Shirinian, A. A. Shimkin, V. F, Traven, A.Watson, S. Yagi., 2008, **14**.

107. Z. Francesco, M. Fanti, D. A. Leigh, S. W. Zhang and M. Asakawa, *Abstracts of Papers of the American Chemical Society*, 1999, **218**, 337-PHYS.

108. M. Asakawa, G. Brancato, M. Fanti, D. A. Leigh, T. Shimizu, A. M. Z. Slawin, J. K. Y. Wong, F. Zerbetto and S. W. Zhang, *Journal of the American Chemical Society*, 2002, **124**, 2939-2950.

109. V. Bermudez, P. A. Chollet, F. Kajzar, A. Lorin, G. Bottari, F. G. Gatti and D. A. Leigh, 2002.

110. V. Bermudez, T. Gase, F. Kajzar, N. Capron, F. Zerbetto, F. G. Gatti, D. A. Leigh and S. Zhang, 2003.

111. J. W. Choi, A. H. Flood, D. W. Steuerman, S. Nygaard, A. B. Braunschweig, N. N. P. Moonen, B. W. Laursen, Y. Luo, E. DeIonno, A. J. Peters, J. O. Jeppesen, K. Xu, J. F. Stoddart and J. R. Heath, *Chemistry-a European Journal*, 2006, **12**, 261-279.

112. C. Yang, Y. H. Ko, N. Selvapalam, Y. Origane, T. Mori, T. Wada, K. Kim and Y. Inoue, *Organic Letters*, 2007, **9**, 4789-4792.

113. W. Abraham, A. Wlosnewski, K. Buck and S. Jacob, *Organic & Biomolecular Chemistry*, 2009, **7**, 142-154.

114. S. Altobello, K. Nikitin, J. K. Stolarczyk, E. Lestini and D. Fitzmaurice, *Chemistry-a European Journal*, 2008, **14**, 1107-1116.

115. V. Bermudez, T. Gase, F. Kajzar, N. Capron, F. Zerbetto, F. G. Gatti, D. A. Leigh and S. Zhang, *Optical Materials*, 2003, **21**, 39-44.

116. A. B. Braunschweig, B. H. Northrop and J. F. Stoddart, *Journal of Materials Chemistry*, 2006, **16**, 32-44.

117. A. M. Brouwer, S. M. Fazio, C. Frochot, F. G. Gatti, D. A. Leigh, J. K. Y. Wong and G. W. H. Wurpel, 2003.

118. A. M. Brouwer, C. Frochot, F. G. Gatti, D. A. Leigh, L. Mottier, F. Paolucci, S. Roffia and G. W. H. Wurpel, *Science*, 2001, **291**, 2124-2128.

119. C. P. Collier, G. Mattersteig, E. W. Wong, Y. Luo, K. Beverly, J. Sampaio, F. M. Raymo, J. F. Stoddart and J. R. Heath, *Science*, 2000, **289**, 1172-1175.

120. E. DeIonno, H. R. Tseng, D. D. Harvey, J. F. Stoddart and J. R. Heath, *Journal of Physical Chemistry B*, 2006, **110**, 7609-7612.

121. F. G. Gatti, S. Lent, J. K. Y. Wong, G. Bottari, A. Altieri, M. A. F. Morales, S. J. Teat, C. Frochot, D. A. Leigh, A. M. Brouwer and F. Zerbetto, *Proceedings of the National Academy of Sciences of the United States of America*, 2003, **100**, 10-14.

122. P. Hirva, M. Haukka and T. A. Pakkanen, *Journal of Molecular Modeling*, 2008, **14**, 879-886.

123. D. C. Jagesar, F. Hartl, W. J. Buma and A. M. Brouwer, *Chemistry-a European Journal*, 2008, **14**, 1935-1946.

124. S. I. Jun, J. W. Lee, S. Sakamoto, K. Yamaguchi and K. Kim, *Tetrahedron Letters*, 2000, **41**, 471-475.

125. K. Nikitin, E. Lestini, J. K. Stolarczyk, H. Muller-Bunz and D. Fitzmaurice, *Chemistry-a European Journal*, 2008, **14**, 1117-1128.

126. S. Schmidt-Schaffer, L. Grubert, U. W. Grummt, K. Buck and W. Abraham, *European Journal of Organic Chemistry*, 2006, 378-398.

127. A. Trabolsi, M. Hmadeh, N. M. Khashab, D. C. Friedman, M. E. Belowich, N. Humbert, M. Elhabiri, H. A. Khatib, A. M. Albrecht-Gary and J. F. Stoddart, *New Journal of Chemistry*, 2009, **33**, 254-263.

128. D. Tuncel and M. Katterle, *Chemistry-a European Journal*, 2008, **14**, 4110-4116.

129. Y. L. Zhao, W. R. Dichtel, A. Trabolsi, S. Saha, I. Aprahamian and J. F. Stoddart, *Journal of the American Chemical Society*, 2008, **130**, 11294-11296.

130. W. D. Zhou, J. B. Li, X. R. He, C. H. Li, J. Lv, Y. L. Li, S. Wang, H. B. Liu and D. B. Zhu, *Chemistry-a European Journal*, 2008, **14**, 754-763.

131. V. Bermudez, N. Capron, T. Gase, F. G. Gatti, F. Kajzar, D. A. Leigh, F. Zerbetto and S. W. Zhang, *Nature*, 2000, **406**, 608-611.

2 PHOTOPHYSICAL CHARACTERIZATION OF THE FLUORECENT DYES FOR BIOANALYTICAL APPLICATION

2.1 Introduction

Some of the Vis-NIR dyes compounds used for bioanalytical applications are typically classified by their chromophoric moieties and most often cyanine families of dyes. For example, commonly applied dyes include categories such as, oxonol, merocyanine, and so forth. They are also named by the heterocyclic moiety at the end of the polymethine chains, whereby the polymethine chain itself can be further classified by the number of methine; mono-, tri-, penta-, heptamethine, etc. The two heteroaromatic ring systems linked to the polyene consist of imidazole, pyridine, pyrrole, quinoline, thiazole, etc. of the various probes. Because of the abundance of tryptophan, phenylalanine and tyrosine amino acids in naturally occurring biomolecules (with exception for the non-proteinated sugars), the strong auto-fluorescence in the ultraviolet band associated with tissue specimens is rather problematic in spectroscopic analyses. For this reason, the use of the Vis-NIR region separates the overlapping of the spectrum between a dye and a target biomolecule. Furthermore, one strong advantage of the Vis-NIR dyes is that during synthesis, unreacted starting materials of dyes, which commonly show spectra in UV region, can be excluded the spectra from NIR region due to the spectral separation. In addition, when separating conjugates using techniques such as capillary electrophoresis and chromatography or other methods with a single wavelength, the detection signal only respond to free Vis-NIR dyes and/or labeled NIR dyes. Furthermore, only a few biomolecules at long wavelengths undergo vibronic electronic transitions with subsequent strong Raman scattering, thus enabling improved signal-to-noise ratio. Finally, the availability and use of compact and cheap GaAlAs laser diodes with high power output and long lifetime (≥100,000 hrs.) make Vis-NIR biomolecular labeling even more attractive[1, 2].

Recently, other research groups have investigated the use of Vis-NIR dye for protein analysis. Colyer *et al*. reported non-covalent labeling scheme by using capillary Zone electrophoresis with laser-induced fluorescence detection (LIF-CZE). Symmetric (NN127), asymmetric (SQ-3) dyes and Indocyanine Green (ICG) (the only NIR dye approved by the FDA for biological applications), are often time used for protein analyses and studying key biological processes. These dyes typically exhibit poor photophysical properties (notably absorbance and emission) in aqueous solution but may or may not show improved spectral behavior upon binding to biomolecules. Thus it is imperative that these dyes be characterized for their light stability, solvatochromic properties and linear behavior when dissolved in different solvents. Previous studies of trimethine (carbocyanine) dyes demonstrated that there are strong correlations between; the chromophore moiety, *N*-indolium sidechain as well as polymethine linker of these probes and their bioanalytical usefulness. Also, our earlier studies of these dyes revealed that the structural properties of Oxazine dyes (Nile Red derivatives) is rather important in studying their application as biological probes[3,4]. Those compounds possessing highly functionalized sidechains can be incorporated in elucidating the structural dependence of small molecules and biomolecules such as proteins. However, due to their poor photostability they were considered less favorable for optimization in developing the CZE based bioassay. Nonetheless, the more photostable Fischer based dyes were determined to be more ideal.

Even though the previous studies revealed that the cyanine dyes are more promising as analytical tools in studying the enzyme catalysis reaction, the complete evaluation of these dyes along with the Nile Red derivative will be beneficial for understanding the dye-protein interaction for developing new bioanalytical protocols.

2.2 Dye synthesis

Symmetrical carbocyanine dyes were synthesized by linking two similar nitrogen-containing heterocycles by a three-carbon methine bridge. The common synthetic pathway involved quaternization of the nitrogen atom and base-catalyzed condensation of two salts using triethyl orthoformate. Detailed chemical synthesis of these dyes will be described elsewhere (Henary et al., manuscript in preparation). These compounds are designed to display unique photo physical characteristics that directly relate to the heterocyclic structure and N-substituted moieties. We described the analyses of three classes of symmetrical carbocyanines containing the benz[*c,d*]indole, benz[*e*]indole, and Fischer indole structures, shown in figure 2.1. These carbocyanine dyes possessed substituents displaying a varied degree of hydrophobicity to study their effects at the hydrophobic binding pockets of serum albumin.

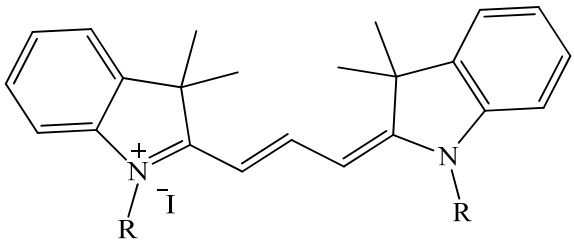

E-14: R = -CH_2CH_3
E-06: R = -$CH_2(CH_2)_2CH_3$
E-04: R = -$CH_2(CH_2)_2Ph$

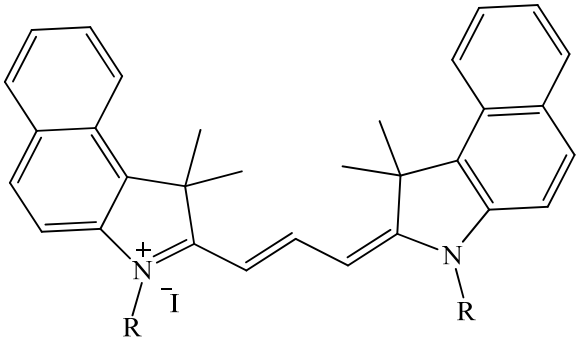

E-05: R = -CH_2CH_3
E-18: R = -$CH_2(CH_2)_2CH_3$
E-08: R = -$CH_2(CH_2)_2Ph$

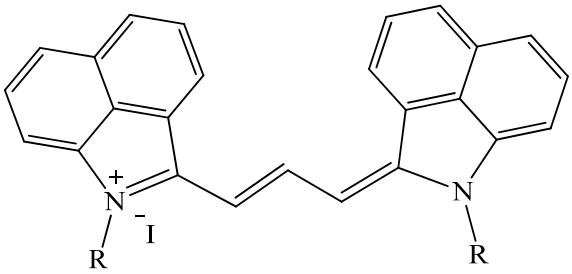

MHI-21: R = -CH_2CH_3
MHI-06: R = -$CH_2(CH_2)_2CH_3$
MHI-36: R = -$CH_2(CH_2)_2Ph$

Figure 2.1 Molecular structure of Indolium cyanine dyes studied, *I;* Fischer indole, *II*; benz[*e*]indole, and *III*; benz[*c,d*]indole structures. These Dye were designed and synthesized by the Henary Research Group, GSU.

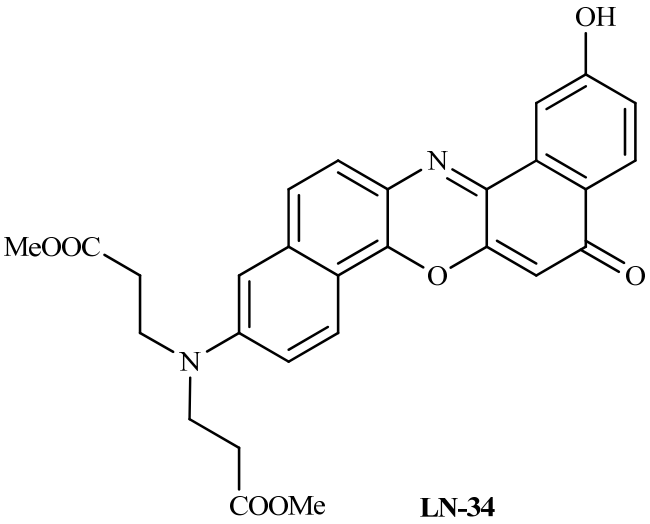

LN-34

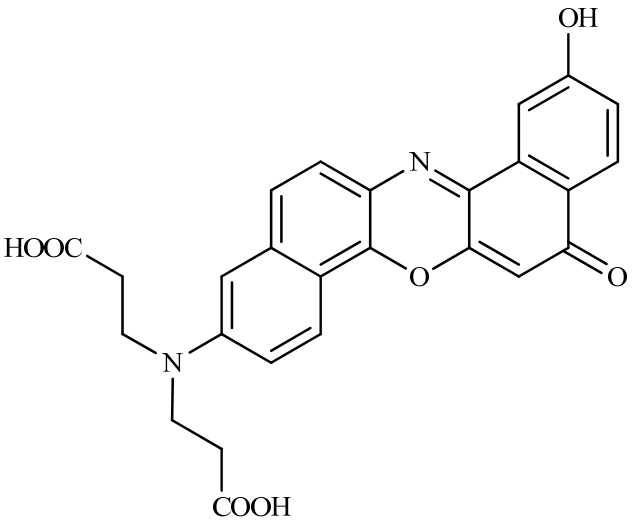

LN-36

Figure 2.2 Molecular structure of Nile red derivatives tested for potential suitability as photo-sensitive enzyme substrates.

2.3 Photophysical characterization of dyes absorbance spectroscopy

2.3.1 Instrumentation

Absorption measurements were performed with a Perkin-Elmer Lambda 20 UV/VIS-NIR (Lambda 50) Spectrophotometer (Norwalk, CT). All measurements were performed in 1 cm two-sided quartz cuvettes (VWR, Suwanee, GA, USA). The appropriate mass of sll dye samples were initially dissolved in methanol to a final concentration of 1.0×10^{-3} Molar, sonicated while being ice cooled at 20 ^{0}C for 30 min. and then stored in the dark at 4 ^{0}C until further diluted and used.

2.3.2 Solution preparation and analyses

2.3.2.1 Molar Absorptivity determination

For the molar absorptivity studies, the trimethine cyanine and Nile Red dyes were prepared by diluting the 1.0×10^{-3} M stock solutions in methanol to the desired concentrations. Series dilutions of 1.0×10^{-6} to 10.0×10^{-6} M in 1.0×10^{-6} M increments were prepared and scanned from 1100 t0 400 nm in two-sided quartz cuvettes. The absorbance values were determined and plotted against concentration for molar absorptivity determinations.

2.3.2.2 Solvatochromic (hydrophobicity) Studies

Phosphate buffer (10.0×10^{-3} M, pH 7.4) was prepared from sodium phosphate monobasic (monohydrate) and sodium phosphate dibasic (monohydrate) obtained from Fisher Scientific (Fair Lawn, NJ) to a final pH of 7.4. The water used was nanopure (Bernard Model D4751 ultrapure water system). HPLC grade methanol was obtained from the Aldrich Chemical Company

(Milwaukee, WI). At constant dye concentration of 10.0×10^{-5} M, the absorbance values in determined hydrophobic characteristics of the dyes were evaluated by acquiring absorbance spectra of the dyes in varying ratios of methanol-phosphate buffer (10.0×10^{-3} M, pH 7.4) mixture (in the range of 1 to 100% phosphate buffer/ methanol) until there was no further discernible spectral changes, at which point the spectra overlapped as percent methanol increased, as shown in figures 2.8 to 2.10. This was then repeated for other less polar solvents as demonstrated in table.

2.4 Photophysical characterization of dyes by Fluorescence Spectroscopy

2.4.1 Instrumentation

Laser Induced Fluorescence (LIF) emission spectra were acquired using a K2 Spectrofluorometer (ISS, Champaign, IL) equipped with a R298 Hamamatsu Photomultiplier Tube (Bridgewater, NJ). Excitation was achieved with GaAlAs laser diodes (Laser Max, Rochester, NY) at 690 nm. Slit widths were set to 2 mm and integration time of 3 s.

2.5 Photostability Studies

The photo (light) stability of Ficsher based trimethine dyes and Nile Red derivatives is a rather complex phenomenon which often times results in poor stability, photobleaching (fading) or photoisomerization of the fluorophores. While numerous NIR fluorescent dyes undergo chemical photobleacing, light induced photofading [5-14] is usually considerably more consequential and play a greater role in determining the bioanalytical potential of the dye.

In the possible mechanisms of the photofading process three main modes, *via*, radical, reductive and oxidative, need to be considered. This process however, often follows mixed mechanism pathways. As Egerton and Morgan reported[5, 8, 10, 14], the presence of moisture can plays an important role in this process, usually increasing the rate of photofading [15-17]. In addition the stability of fluorophores is can be further affected by the nature of the surrounding media, e.g. presence of oxygen, the humidity which can often accentuate fading and degradation reactions, the type of light source and the temperature of the irradiation conditions. Many bioanalytical applications of fluorescent dyes are thus hindered by such problems despite tremendous efforts to develop new additives that are useful and photo-stabilizing agents. Also, Intermolecular H-bonds bring about aggregation of the dye molecules, thus improving the light stability[5-14]. To the contrary, the presence of too many electron withdrawing substituents in the dye molecule can significantly lower the light stability through intra-molecular dye quenching. Having developed dyes that are rather photostable and resist the tendencies to photofade under normal test conditions would fulfill one fundamental requirement of any fluorescent compounds created for the purpose designing new bioanalytical techniques. Besides, considering that these compounds will be illuminated for detection, further illustrate the need for high photostability.

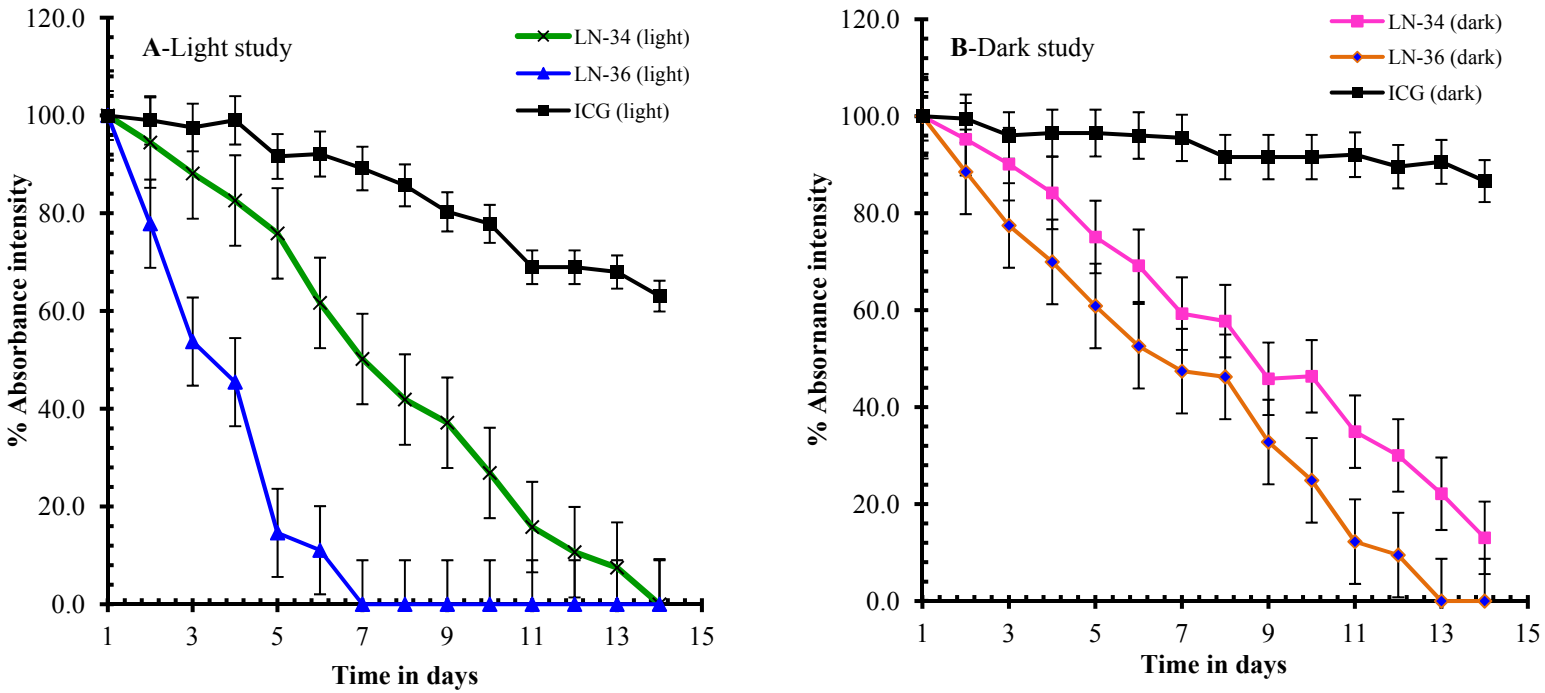

Figure 2.3 Photostability plots of oxazine (Nile Red) dyes. A; One set of 1.0×10^{-6} M dye solution was irradiated with a 250W Sylvania/Osram Vis-NIR lamp over 14 days period with constant cooling at 25 ^{0}C. B; Another set of 1.0×10^{-6} M dye solution was kept in a dark room for the same period. Absorbance values were taken daily. Lamp was kept 24 inches away from sample as to prevent any localized heating within the testing area that could result in dye degradation or solvent evaporation.

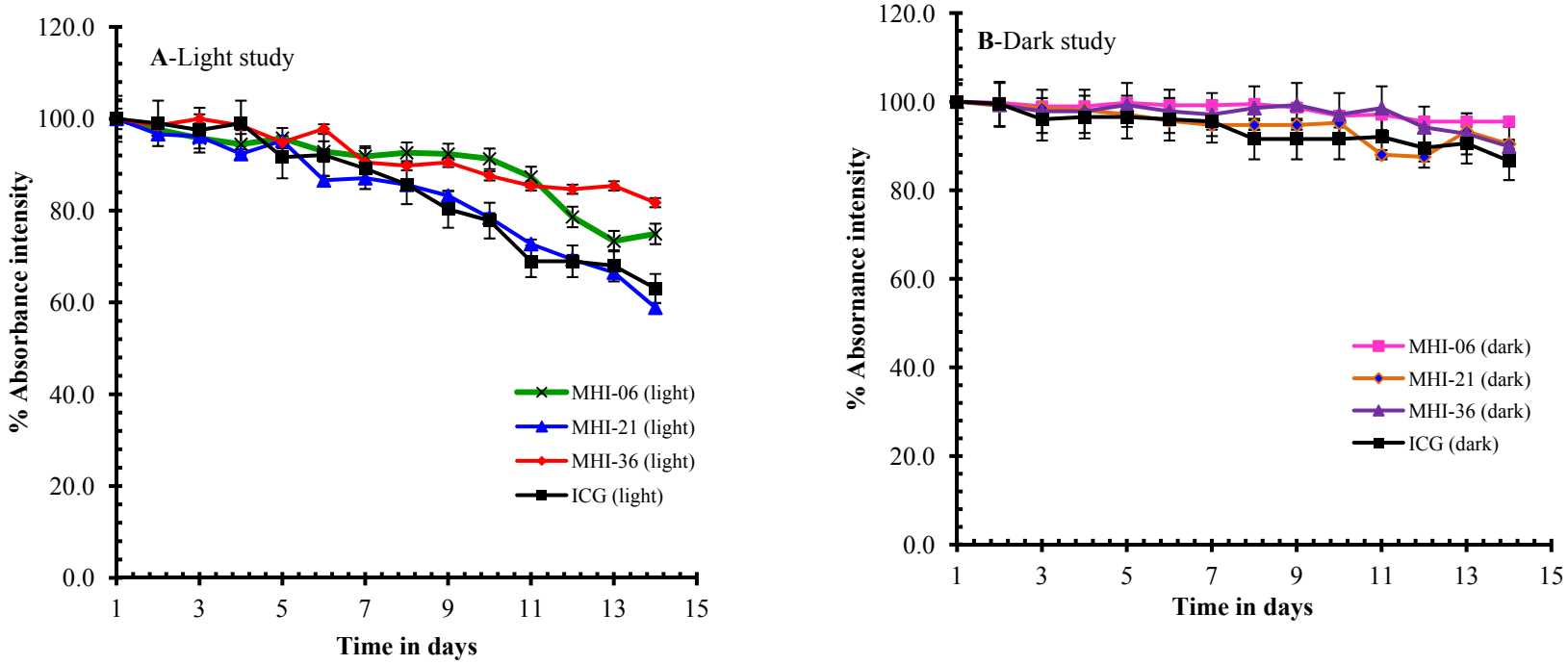

Figure 2.4 Photostability plots of Benz*[c,d]*indolium dyes (class *III*). A; One set of 1.0 × 10^{-6} M dye solution was irradiated with a 250W Sylvania/Osram Vis-NIR lamp over 14 days period with constant cooling at 25 ^{0}C. B; Another set of 1.0 × 10^{-6} M dye solution was kept in a dark room for the same period. Absorbance values were taken daily. Lamp was kept 24 inches away from sample as to prevent any localized heating within the testing area that could result in dye degradation or solvent evaporation.

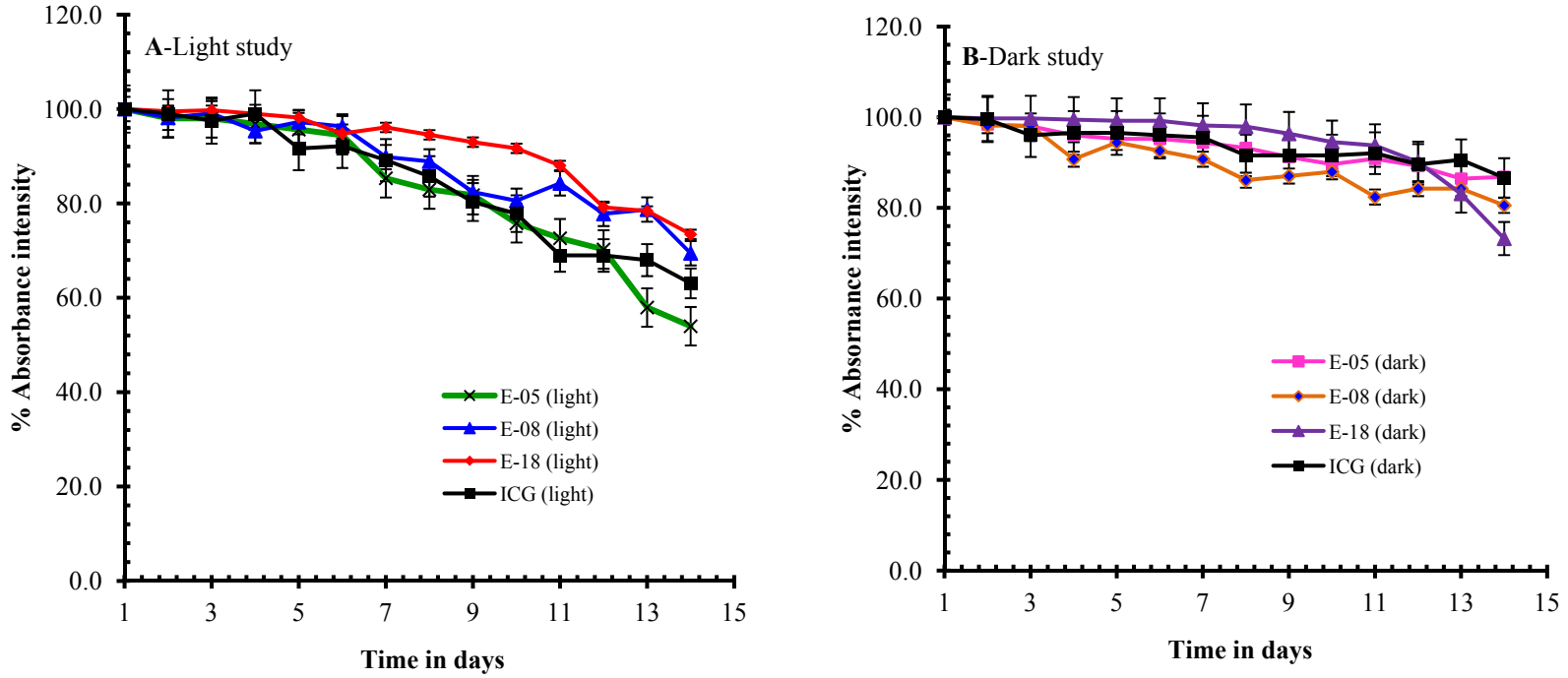

Figure 2.5 Photostability plots of Benz*[e]*indolium dyes (class *II*). A; One set of 1.0 × 10^{-6} M dye solution was irradiated with a 250W Sylvania/Osram Vis-NIR lamp over 14 days period with constant cooling at 25 ^{0}C. B; Another set of 1.0 × 10^{-6} M dye solution was kept in a dark room for the same period. Absorbance values were taken daily. Lamp was kept 24 inches away from sample as to prevent any localized heating within the testing area that could result in dye degradation or solvent evaporation.

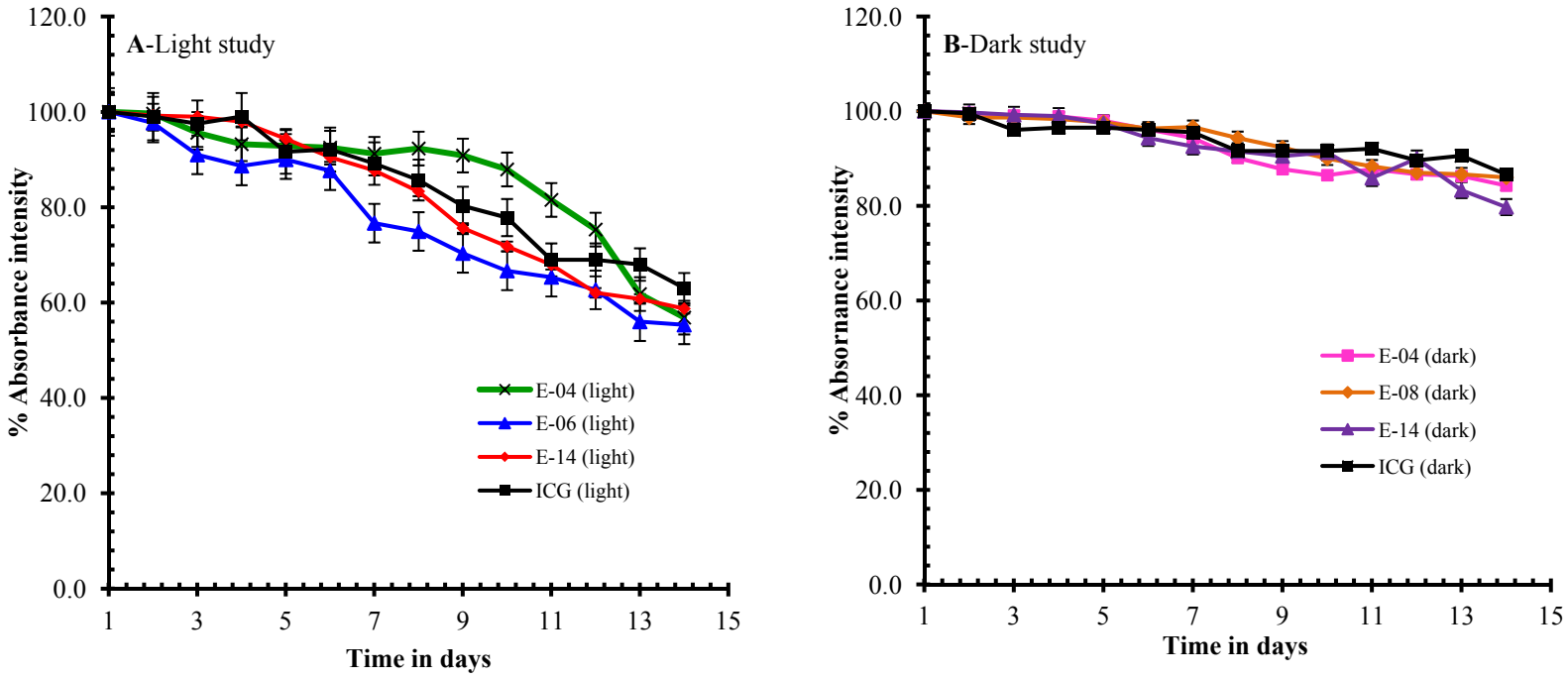

Figure 2.6 Photostability plots of Fischer indolium dyes (class *I*). A; One set of 1.0×10^{-6} M dye solution was irradiated with a 250W Sylvania/Osram Vis-NIR lamp over 14 days period with constant cooling at 25 ^{0}C. B; Another set of 1.0×10^{-6} M dye solution was kept in a dark room for the same period. Absorbance values were taken daily. Lamp was kept 24 inches away from sample as to prevent any localized heating within the testing area that could result in dye degradation or solvent evaporation.

Results obtained from studying the dyes in both light and dark revealed that the cyanine dyes are much more photo stable than the oxazine (Nile Red) derivatives. The oxazines were rather very unstable whereby **LN-34** completely photo-bleached after only 14 days of exposure to the light source compared to the ICG standard that maintained 63.1% of the absorptivity over the same period. In the dark the Nile Red dye did not behave much different and only maintained 13.0% at the end of the 14 days test period. **LN-36** was however quite different and was photo-bleached only after 7 and 13 days in the light and dark respectively. Having seen this poor stability of the oxazine derivatives it is inferred that these dyes are not very photo stable and are thus less suitable for further bioanalytical testing with the hope to develop new bioanalytical assays. While the two molecules are similar in structure, the presence of the strong electron withdrawing groups on **LN-34** and the strong electron releasing moieties associated with **LN-36** could explain the difference in photo stability. This suggests that the ionizing carboxylate groups make **LN-36** extremely less photo stable and thus less favorable as a contrasting agent or for this bioanalytical utility.

Unlike the Nile Red dyes, the Fischer based dyes were much more photo-stable throughout the test period. In comparison, these dyes behave similar to the ICG standard and exhibit less that 30% absorbance loss after 14 days when irradiated with the light source. Among the ones exposed to the light, the phenylpropyl (**MHI-36**) Benz*[c,d]*indolium was most stable and the ethyl (**MHI-21)** the least. For the Benz*[e]*indolium the butyl (**E-18)** was most photo stable and the ethyl (**E-05**) the least. However, Fischer indolium dyes, ethyl (**E-04)** was just as stable and the phenyl propyl (**E-14)** but less photo stable than the butyl derivative (**E-06**). This results suggests that the incorporation of the longer indolium chain to the heterocycle improves photo

stability of the Fischer based dyes, shown in figure 2.3 to 2.5. After 14 days of testing, all three classes of dyes maintained more than 50% of their absorptivity. This was further corroborated by the strong photo stability displayed by the dyes in the dark. Again, the dyes maintained their strong light absorbing properties above 73% with the 14 days of testing. The results clearly suggested that these dyes are very photo stable as compared to the FDA approved ICG and can be further assessed for uses in bioanalyses such as tissue contrasting and imagery along with other enzyme based bioassays. Furthermore, light stability serves as an early indication that these molecules are less susceptible to light degradation and production of reactive oxygen species that can be very damaging to live tissue specimens which would inadvertently limit their bio-applicability.

2.6 Solvatochromic (hydrophobicity) Studies

Similar to the absorbance analyses, the linear relationship of the dyes in various solvents was determined to ensure full dissolution with minimal aggregation. As previously mentioned, the sulfonated cyanine dyes dissolve readily in polar solvents due to the solubilizing sulfonate group attached to the indolium alkyl chain and display high emission properties. However, the new dye derivative formed with display strong aggregation due to the loss of the solubilizing group and is further characterized by diminished emission signal. To illustrate these unique solvatochromism properties, working solutions within the concentration range of 1.0×10^{-7} to 10.0×10^{-7} molar were prepared from the stock solutions, and the emission scans were collected from 690 to 850 nm with an excitation source of 690 ± 2 nm. Also, successive dilution of dyes were prepared and evaluated for their solvatochromic characteristics of by acquiring emission spectra of the dye samples in varying ratios of methanol-phosphate buffer (10.0×10^{-3} Molar, pH

7.4) mixture (in the range of 1 to 100% phosphate buffer/ methanol) until there was no further discernible spectral changes, at which point the spectra overlapped as percent methanol increased. This was then repeated for other less polar solvents as demonstrated in table**s 2.1 to 2.3.**

Table 2.1 Solvent effects on the spectral characteristics of Benz[*c,d*]indolium dyes; MHI-06, 21 and 36.

	Dyes (λ_{max} [nm]/ Em_{max} [nm])			Stokes Shift [nm]			Monomeric Peak Extinction Coefficient (ε) Mol^{-1} cm^{-1}		
Solvents	**MHI-06**	**MHI-21**	**MHI-36**	**MHI-06**	**MHI-21**	**MHI-36**	**MHI-06**	**MHI-21**	**MHI-36**
Water	753/770	755/768	755/773	17	13	18	14,800	6,000	14,500
Methanol	758/774	764/780	758/775	16	16	17	116,000	143,000	124,000
Ethanol	763/778	760/775	760/778	15	15	18	92,400	124,000	108,500
1-Propanol	765/780	763/780	766/780	15	17	14	96,300	127,200	109,400
Sec-butanol	766/780	764/777	766/780	14	13	14	93,100	121,200	101,200
Benzanol	777/797	774/794	777/796	20	20	19	86,600	116,400	104,000
Acetonitrile	757/776	754/772	757/776	19	18	19	95,000	118,500	99,200
DMSO	769/787	771/795	773/798	18	24	25	90,700	116,900	99,200

Table 2.2 Solvent effects on the spectral characteristics of Benz[*e*]indolium dyes; E-04, 06 and 14.

	Dyes (λ_{max} [nm]/ Em_{max} [nm])			Stokes Shift [nm]			Monomeric Peak Extinction Coefficient (ε) Mol^{-1} cm^{-1}		
Solvents	**MHI-06**	**MHI-21**	**MHI-36**	**MHI-06**	**MHI-21**	**MHI-36**	**MHI-06**	**MHI-21**	**MHI-36**
Water	541/556	544559	546/563	15	15	17	96,500	72,000	79,100
Methanol	546/561	548/561	549/565	15	13	16	149,100	106,900	149,500
Ethanol	548/563	550/565	552/567	15	15	15	117,400	92,300	173,400
1-Propanol	550/564	552/566	553/569	14	14	16	115,200	96,500	138,300
Sec-butanol	550/563	552/556	554/568	13	14	14	121,200	102,000	140,900
Benzanol	556/569	559/571	559/575	13	12	16	117,500	98,600	136,500
Acetonitrile	552/559	554/560	555/564	7	6	9	121,000	92,700	147,900
DMSO	552/569	554/569	555/571	17	15	16	110,100	99,800	145,400

Table 2.3 Solvent effects on the spectral characteristics of Fischer indolium dyes; E-05, 08 and 18.

	Dyes (λ_{max} [nm]/ Em_{max} [nm])			Stokes Shift [nm]			Monomeric Peak Extinction Coefficient (ε) Mol^{-1} cm^{-1}		
Solvents	**MHI-06**	**MHI-21**	**MHI-36**	**MHI-06**	**MHI-21**	**MHI-36**	**MHI-06**	**MHI-21**	**MHI-36**
Water	580/596	605/617	583/600	16	12	17	62,900	48,000	56,300
Methanol	586/603	589/607	588/605	17	18	17	122,700	117,300	103,300
Ethanol	589/604	592/606	590/605	15	14	15	106,800	77,500	99,100
1-Propanol	590/606	594/608	592/608	16	14	16	109,200	81,700	92,600
Sec-butanol	592/605	595/609	593/607	13	14	14	104,400	81,100	98,200
Benzanol	598/612	601/616	600/614	14	15	14	103,300	83,000	95,900
Acetonitrile	592/601	594/604	586/602	9	10	16	113,200	89,700	99,000
DMSO	592/609	594/610	594/610	17	16	16	104,800	86,300	99,900

2.7 Discussion

Dye characterization studies were performed to evaluate the hydrophobic characteristics of three classes of cyanine dyes along with two Nile Red derivatives. As was reported in previous work by Kim *et al*.[2, 18], NIR molecules typically display moderate to high hydrophobic behavior based on the specific conjugated chromophore as well as the alkyl substituted indolium moiety. Varying the volume ratio of increased methanol to phosphate buffer at constant pH of 7.4 resulted in a general absorbance enhancement of the monomeric band. This unique spectral characteristic associated with decreased solvent polarity was observed among all three classes of dyes as depicted in figures 2.7 to 2.9. This change in solvent polarity also resulted in changes to other intrinsic spectral properties of the dyes such as maximum absorbance values. As the percent methanol in the solvent increases from 1 to 100% there is a general increase in the ratio of the maximum absorbance intensity of the monomer dye (monomeric or M-band) ca. 758 nm to the blue shifted aggregate (Hypsochromic or H-band) absorbance band. This increased in absorbance is associate with the breakup of the H-aggregate to form monomers which is evidenced by a simultaneous reduction in the aggregate peaks [19]. The aggregation is predominantly due to the plane-to-plane stacking of the dye molecules to form a sandwich type arrangement which is characterized by a broad H-band. Upon exposure to more hydrophobic solvent, this highly organized plane-to-plane arrangement is disrupted which subsequently gives rise to the formation of the randomized monomer arrangement characterized by a sharp M-band. This is further evident in tables 2.1 to 2.3 whereby the dyes exhibit an increase in the measured molar absorptivity values in less polar solvents such as methanol as opposed to the less hydrophobic buffer solution. Since cyanine dyes lacking key solubilizing moieties like sulfonate or carboxylic groups are commonly known to exhibit intrinsic H-aggregation in highly polar solvents, these unique spec-

tral properties make these dyes much more attractive as NIR biological probes and further enable the possibility for the development of a bioanalytical assay necessary to study key enzymatic catalysis.

In agreement with prior published data by Zhang *et al*. [20], the increase in chain length and subsequent hydrophobicity of the indolium side chain from the ethyl to butyl moiety among the class **III** type dyes resulted in a blue shift of the absorbance maxima from 764 nm to 758 nm in methanol [21-24,25, 26]. While these solvatochromic shifts may indicate interaction between the solvent and the dye in the ground state, a smaller shift suggests that the distribution of the ground state dye is virtually unaffected by the solvent polarity[27-30]. Unexpectedly, the molar absorptivity was also reduced from143,000 $M^{-1}cm^{-1}$ to 116,000 $M^{-1}cm^{-1}$ due to increased dimerization. From the results, we observed that carbocyanine dyes bearing less hydrophobic side chains display greater tendencies to self-associate in less polar solvent to form the intra-molecular aggregate species. These aggregate species are generally weakly fluorescent and often exhibit a lower molar coefficient than their monomeric counterparts. Similar patterns were observed with the other two classes of NIR molecules. Although effective use of these fluorescent molecules as biological sensors depends significantly on their molecular structure, hydrophobic character is an important factor in their overall biological utility [31]. The incorporation of the Benz[*e*]indolium or Fischer indolium chromophore improves quantum efficiency but reduces the hydrophobicity of the molecules. Ideally this improved quantum efficiency results in enhanced optical contrast for *in vivo* studies; however, the diminished hydrophobic nature cannot be overlooked as the molecules have effectively become less biocompatible with regard to their uptake and transportation by key plasma transporter complexes [32, 33]. Despite the potential reduction in the ability to com-

plex biomolecules and subsequent molecular activity resulting from this hydrophobicity change, the effect of the dyes improves solubility is considered quite useful. Moreover, this makes the molecule more attractive as novel NIR biological probes in other aspects such as studying conformational changes in various target proteins [34]. In addition, figure 2.1 illustrate that the increased quantum yield associated with the presence of the Benz[*e*]indolium moiety confirms the idea that increased rigidity or reduced free rotation within the molecule is important in reducing photo-isomerization and subsequently stabilizes the ground state distribution of the dyes [35-38].

In an effort to fully understand the unique binding characteristics of fluorescent dyes with biomolecules, logarithmic partition coefficient (*Log P*) values were determined. These results were used primarily to predict the fluorescent molecules hydrophobicity with respect to the various indolium side chains. Successful prediction of the molecular hydrophobicity enables an early indication of dye affinity for the hydrophobic binding domains of the tested biomolecules. This data becomes important factor in the overall screening process of potential dye substrates as it further provides fundamental details on the binding parameters with the hydrophobic active sites of the monooxygenase enzyme.

Using a logarithmic partition coefficient scale (*Log P*) **MHI-36** exhibits a relatively high value of 11.03 and is thus expected to display more aggregation tendencies than the N-butyl analog in the polar phosphate buffer solution. The *Log P* values are used to determine the distribution ratio of concentrations of the dyes in the two immiscible solvents at equilibrium. This measure of molecular hydrophobic properties not only provides useful qualitative data on the hydrophobic behavior of the test molecule but is also useful in assessing a molecules ability to cross

the bilipid membrane of living cells. Information obtained from this value can also be very useful in the determination of the test ligand's ability to interact with the three dimensional hydrophobic binding domains of carrier protein and nucleic acid macromolecules. This feature is imperative to the development of this new bioanalytical assay to investigate various enzyme controlled processes. Dyes exhibiting higher values are usually more hydrophobic and are thus more suitable for non-polar solvents. However, mere analysis of these data shows, **MHI-36** displayed less favorable aggregation tendencies than **MHI-06** with a *Log P* value of 9.26. This is further illustrated in table 2.1 which shows values of 124,000 and 116,000 $M^{-1}cm^{-1}$, respectively. Similar patterns were observed among the class **I** and **II** type dyes as well. Even though the phenylpropyl derivatives of all three classes of dyes are considerably more hydrophobic with higher *Log P* values, the data did not reveal any significant changes in the overall molar absorptivity values. Thus, it is inferred that the excitation properties of these molecules are not merely governed by hydrophobicity properties but may be further influenced by the molecular conformation of the molecules in different solvent media. However, this pattern was less evident among the individual classes of dyes, whereby the phenylpropyl derivatives continued to display the highest molar absorptivity values which can be further explained by enhanced π-π electron stacking of the indolium aromatic system, an arrangement uncharacteristic of the aliphatic indolium side chains. These same characteristics of molecular orientation in liquid media, along with hydrophobic behavior of the dyes are applied in explaining the difference in absorbance and emission spectra exhibited among the three derivatives in the three classes of novel trimethine dyes. The solvatochromism studies revealed that each dye exhibit different spectral properties in going from the less hydrophobic phosphate buffer to the more hydrophobic methanol solvent. Previous studies have revealed that often times solvatochromism represents the solvent-induced spectral

band shift. This shift is due to changes in the $\pi \rightarrow \pi^*$ and $n \rightarrow \pi^*$ transition energy resulting from differential solvation of ground and excited states of the NIR dye[39, 40]. With decreasing polarity of the solvent or increase in percent methanol to phosphate buffer ratio, the spectral band can undergo a marginal bathochromic shift depending on the electronic structure of the probe and its interaction with the micro-environment given by the solvent shell. Accordingly, a negative or positive solvatochromism can be determined, which gives qualitative and quantitative conclusions about the energetics of the dye solvation. Probes exhibiting this solvatochromic behavior generally display steady bathochromic (positive solvatochromism) and are important in studying the structural orientation of the primary binding domains of key ligand binding proteins[39, 41-44]. In fact, the change in absorbance and emission further demonstrate the possibility to obtain qualitative information as to the expected binding patterns about whether or not these probes are restricted within ligand binding domains [39, 43-48].

Representational absorbance spectra revealed that among the three classes of carbocyanine dyes, the Benz[*c,d*]indolium exhibited the greatest positive solvatochromic effects. For example, with **MHI-06**, the ratio of the aggregation band at 659 nm to the monomeric band 763 nm decreased sharply with the increased methanol content. This observation was evident with the ethyl and phenylpropyl derivatives. To the contrary, this behavior was less pronounced for the Benz[*e*]indolium and Fischer indolium dyes suggesting that the Benz[*c,d*]indolium chromophore was most suited as a bioanalytical probe for investigating photophysical properties in different solvent media, as shown in figures 2.8 to 2.10 depicting the results of the absorbance studies. However, despite its favorable results obtained from the solvatochromism studies, the Fischer indolium dyes were selected in preference to both the Benz[*e*]indolium and Benz

[*e*]indolium derivatives. This in part is due to the fact that all dyes displayed quite similar photostability but since the Fischer indolium compounds possess the less bulky heterocyclic systems among the three.

The Fischer indolium dyes were designed to possess the considerably less bulky heterocycles, therefore the loss in solvatochromism properties from selecting this less bulky dye structure is rather insignificant in comparison to the potential risk of reduced substrate-enzyme interaction that could have resulted if the more bulky Benz[*c,d*]indolium heterocyclic systems were chosen. This poses the potential to affect the delicate and highly specific lock-and-key binding model that must be established to facilitate enzyme catalysis. Besides, each class of dye exhibited similar absorption and emission properties, thus the selection of the Fischer indolium derivatives would not affect the fluorescence signal output for the subsequently enzyme detection.

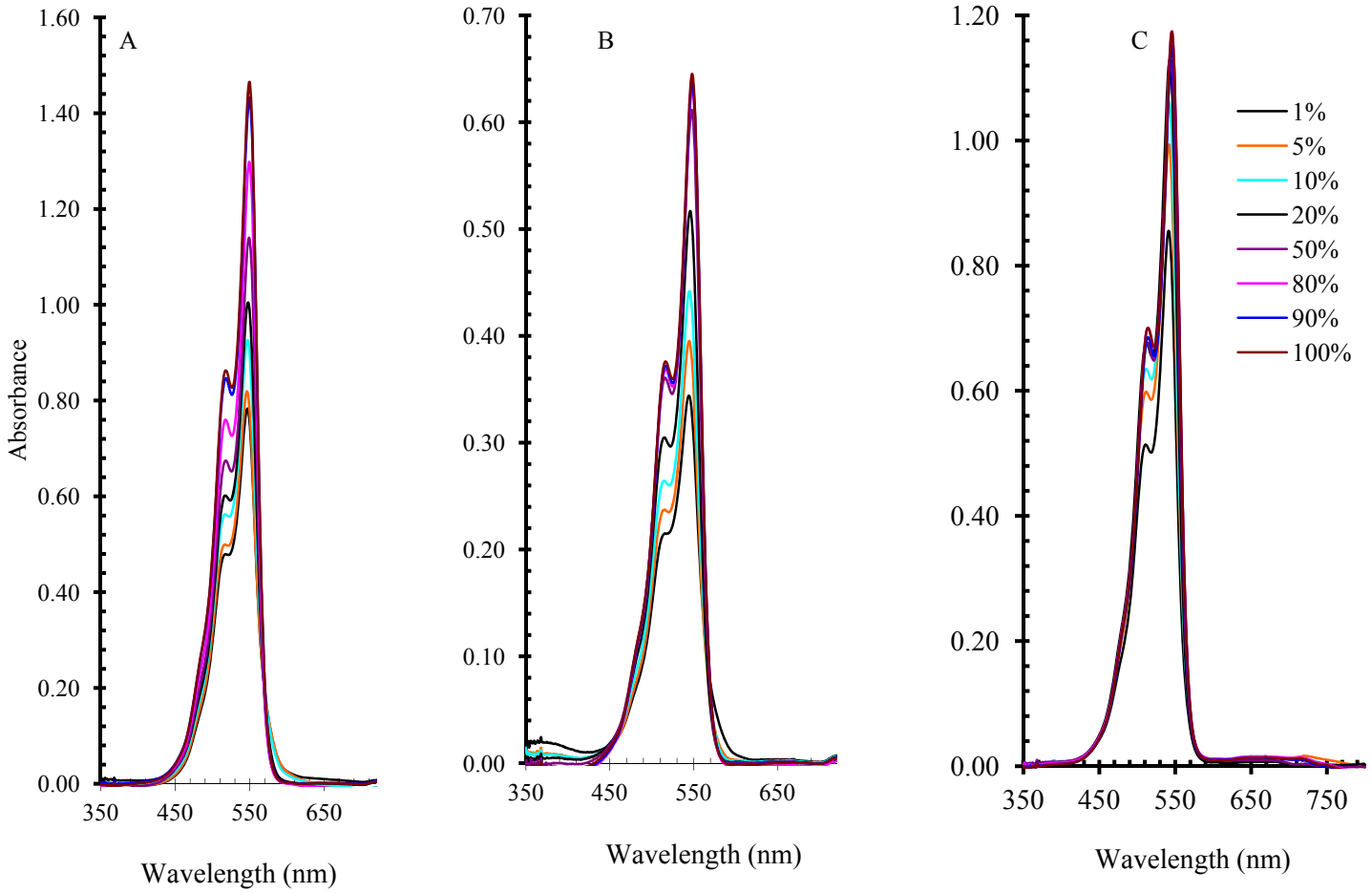

Figure 2.7 Absorbance as a function of solvent hydrophobicity (% Methanol) at Dye concentration of 10.0 µM of the Fischer indolium family of dyes (class *I*). Increased percent methanol resulted in aggregation disruption and give rise to the monomeric peak. A; E-04, B; E-06 and C; E-14.

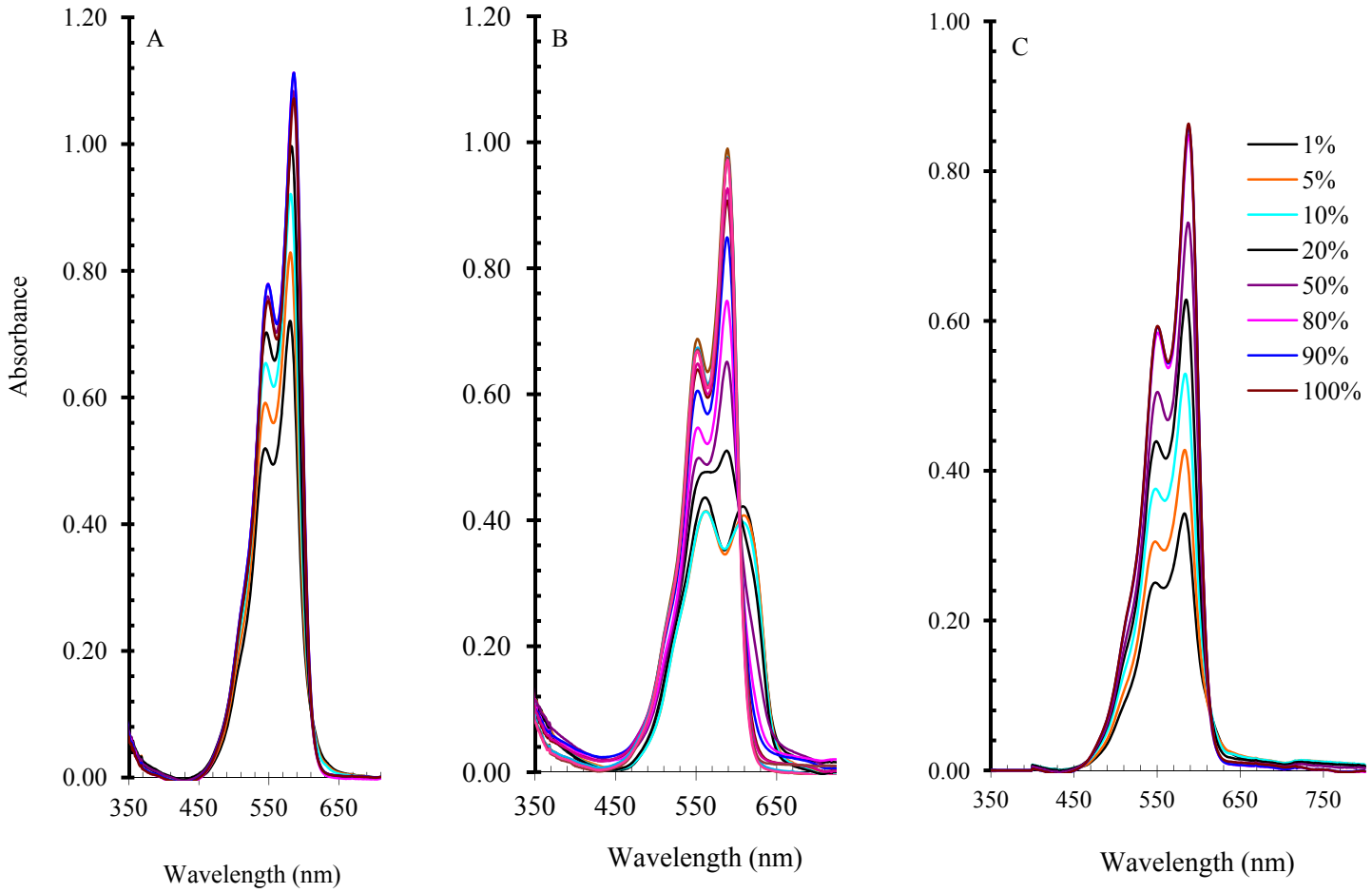

Figure 2.8 Absorbance as a function of solvent hydrophobicity (% Methanol) at Dye concentration of 10.0 µM of the Fischer indolium family of dyes (class *II*). Increased percent methanol resulted in aggregation disruption and give rise to the monomeric peak. A; E-05, B; E-08 and C; E-18.

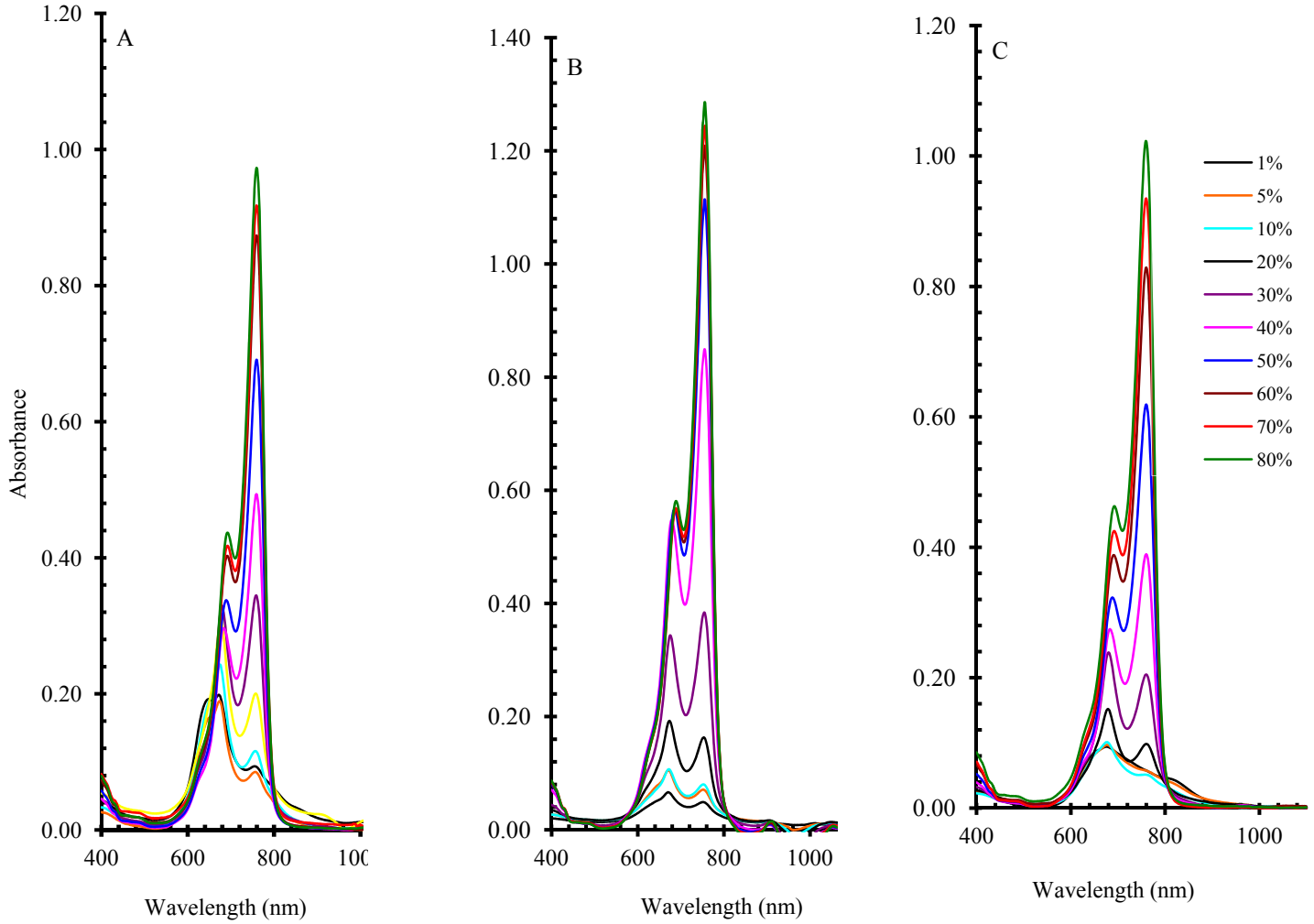

Figure 2.9 Absorbance as a function of solvent hydrophobicity (% Methanol) at Dye concentration of 10.0 µM of the Benz*[c,d]*indolium family of dyes (class *III*). Increased percent methanol resulted in aggregation disruption and give rise to the monomeric peak. A; MHI-06, B; MHI-21 and C; MHI-36.

Even though class ***III*** seemed most suitable for further structural and photophysical "fine tuning" and the agent a bioassay development more consideration to other biophysical properties such as dye-ligand interaction once the probe is conjugated with a complex biomolecule.

2.8 Summary

As previously discussed, one important spectral property of any ideal photophysical probes for bio-analysis is strong photo stability. These studies have demonstrated that despite the popularity of oxazines and their Nile Red derivatives, the cyanine dyes are more superior as bioanalytical probes based on their overall photo stability when stored or exposed to light for prolong time periods. Not only are the cyanine dyes and in particular those possessing the Fischer indolium chromophore more stable, but they are less susceptible to deleterious photo-degradation and thus the formation of side products under normal storage conditions. As shown in figures 2.3 to 2.6 these compounds were still highly absorbing after 14 days of exposure to light and in fact maintained at least 60% absorbance beyond this period unlike the Nile Red dyes that were completely photo bleached within the same period.

As a criterion for the successful development of any dye based bioassay, the dyes must firstly be photostable for relatively long periods considering the fact that these compounds will be strongly irradiated for detection. Not only will poor photostability limit the overall detection and by extension the effectiveness of the technique. The possibility of photo fading could limit key analytical components of the technique such as lower detection limits and lower limits of quantification; which are some of the main advantages for the development of this new technique in comparison to classical bioanalytical methods.

The photophysical properties of the trimethine dyes remained in the visible to NIR band and have exhibited very distinguished characteristics in comparison to the oxazine derivatives. As is shown in tables 2.2 and 2.5, the absorption and emission maxima all fall above 640 nm for all the Fischer based indolium dyes. However, the Benz[*c,d*]derivatives were much higher in the 750 to 790 nm range. This unique observation is in agreement with the general rule that, increase in conjugation of the heterocyclic systems increases the absorbance maxima. In addition, the extra aromaticy contributes to increased hydrophobicity which is evident in the increased aggregation tendencies when the compounds are dissolved in more polar solvents such as phosphate buffer or water, thus resulting in a slight hypsochromic shift in absorption and emission of up to about 10 nm. This shift is primarily attributed to the changes in the $\pi \rightarrow \pi^*$ and $n \rightarrow \pi^*$ transition energy resulting from differential solvation of ground and excited states of the NIR dye. These results clearly indicated that the cyanine dyes are more favorable as analytical probes and are more suitable for the development of the new bioanalytical technique.

2.9 References

1. G. Beckford, E. Owens, M. Henary and G. Patonay, *Talanta*, 2012, **92**, 45-52.
2. G. Patonay, G. Beckford, L. Strekowski, M. Henary, J. S. Kim and S. Crow, 2009.
3. G. I. Nosova, D. A. Lypenko, R. Y. Smyslov, I. A. Berezin, E. V. Zhukova, E. I. Mal'tsev, A. V. Dmitriev, L. S. Litvinova, N. A. Solovskaya, O. V. Dobrokhotov, I. G. Abramov and A. V. Yakimanskii, *Polymer Science Series B*, 2014, **56**, 59-76.
4. M. Omedes Pujol, D. J. L. Coleman, C. D. Allen, O. Heidenreich and D. A. Fulton, *Journal of controlled release : official journal of the Controlled Release Society*, 2013, **172**, 939-945.

5. M. Ahmad, *Optics Communications*, 2007, **271**, 457-461.

6. M. Ahmad, T. A. King, D. K. Ko, B. H. Cha and J. Lee, *Optics Communications*, 2002, **203**, 327-334.

7. Y. Kohno, K. Totsuka, S. Ikoma, K. Yoda, M. Shibata, R. Matsushima, Y. Tomita, Y. Maeda and K. Kobayashi, *Journal of Colloid and Interface Science*, 2009, **337**, 117-121.

8. M. S. Mackey and W. N. Sisk, *Dyes and Pigments*, 2001, **51**, 79-85.

9. J. Mahmoudian, R. Hadavi, M. Jeddi-Tehrani, A. R. Mahmoudi, A. A. Bayat, E. Shaban, M. Vafakhah, M. Darzi, M. Tarahomi and R. Ghods, *Cell Journal*, 2011, **13**, 169-172.

10. H. M. Marwani, A. M. Asiri and S. A. Khan, *Russian Journal of Bioorganic Chemistry*, 2012, **38**, 533-538.

11. B. Song, Q. Zhang, W. H. Ma, X. J. Peng, X. M. Fu and B. S. Wang, *Dyes and Pigments*, 2009, **82**, 396-400.

12. T. Suratwala, Z. Gardlund, K. Davidson, D. R. Uhlmann, J. Watson, S. Bonilla and N. Peyghambarian, *Chemistry of Materials*, 1998, **10**, 199-209.

13. P. N. Thanki and R. P. Singh, *Macromolecular Materials and Engineering*, 2001, **286**, 756-760.

14. S. J. Yang, F. S. Meng, H. Tian and K. C. Chen, *European Polymer Journal*, 2002, **38**, 911-919.

15. S. A. El-Daly, A. M. Asiri, K. A. Alamry and A. G. Al-Sehemi, *Journal of Molecular Structure*, 2013, **1037**, 323-331.

16. H. M. Marwani, A. M. Asiri and S. A. Khan, *Journal of Luminescence*, 2013, **136**, 296-302.

17. V. E. Shershov, M. A. Spitsyn, V. E. Kuznetsova, E. N. Timofeev, O. A. Ivashkina, I. S. Abramov, T. V. Nasedkina, A. S. Zasedatelev and A. V. Chudinov, *Dyes and Pigments*, 2013, **97**, 353-360.

18. G. Patonay, J. S. Kim, R. Kodagahally and L. Strekowski, *Applied Spectroscopy*, 2005, **59**, 682-690.

19. J. S. Kim, R. Kodagahally, L. Strekowski and G. Patonay, *Talanta*, 2005, **67**, 947-954.

20. Y. Z. Zhang, H. Y. Du, Y. L. Tang, G. Z. Xu and W. P. Yan, *Biophysical Chemistry*, 2007, **128**, 197-203.

21. H. Lee, M. Y. Berezin, K. Guo, J. Kao and S. Achilefu, *Organic Letters*, 2009, **11**, 29-32.

22. H. Lee, M. Y. Berezin, M. Henary, L. Strekowski and S. Achilefu, *Journal of Photochemistry and Photobiology a-Chemistry*, 2008, **200**, 438-444.

23. H. Lee, K. Lee, I. K. Kim and T. G. Park, *Biomaterials*, 2008, **29**, 4709-4718.

24. J. S. Lee, Y. K. Kim, M. Vendrell and Y. T. Chang, *Molecular Biosystems*, 2009, **5**, 411-421.

25. L. Strekowski, *Heterocyclic polymethine dyes : synthesis, properties and applications*, Springer, Berlin, 2008.

26. L. Strekowski and B. Wilson, *Mutation Research-Fundamental and Molecular Mechanisms of Mutagenesis*, 2007, **623**, 3-13.

27. M. A. Rauf, J. P. Graham, S. B. Bukallah and M. A. S. Al-Saedi, *Spectrochimica Acta Part a-Molecular and Biomolecular Spectroscopy*, 2009, **72**, 133-137.

28. F. L. Dickert, U. Geiger, P. Lieberzeit and U. Reutner, *Sensors and Actuators B-Chemical*, 2000, **70**, 263-269.

29. B. Jedrzejewska, M. Pietrzak and J. Paczkowski, *Journal of Fluorescence*, 2010, **20**, 73-86.

30. M. J. Sawicka, J. A. Soroka, E. K. Wroblewska and I. K. Zawadzka, *Polish Journal of Chemistry*, 2006, **80**, 1337-1351.

31. S. H. Kim, S. Y. Lee, S. Y. Gwon, Y. A. Son and J. S. Bae, *Dyes and Pigments*, 2010, **84**, 169-175.

32. X. H. Gao, L. L. Yang, J. A. Petros, F. F. Marshal, J. W. Simons and S. M. Nie, *Current Opinion in Biotechnology*, 2005, **16**, 63-72.

33. M. Henary, V. Pannu, E. A. Owens and R. Aneja, *Bioorganic & Medicinal Chemistry Letters*, 2012, **22**, 1242-1246.

34. M. Y. Berezin, H. Lee, W. Akers and S. Achilefu, *Biophysical Journal*, 2007, **93**, 2892-2899.

35. S. Murphy and G. B. Schuster, *Journal of Physical Chemistry*, 1995, **99**, 8516-8518.

36. C. Eggeling, J. Widengren, L. Brand, J. Schaffer, S. Felekyan and C. A. M. Seidel, *Journal of Physical Chemistry A*, 2006, **110**, 2979-2995.

37. C. Eggeling, J. Widengren, R. Rigler and C. A. M. Seidel, *Analytical Chemistry*, 1998, **70**, 2651-2659.

38. T. Shibata, T. Hattori, S. Onodera and T. Kaino, *Nippon Kagaku Kaishi*, 1998, 831-836.

39. M. Panigrahi, S. Dash, S. Patel, P. K. Behera and B. K. Mishra, *Spectrochimica Acta Part a-Molecular and Biomolecular Spectroscopy*, 2007, **68**, 757-762.

40. M. Panigrahi, S. Patel and B. K. Mishra, *Journal of Molecular Liquids*, 2013, **177**, 335-342.

41. J. Catalan, *Dyes and Pigments*, 2012, **95**, 180-187.

42. E. O. l. Moradi-e-Rufchahi and A. Ghanadzadeh, *Journal of Molecular Liquids*, 2011, **160**, 160-165.

43. J. A. Soroka and K. B. Soroka, *Journal of Physical Organic Chemistry*, 1997, **10**, 647-661.

44. A. C. Yu, C. A. Tolbert, D. A. Farrow and D. M. Jonas, *Journal of Physical Chemistry A*, 2002, **106**, 9407-9419.

45. G. Jung, S. Gerharz and A. Schmitt, *Physical Chemistry Chemical Physics*, 2009, **11**, 1416-1426.

46. C. T. Martins, M. S. Lima, E. L. Bastos and O. A. El Seoud, *European Journal of Organic Chemistry*, 2008, 1165-1180.

47. E. O. Moradi-e-Rufchahi and A. Ghanadzadeh, *Journal of Molecular Liquids*, 2011, **160**, 160-165.

48. E. K. Wroblewska, J. A. Soroka, K. B. Soroka and M. Gasiorowska, *Journal of Physical Organic Chemistry*, 2005, **18**, 347-352.

3 PROTEIN LABELING USING VISIBLE TO NEAR INFRARED DYES

3.1 Introduction

3.1.1 Protein labeling with Vis-NIR fluorescent dyes

Optical probes designed for the purpose of labeling of biomolecules have become widely accepted a tool used in bioanalytical research. To achieve successful labeling, the target molecule typically possesses the necessary functionality to facilitate covalent attachment or alternatively, a biomolecule of interest maybe a non-functionalized marker and exhibit a strong non-covalent interaction with the probe that allows for the formation of a stable conjugate. Although the two modes of labeling techniques yield similar results, unlike the non-covalent, covalent labeling of biomolecule for bioanalysis usually occurs at a more rapid rate and quite is limited to physiological pH range. Also, once a conjugate is formed purification steps are usually unnecessary when the stoichiometry of the complex is known or if non-covalent labeling is used in conjunction with separation techniques, e.g. capillary zone electrophoresis as shown in table 1.3. In addition, often times there be multiple binding regions to the biomolecule thus allowing the attachment varying numbers of ligands or probes molecules attached to them, which could result in band broadening and poor resolution [1, 2]. To the contrary, non-covalent labeling typically occurs through hydrophobic linkages but may involve other forms of interactions such as electrostatic, ionic and hydrogen bonding interactions. These interactions are substantially less stable than the covalent linkages but they are useful in studying biomolecules such as proteins and nucleic acids in their native three dimensional structure. This so because; (1) no dye complex derivatization is required when they are non-covalently attached to biomolecules, (2) there is no separation method needed post conjugate formation and (3) because the conjugate is formed through weak intermolecular linkages such as van der waals, hydrophobic and dipole-dipole interactions, both the dye and biomolecule are less likely to undergo structural alteration that could possible affect

the structural integrity of either molecules. These advantages render the non-covalent labeling technique even more attractive in the design of this novel bioassay.

3.1.2 Covalent labeling of biomolecules

For the application of covalent labeling in bioanalyses, there are numerous encountered, generic functional groups. Linkages to the α- and ε-NH2 terminal in amino acid usually involves; succinimidyl esters, isothiocyanates and sulfonyl chlorides. Thiol groups on the other hand may require an alkyl halide or a maleimide moiety[3, 4]. Despite the labeling mode or type of linkage, it is believed that there can be notable changes to the specificity of the amino acid of a protein upon reacting with a functionalized dye. For example, pH dependant *N*-terminal of amino acids such as lysine and histidine can undergo protonated or deprotonated dependent on pH of the solution in order to facilitate covalent conjugation. This pH dependent conjugation can further lead to the covalent attachment to a protonated or deprotonated non-terminal amino group thus controlling the rate and efficiency of bio-conjugation. While there are many types of possible dye functionalities for amine, thiol groups as well as other side chains. Studies have demonstrated that these types of covalent bio-conjugation occur primarily with a side chain of an amino acid and follows substitution reaction in distinct environment[5-7]. Besides, these interactions exhibit the potential to chemically alter the functional groups within the target molecules and may ultimately lead to expected loss or disruption to macromolecules functional integrity. In addition, there is always the need for complex separation techniques to study the hybridized molecule once conjugation is achieved, making the technique in general less favorable to for simple and straight forward novel bioassays.

3.1.3 Non-covalent labeling of biomolecules

Unlike the covalent labeling, non-covalent labeling of complex biomolecules is more binding specific and requires at least one binding site on the biomolecule with the requisite functionality. For example, current NIR probes are being designed with strong hydrophobic characteristics to interact with interior hydrophobic binding domains on globular proteins. Because of the simplicity of this type of interaction, a dye can be readily mixed with a protein or the appropriate biomolecule that provides favorable binding properties for the probe. This ligand binding interaction can thus be then monitored by molecular spectroscopy, mobilities in chromatography and circular dichroism. In nucleic acid studies, non-covalent labeling provides the role of minor and major grooves. The non-covalent interaction is dependent on mainly dipole-dipole forces, dispersion forces and hydrogen bond between a ligand and a biomolecule [8]. In addition, two forms of linkage may even be codependent and thus influencing each other, or only a single factor influences the binding. However, in protein noncovalent labeling the probes more commonly interact through hydrophobic interaction or electrostatic interaction which can be further influenced by pH of the micro-environment [8-15].

It is well established that NIR cyanine dyes self-aggregate in aqueous buffer solutions resulting from the planar π-electron conjugation systems [16]. It has been reported that the aggregation gives rise to two different structures depending on the angle of slippage (α); these are commonly referred to as J-aggregation (bathochromic) and H-aggregation (hypsochromic)[16, 17]. Studies have shown that a small angle of molecular slippage ($\alpha < \sim 32^{0}$) results in H-aggregation while large slippage ($\alpha > \sim 32^{0}$) leads to J-aggregation formation[18, 19].

Figure 3.1 **Representation of cyanine dye aggregation in liquid media. Dye may form three distinct aggregation patterns. A; brick work, B; ladder, C; stair case molecular arrays. α is the angle of slippage.**

The type of aggregation is largely dependent on the solvent polarity, but it may also be affected by other factors such as temperature, pH, dye concentration and ionic strength[16, 19, 20]. Kim and coworkers among others have studied the hydrophobic characteristics of the Bis(heptamethine cyanine) dyes, but relatively few recent experimental studies have dealt with the trimethine family of dyes [8, 16]. Some interesting results have been reported on their hydrophobic behavior and aggregation formation. Such as a prominent red-shifted spectral transition influenced by the increased $\pi \rightarrow \pi^*$ energy gap associated with reduced solvent polarity[8]. As a part of this study three novel classes of trimethine dyes were prepared, characterized and were considered ideal to examine the photophysical behavior and the effects of solvatochromism on their binding characteristics. Among these dyes were Benz[*c,d*]indolium, Benz[*e*]indolium and Fischer indolium derivatives with variations made to the symmetrical indolium side chains (figure 2.1 ***[I-III]***). As expected, the photophysical chemistry of cyanine dyes is determined primarily by the conjugated backbone carbon structure. However, the nature of the indolium side chains is critical to the overall hydrophobic properties of these fluorescence compounds is the basis of their distinct

spectral variations. It has been shown that most NIR cyanine H-aggregates in aqueous media usually display virtually no fluorescence activity[16, 21-24]. Interaction with HSA, however, results in a marked increase in fluorescence intensity thus providing a viable option for non-covalent labeling of proteins as well as their utilization as binding site probes.

A full understanding of the binding equilibria can explain the enhanced sensitivity and reduced detection limits attained with Vis-NIR dyes for proteomic studies. The spectral characteristics and structure of these probes are determined predominantly by their microenvironment, and any conjugation with biomolecules would subsequently lead to a concomitant change in these intrinsic properties. Furthermore, the polarity of the microenvironment can further influence the spectral properties of these molecules. For example, newly designed cationic dyes are used in investigating the ground and excited states of 1,1',3,3'-tetraethyl-5,5',6,6'-tetrachlorobenzimidazolocarbocyanine (TTBC) dyes in solvent [25]. Increased interest in the study of these fluorescence probes has focused tremendously on investigating the non-covalent interaction with proteins for both clinical and biomedical applications [26]. In addition, although more commonly recognized as bio-analytical probes, trimethine cyanine dyes have also demonstrated their suitability as ion selective metal probes for *in vitro* metal ion analyses [27, 28]. But more importantly, the Fischer based cyanine dyes introduced in this method development have shown unique spectral and solvatochromism patterns that are quite useful to study the enzymatic catalysis of the alkyl sulfonated substrate *in vitro* with strong potential for *in vivo* applications.

Non-covalent labeling offers considerable advantages to the numerous applications of cyanine dyes. Studies have reported significant spectral changes with direct interaction of these

dyes with the hydrophobic binding pockets of HSA [8, 12, 16, 18, 29, 30]. Given the importance of serum albumin in maintaining many vital processes, a myriad of new fluorescence probes are being developed to study the hydrophobic effect on binding site specific interactions [31]. Furthermore, NIR fluorescence probes exhibiting spectral profiles that are significantly influenced by solvation are becoming more popular in proteomic studies [32]. Binding of the novel cyanine dyes reported herein with specific protein molecules can provide useful information on binding site location and conformational changes within the target molecules.

Herein, we report a systematic study of the effect of side chain on the binding interaction of three classes of cyanine dyes. Our studies demonstrate how the nature of the side chain may influence the overall quantum efficiency and other key spectral characteristics of the probes. In addition, molecular size of the indolium side chain have important ramifications for the interaction of cyanine dyes with serum albumin and their applications in developing new bioanalytical techniques.

3.1.4 HSA Binding Interaction

In order to investigate the hydrophobic binding domains of the serum albumin, binding studies were conducted by titration of a fixed volume of dye at constant concentration (*10 μM for absorbance and 1.0 μM for emission*) with HSA. Each sample was vortexed for 30 s and then left for 5 min to equilibrate. Analyses were performed until there were no further spectral changes with further addition of the HSA. A fresh batch of the biomolecule solution was prepared every 24 h period. As already explained, these studies will form the basis of confirming the occurrence of enzyme catalysis. The loss of emission signal resulting from the conversion highly

solubilizing alkyl sulfonate moiety to the aggregate forming alkyl aldehyde is restored when the latter interacts with albumin. On the one hand it confirms the enzyme catalysis but on the other it also serves as a quantitative tool for the overall method development. Change in emission signal is rather linear with production of the straight chain aldehyde product or even extent of catalysis. In addition, dye albumin interaction also provides an early indication to the dye enzyme interaction considering that both the enzyme active site and the serum albumin binding domains have similar binding characteristics and are similarly hydrophobic in nature.

3.2 Results and discussion

3.2.1 HSA binding interactions with NIR cyanine Dyes

The conjugate formation of the cyanine dyes with the serum albumin was studied in phosphate buffer at pH 7.4. The binding interaction was monitored by evaluating the changes in absorbance and emission intensities at a fixed concentration of dye with micro molar concentrations of protein. Based on the dye structure, this results in up to as much as a five-fold increase in absorbance intensity of the monomeric peak among all three families of dyes.

Having displayed moderate affinities for the serum albumin, the variation in the alkyl indolium moiety of the cyanine dyes had a profound effect on overall conjugation with the biomolecule. In recent literature Kim and coworkers characterized the hydrophobic binding pockets of the HSA molecule[8, 31] and observed that changes in binding affinity are attributed to the substitution of hydrophobic moieties at the heterocyclic ring of the cyanine dyes. Table 3.2 summarizes the effects of indolium side chain modifications on the binding affinity of these novel cyanine molecules.

As earlier mentioned, cyanine dyes self-assemble in polar solvents such as the phosphate buffer solution owing to the strong intermolecular van der Waals interactions between the heterocyclic moieties to form H-aggregation [16]. Conjugate formation with HSA disrupts the aggregation thereby increasing monomer formation and subsequently increasing fluorescence emission and molar absorptivity values of the bound dye.

It was suggested that cyanine dyes are binding site specific and exhibit a high specificity for the subdomain **III** commonly referred to as the site II of the HSA molecule [12, 13, 33]. Within this context these investigations suggested that the binding affinity of these dyes is not only hydrophobicity dependent, but may be influenced by steric interferences within the binding sites. There is a general pattern of increased binding affinity with increased hydrophobicity among the dyes and at pH 7.2 it is unlikely that the delocalized positive charge on these molecules will have any electrostatic effect within the binding cavity. However, further analysis of the data as shown in table 3.2 reveals that among the class ***III*** derivatives, despite **MHI-36** exhibiting a binding constant of $3.51 \times 10^5\ M^{-1}$, it is the most hydrophobic of the class (as indicated by the hydrophobicity 11.03 *Log P* value). In comparison to the other two analogs, there is increased binding when the more hydrophobic phenylpropyl group is substituted with the less hydrophobic butyl moiety with a *Log P* value of 9.26.

Although it is a general trend for the more hydrophobic group to bind more strongly to the valine rich hydrophobic pocket of the HSA, to the contrary, our conjugation experiments yielded some unexpected binding results. This type of binding pattern resulted from the occurrence of steric hindrances within the binding cavities which increases with the presence of the more bulky indolium side chain aromatic system. Therefore it can be inferred that beyond a certain ligand size steric factors will decrease binding affinity with the HSA molecule. Interestingly, inspite of the variation in binding patterns, extrapolation of the linear Scatchard plot of figure 3.3 illustrates that at HSA of concentration of 7.97×10^{-6} M all three class ***III*** cyanine dyes yielded similar binding parameters. As depicted in the figure, at this concentration and in the absence of the biomolecule, the unconjugated dye remains in the virtual non-fluorescing aggregat-

ed form. It is thus believed that the emission intensity of the bound dye is primarily dependent on the degree of conjugation and is unaffected by the hydrophobicity of the solvent when the biomolecule is added. In addition, recent studies have revealed that the interaction of bulky hodrophobic ligands with HSA can lead to the perturbation of the secondary conformation. This may further result in the rearrangement of the **I – II** and **II – III** binding domain interfaces and conformation changes of the key hydrophobic binding sites [34]. Similarly, the Scatchard plots of the class ***I*** and ***II*** dyes also illustrate that the binding affinity is dependent on the hydrophobicity but is further influenced by steric size of the indolium side chain of the dyes. However, for the former families of dyes, the binding data did not support the theory of similar binding patterns at a specific HSA concentration. In addition, the more conjugated heterocyclic class ***III*** derivatives have proven to bind more strongly with the biomolecule as indicated by the comparatively higher binding constants ranging from 3.51 to 10.60 $\times$ 10^5 M^{-1} despite the influence of steric hindrance.

Albumin is known to bind a large variety of other compounds such as fatty acids, nucleic acids and oligoproteins and antibodies; thus, it is of potential interest to develop methods that can reveal information on the hydrophobic character and steric specificity of the binding cavities. This unique binding effect of these novel NIR cyanine probes further demonstrates the utility of a host of bioanalytical applications including monitoring changes in protein binding sites, conformational changes and activities of biological molecules and target proteins.

Previous research by Kim *et al.* suggested that most cyanine dyes bind in a 1:1 stoichiometry with HSA, [8, 11, 18, 31]. This arrangement is confirmed by the Job's Plot method [35]. A method of continuous variation of both dye and HSA concentrations (varied dye to HSA ratio) at con-

stant total concentration yielded maximum absorbance intensity at 0.492 ± 0.12 HSA mole fraction, which, by application of the Job's method, corresponds to a 1:1 binding stoichiometry.

In this method, the measured corrected absorbance intensity is plotted against the mole fraction of one reactant while the sum of the reactant concentrations remained constant. For association equilibria of this type, the highest concentration of the labeled complex is depicted by the maximum ordinate in the Job's plot. Clearly, this relationship makes Job's method an extremely useful technique to determine the stoichiometries of equilibrium reactions.

However, while the of the plot allows for the immediate determination of other empirical ratios of the reactants in a chemical equilibrium by the location of the maximum in the plot, distinguishing between 1:1, 2:2, and higher n:n stoichiometries on the basis this plot can be proven more complex, this is because they all exhibit a similar maximum at the same mole fraction (i.e., $f = 0.5$). But with previous reported data of 1:1 stoichiometry, the 0.492 ± 0.12 maximum value obtained further confirms this binding relationship, as shown in figure 3.2.

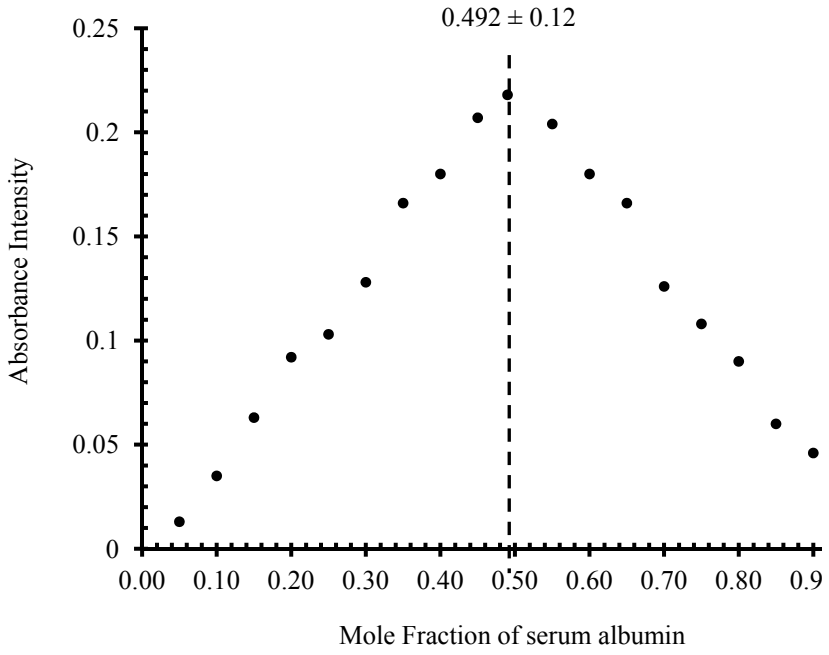

Figure 3.2 Representation of the Job's Plot for the binding interaction between serum albumin and the NIR dyes studies. All dyes yielded maximum plot value ca. 0.500 with a mean value of 0.492 ± 0.12 confirming 1:1 binding stoichiometry reported in the literature.

Assuming all the NIR probes are conjugated with the free HSA, an equilibrium is reached. In order to determine the binding affinities of the NIR cyanine, the binding interactions were evaluated with the Scatchard method [16, 18, 27, 28, 30]. In accordance with this method, the concentrations (activities) of the different reaction species are measured at equilibrium. Applying the equation,

$$\text{Dye} + \text{HSA} \rightleftharpoons^{K_s} \text{Dye-HSA} \qquad (1)$$

and assuming activity coefficient to be unity *(and 1:1 reaction stoiciometry)*,

$$K_s = \frac{[\text{Dye-HSA}]}{[\text{Dye}]\,[\text{HSA}]} \qquad (2)$$

The affinity constant is determined from the linear fit of the data of the fluorimetric titration of a fi centration of dye with HSA according to equation (3)[16, 18, 27, 28, 30].

$$\frac{1}{\Delta F} = \frac{1}{k[\text{Dye}]} + \left(\frac{1}{k[\text{Dye}]Ks}\right)\frac{1}{[\text{HSA}]} \qquad (3)$$

Where ΔF is the change in emission intensity of the Dye-HSA conjugate and k is a constant that is dependent on the quantum efficiency of the process and the instrumentation. A plot of the reciprocal of ΔF versus the reciprocal of HSA concentration should give a linear relationship that intersects the ordinate *(x-axis)* as depicted in figures 3.3 to 3.5. The affinity constant is calculated by dividing the intercept by the slope of the line.

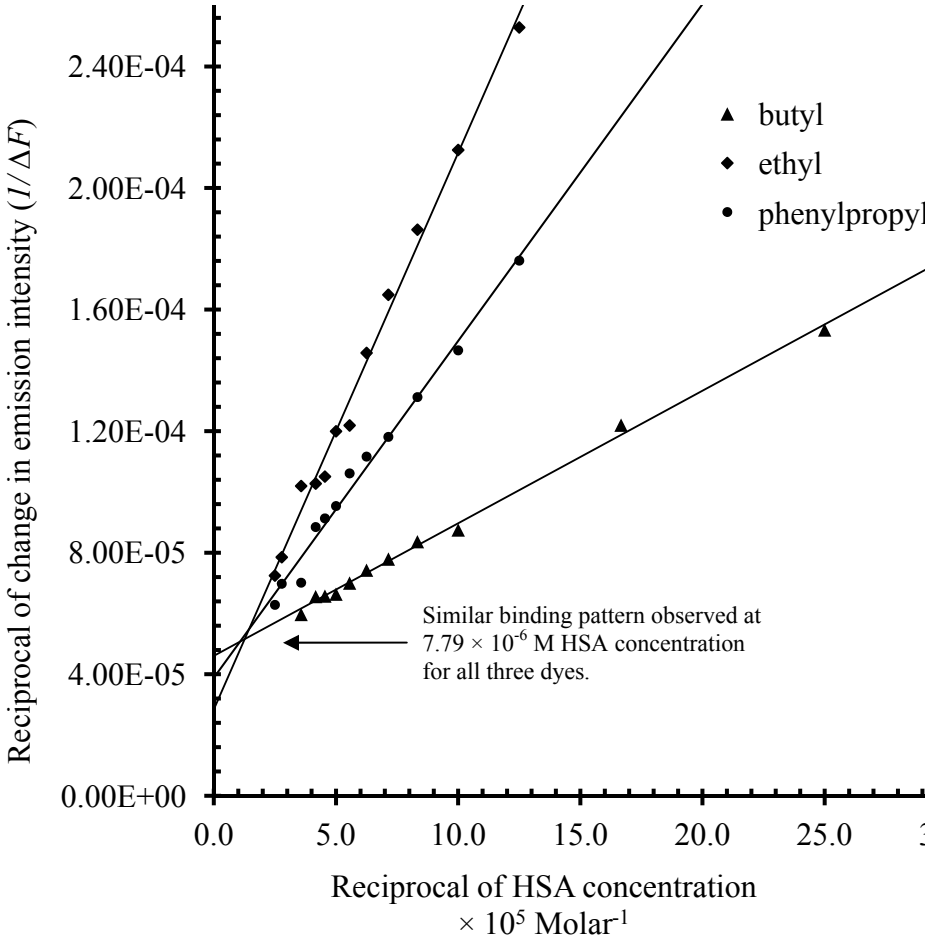

Figure 3.3 Scatchard Plots of cyanine dyes at constant concentration of 1.0 μM and increasing HSA concentration in the 0 to 2.0 μM range. Benz[*c,d*]indolium cyanine dyes with different indolium substituents.

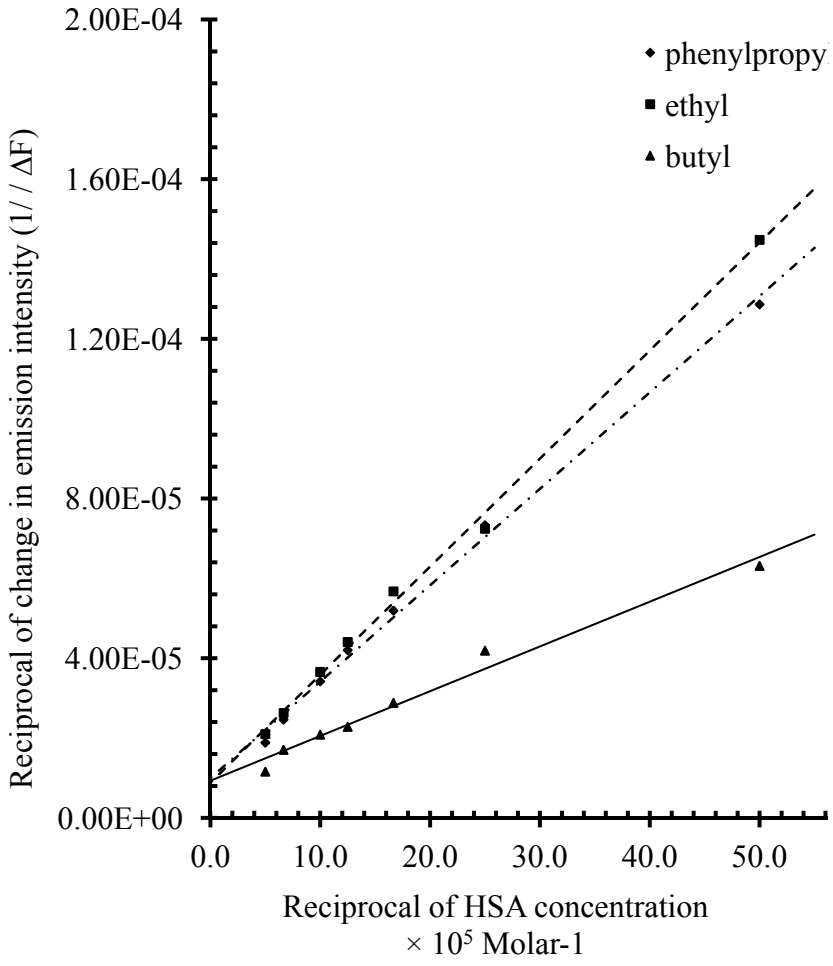

Figure 3.4 Scatchard Plots of cyanine dyes at constant concentration of 1.0 μM and increasing HSA concentration in the 0 to 2.0 μM range. Benz[*e*]indolium cyanine dyes with different indolium substituents.

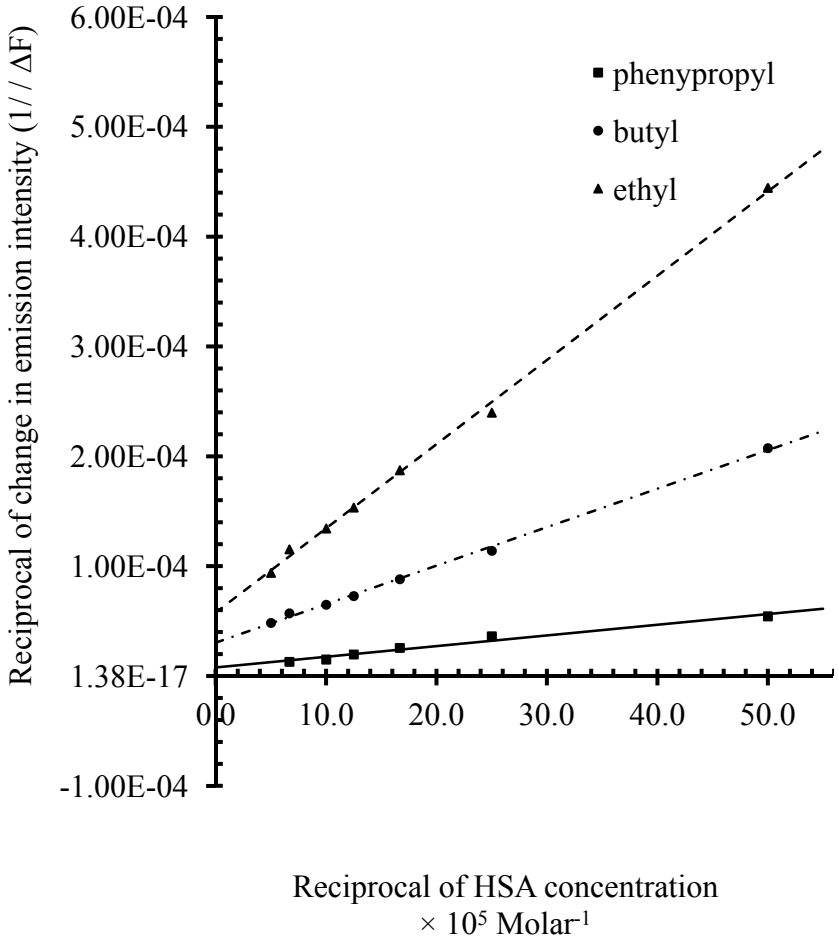

Figure 3.5 Scatchard Plots of cyanine dyes at constant concentration of 1.0 μM and increasing HSA concentration in the 0 to 2.0 μM range. Fischer indolium cyanine dyes with different indolium substituents.

Table 3.1 Preliminary results showing the effects *N*-indoline sidechain substitution on the photophysical properties of trimethine dyes. Binding to the hydrophobic binding domains of the serum albumin improves with increased hydrophobicity of the ligands.

Cyanine Dye	Indolium Side chain	Abs (λ_{max}) [nm]	Em (Em_{max}) [nm]	Molar Absorptivity (ε) $M^{-1}cm^{-1}$	*Log P* value*	Binding Affinities (K_a) $\times 10^5 M^{-1}$	Quantum Yield (in methanol)
MHI-06	- $(CH_2)_3CH_3$	758	774	116,000	9.26	10.60	0.0047
MHI-21	- CH_2CH_3	764	771	143,000	7.46	1.55	0.0036
MHI-36	- $(CH_2)_3C_6H_5$	758	775	124,000	11.03	3.51	0.0061
E-6	- $(CH_2)_3CH_3$	531	605	106,900	8.57	8.75	0.0112
E-14	- CH_2CH_3	529	561	149,500	7.68	7.54	0.0200
E-04	- $(CH_2)_3C_6H_5$	532	565	149,100	10.34	8.03	0.0058
E-18	- $(CH_2)_3CH_3$	572	605	103,000	10.09	8.33	0.0124
E-05	- CH_2CH_3	569	603	122,700	9.19	3.25	0.0041
E-08	- $(CH_2)_3C_6H_5$	572	607	117,300	11.60	4.14	0.0171

*PC MODEL v. 9.0

Indocyanine Green (ICG) is used as standard for quantum yield determination of Benz[*c,d*]indolium dyes, with Φ_f value of 4.2% determined by Reindl *et al*. [36]

Fluorescein is used as standard for quantum yield determination Benz[*e*]indolium and Fischer indolium dyes , with Φ_f value of 79% determined by Magde *et al*. [37]

3.3 Summary

The utility of near-infrared cyanine dyes in biomedical and clinical research highlights their unique hydrophobic characteristics in aqueous solutions and has been quite useful for protein labeling, DNA sequencing, DNA intercalation, *in vivo* tissue imaging among numerous other bioanalytical assays. Owing to the ability to self-aggregate in polar solvents due to the planar π-π electron conjugation systems, changes in the hydrophobic moieties of the dyes serve a viable option of monitoring binding affinity with biomolecules such as serum albumin. In addition to the enhanced binding site specificity, the unique hydrophobic behavior of the three classes of cyanine dyes presented in this article reveals photophysical properties that are suitable for binding site characterization and changes the overall 3-dimensional structure. Whereas previous results have sought to examine the effect of hydrophobicity on the overall conjugate formation of these fluorescence chromophores with serum albumin, these studies demonstrate how the combination of ligand size and hydrophobic properties may also affect conjugation. There is a general pattern of increased binding affinity with increased hydrophobicity among these dyes. However, this pattern is also affected by steric hindrance beyond a certain ligand size. Nonetheless, further studies are needed to fully examine the utility of the hydrophobic characterization of these novel carbocyanine chromophores for binding site specific bioanalytical assay. Besides it would be quite useful to establish a relationship between ligand size and hydrophobic properties for key albumin binding small molecules. This binding data would not only provide useful information on the effect of side chain substitution as it relates enzyme interaction, but would also give a better understanding as to the role played by the alkyl sulfonate side chains in relationship to the overall enzyme catalysis. Any experimental result that directly or indirectly relates dye structure to enzyme activity is considered a tool in the design of this new bioassay being developed to

study the catalytic activity of alkane monooxygenase. Thus in optimization of ligand design for best biomolecular interaction any three of the chromophores could be equally as useful, possessing an *N*-butyl substituents is the more important factor. However, other previous experiments suggest that the Fischer indolium chromophore backbone is applicable.

3.4 References

1. C. Colyer, *Cell Biochemistry and Biophysics*, 2000, **33**, 323-337.
2. N. S. Kosower, E. M. Kosower, G. L. Newton and H. M. Ranney, *Proceedings of the National Academy of Sciences of the United States of America*, 1979, **76**, 3382-3386.
3. R. K. Behera, A. Mishra and G. B. Behera, *Indian Journal of Chemistry Section B-Organic Chemistry Including Medicinal Chemistry*, 2000, **39**, 783-786.
4. A. Mishra, R. K. Behera, P. K. Behera, B. K. Mishra and G. B. Behera, *Chemical Reviews*, 2000, **100**, 1973-2011.
5. T. Fukushima, N. Usui, T. Santa and K. Imai, *Journal of Pharmaceutical and Biomedical Analysis*, 2003, **30**, 1655-1687.
6. K. Ohno, S. Suzuki, T. Fukushima, M. Maeda, T. Santa and K. Imai, *Analyst*, 2003, **128**, 1091-1096.
7. H. A. Bardelmeijer, H. Lingeman, C. de Ruiter and W. J. M. Underberg, *Journal of Chromatography A*, 1998, **807**, 3-26.
8. G. Patonay, J. S. Kim, R. Kodagahally and L. Strekowski, *Applied Spectroscopy*, 2005, **59**, 682-690.
9. F. Meadows, N. Narayanan and G. Patonay, *Talanta*, 2000, **50**, 1149-1155.
10. G. Patonay, G. Beckford, L. Strekowski, M. Henary, J. S. Kim and S. Crow, 2009.

11. A. J. Sophianopoulos, J. Lipowski, N. Narayanan and G. Patonay, *Applied Spectroscopy*, 1997, **51**, 1511-1515.

12. J. Sowell, K. A. Agnew-Heard, J. C. Mason, C. Mama, L. Strekowski and G. Patonay, *Journal of Chromatography B*, 2001, **755**, 91-99.

13. J. Sowell, J. C. Mason, L. Strekowski and G. Patonay, *Electrophoresis*, 2001, **22**, 2512-2517.

14. T. G. G. Vo-Dinh, [Cambridge], 2003.

15. R. J. Williams, J. M. Peralta, V. C. W. Tsang, N. Narayanan, G. A. Casay, M. Lipowska, L. Strekowski and G. Patonay, *Applied Spectroscopy*, 1997, **51**, 836-843.

16. J. S. Kim, R. Kodagahally, L. Strekowski and G. Patonay, *Talanta*, 2005, **67**, 947-954.

17. V. Kumar, G. A. Baker and S. Pandey, *Chemical Communications*, 2011, **47**, 4730-4732.

18. Y. Z. Zhang, H. Y. Du, Y. L. Tang, G. Z. Xu and W. P. Yan, *Biophysical Chemistry*, 2007, **128**, 197-203.

19. Y. Z. Zhang, J. F. Xiang, Y. L. Tang, G. Z. Xu and W. P. Yan, *Dyes and Pigments*, 2008, **76**, 88-93.

20. J. K. Jin, J. Z. Sun, Y. Q. Dong, H. P. Xu, W. Z. Yuan and B. Z. Tang, *Journal of Luminescence*, 2009, **129**, 19-23.

21. W. Y. Yan and C. L. Colyer, *Journal of Chromatography A*, 2006, **1135**, 115-121.

22. A. S. Kashin and A. S. Tatikolov, *High Energy Chemistry*, 2009, **43**, 480-488.

23. A. S. Tatikolov, A. A. Ishchenko, M. A. Kudinova and I. G. Panova, *High Energy Chemistry*, 2010, **44**, 304-310.

24. Y. Z. Zhang, Q. F. Yang, H. Y. Du, Y. L. Tang, G. Z. Xu and W. P. Yan, *Chinese Journal of Chemistry*, 2008, **26**, 397-401.

25. S. Karaca and N. Elmaci, *Computational and Theoretical Chemistry*, 2011, **964**, 160-168.

26. F. Luschtinetz, C. Dosche and M. U. Kumke, *Bioconjugate Chemistry*, 2009, **20**, 576-582.

27. L. Tarazi, H. Choi, J. C. Mason, J. Sowell, L. Strekowski and G. Patonay, *Microchemical Journal*, 2002, **72**, 55-62.

28. L. Tarazi, N. Narayanan and G. Patonay, *Microchemical Journal*, 2000, **64**, 247-256.

29. G. Patonay, J. Salon, J. Sowell and L. Strekowski, *Molecules*, 2004, **9**, 40-49.

30. F. Welder, B. Paul, H. Nakazumi, S. Yagi and C. L. Colyer, *Journal of Chromatography B-Analytical Technologies in the Biomedical and Life Sciences*, 2003, **793**, 93-105.

31. M. Y. Berezin, H. Lee, W. Akers, G. Nikiforovich and S. Achilefu, *Photochemistry and Photobiology*, 2007, **83**, 1371-1378.

32. M. Y. Berezin, H. Lee, W. Akers and S. Achilefu, *Biophysical Journal*, 2007, **93**, 2892-2899.

33. E. Peyrin, Y. C. Guillaume and C. Guinchard, *Biophysical Journal*, 1999, **77**, 1206-1212.

34. S.-i. Fujiwara and T. Amisaki, *Chemical & Pharmaceutical Bulletin*, 2011, **59**, 860-867.

35. Y. Y. Zhou, H. W. Xu, H. P. Yu, L. Chun, Q. Lu and L. Wang, *Spectrochimica Acta Part a-Molecular and Biomolecular Spectroscopy*, 2008, **70**, 411-415.

36. S. Reindl, A. Penzkofer, S. H. Gong, M. Landthaler, R. M. Szeimies, C. Abels and W. Baumler, *Journal of Photochemistry and Photobiology a-Chemistry*, 1997, **105**, 65-68.

37. D. Magde, R. Wong and P. G. Seybold, *Photochemistry and Photobiology*, 2002, **75**, 327-334.

4 CAPILLARY ELECTROPHORESIS IN STUDYING COMPLEX DYE-BIOMOLECULE INTERACTIONS

4.1 The principle of Capillary Electrophoresis

Capillary electrophoresis describes a separation technique that is based on the distribution of charged analytes in a buffer solution or slab gel according to their differential electrophoretic mobilities[1]. This separation is facilitated by the application of high direct voltage (or dc current) at both end of a narrow-bore capillary (20-200 microns) which generates both an electroosmotic and electrophoretic flow of buffer solution *(see equation 4.1)*. Typically, the properties of the separation exhibit characteristics resembling both polyacrylamide gel electrophoresis (PAGE) and high performance liquid chromatography (HPLC) in tandem[1, 2].

$$\mu_{ep} = \frac{v_{ep}}{E} = \frac{L_d/t_m}{V/L_t} \qquad (4.1)$$

where μ_{ep} represents electrophoretic mobility (cm^2/Vs), v_{ep} is electrophoretic velocity (cm/s), L_d is the length of the capillary to the detector, L_t is the total length, E is the electric field strength and V is the applied voltage.

These combined properties of liquid chromatography and electrophoresis offers diverse advantages of and can be described as;

- Employs capillary tubing within which the electrophoresis occurs.
- Utilizes very high electrostatic field strengths, often higher than 500 V/cm.
- Uses modern detector technology such that the electropherogram appear similar to a chromatogram.
- Exhibit efficiencies on the order of capillary gas chromatography or even higher.
- Requires minutes sample volume easily automated for precise quantitative analysis.

- Limited consumption of reagents
- Applicable to wider selection of analytes compared to other analytical separation techniques.

The generic instrumental configuration of a typical CE is relative simple with the main focus being the open narrow-bore fused silica capillary with an optical window approximately 7 cm on one end for direct detection, two background electrolyte (BGE) or buffer reservoirs, two stainless steel assemblies and a controllable direct current high voltage power supply. The detection type can vary but are most often either a direct UV absorbance or a diode array detection setup as shown in figure 4.1.

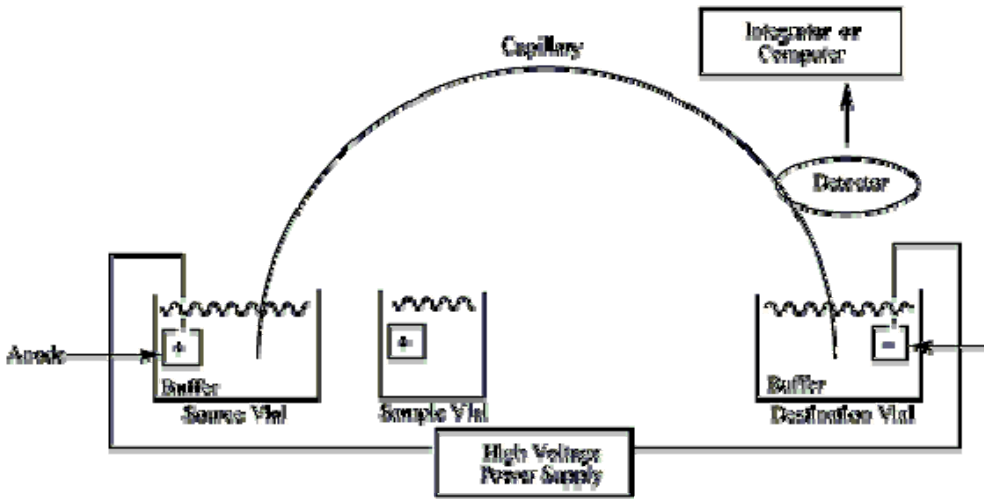

Figure 4.1 Basic configuration of capillary electrophoresis and representation of electroosmotic flow in CE.

Most modern CE instrument in bioanalytical research are also equipped with autosample, electrokinetic and pneumatic injection assemblies, precise temperature control system and a heat dissipation assembly.

4.2 Operation of a Capillary Electrophoresis separation technique

Similar to other commonly purification techniques such as HPLC and GC, effective CE separation with subsequent bioanalyses are influenced by numbers instrumental parameters. Chief among these are the; electroosmotic force (EOF), injection technique, capillary size, separation voltage and temperature.

4.3 The effects of Electroosmosis on separation efficiency

The fundamental driving force in delivering the CE separation is the principle of electroosmosis. This property is the result of the establishment of opposite surface charges on the inner walls of the fused-silica capillary. These wall surfaces are characterized by ionizable silanol groups that are in constant contact with the mobile phase or buffer solution. The ionic potential of the fused silica is ca. 1.5 and the extent of ionization is controlled by the pH of the buffer. This creates a net movement of analytes through the capillary referred to as the electroosmotic flow (EOF). Equation 2 related the EOF to the viscosity of the buffer and the zeta potential[3, 4].

$$v_{eo} = \frac{\epsilon\xi}{4\pi\eta} E \qquad (4.2)$$

Where ϵ represents the dielectric constant, η is the viscosity of the buffer, ξ is the zeta potential measured at the plane of shear close to the liquid-solid interface.

During capillary conditioning, the negatively charges silica walls will attract positively charged ions from the buffer thus creating a charged double layer that facilitates the EOF[5]. Under the application of the high DC potential, cations are transported towards the negatively charged electrode (cathode) under the influence of both the EOF and the established electrophoretic force, neutral analytes are carried with the EOF while negatively charged ions are carried against their innate electrophoretic migration away from the positively charged electrode (anode) towards the cathode by the stronger EOF [6-8]. Thus there is a net migration towards the cathode irrespective of charge. However, molecules arrive at the cathode of the detector end of the capillary base on a positive charge to mass (*z/m*) ratio[9, 10]. Smaller high positively charged species will arrive first followed by the neutral species (in one separation band unless some neutral separator additive is used) while smaller highly negatively charged species arrive last or with the greatest migration time as shown in figure 4.2. The efficiency of the separation is highly affected by the zeta potential, which is inversely related to the charged per unit surface area of the capillary, the number of valence electrons, and the square root concentration of the buffer. Thus, as shown in equation 2, an increase the buffer concentration results in decreased EOF. This is a key phenomenon is achieving bio-separation and developing a NIR dye based bioanalytical technique to study complex enzymatic processes.

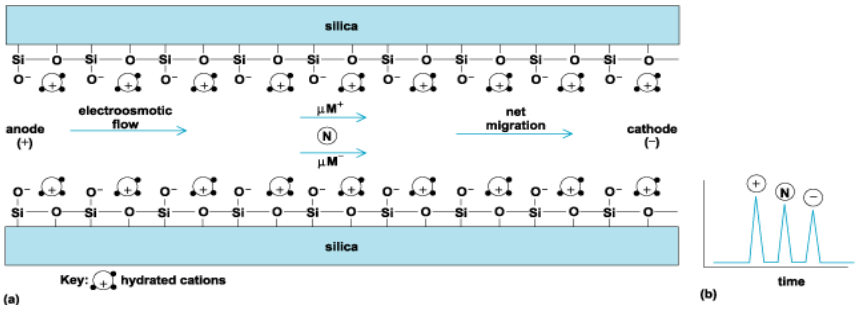

Figure 4.2 Basic configuration of fused-silica capillary showing the migration order of analytes having different charge to size ratio.

4.4 The effects of voltage and temperature on separation efficiency

Voltage and temperature are two of the common separation parameters that can influence the outcome of a CE analysis. Throughout the development of this new bioanalytical technique to study a key enzymatic catalysis all temperatures were maintained at 24 ^{0}C, just below room temperature as the preserve the complex biomolecules. However, in order to develop the technique the applied voltage was among the factors varied to achieve best separation and quantitative analyses.

Both the EOF and the electrophoretic velocities of the CE separation are proportional to the field strength and any increase in voltage would result in reduced run time. Research has revealed[11, 12] that shorter migration time may yield higher efficiencies and limiting other ill-effects such as band broadening and joule heating. However, the with lower migration time, the sample makes less contact with the silanol walls of the capillary which could also result in poor separa-

tion and resolution. To develop this bioanalytical technique, standard analysis were performed at varied potential between 5.0 and 25.0 kilovolts until the optimum separation potential was achieved, having optimized all the other key separation parameters[6-8].

4.5 The effects of capillary size (internal diameter) and joule heating on separation efficiency

Under in influence of high electric field strength, heat production within the capillary is inevitable and must be addressed in order to achieve satisfactory CE separation. Unlike controlling operational delocalized heating which was earlier discussed, monitoring joule heating in a CE separation can be much more problematic and poses a greater threat to the success of the analysis. There are two major limitations that will arise from heat production in the capillary during separation; 1) increase temperature gradients across the capillary and 2) temperature changes with time due to ineffective heat dissipation. Typically, the rate of heat generation in the fused-silica capillary can be expressed as;

$$\frac{dH}{dt} = \frac{iV}{LA} \qquad (4.3)$$

where L represents the capillary length (cm), A is the cross sectional area. Since $i = V/R$ and $R = L/kA$ where k is the conductivity.

$$\frac{dH}{dt} = \frac{kV^2}{L^2} \qquad (4.4)$$

Because the amount of heat generated is directly proportional to the square of the field strength. An increase in the length of the capillary or a decrease in applied voltage can dramati-

cally reduce joule heating and improve separation efficiencies. In addition, lowering the concentration of the buffer (with limits) or using a lower conducting buffer may also produce similar results of reduced joule heat generation. Besides, temperature gradient across the capillary wall is uniform and heat is dissipated by diffusion, temperature at the center of the capillary is greater than at the walls. This is another factor that may affect migration and overall efficiency of the separation.

An increased joule heat production may also affect the viscosity of the separation buffer. Since viscosity displays an inverse relationship with overall temperature, both the EOF and the electrophoretic mobility (EPM) will be increased as well. This phenomenon will lead to the formation of a hydrodynamic flow profile that may introduce band broadening. Besides, lowering the internal diameter of the capillary improves the separation for two main reasons; 1) the current per unit length of the capillary is reduced by the square of the capillary radius and 2) the heat is more easily dissipate across the narrower radial path of the capillary[2, 6, 8]. This results in a thermal gradient that is proportional to the square of the diameter of the capillary, which can be approximated using equation 4.5.

$$\Delta T = 0.24 \frac{Wr^2}{4K} \qquad (4.5)$$

Where W represents the power (iV), r is capillary radius and K is the thermal conductivity.

Variation in capillary size is one other factor that was monitored in order to develop the new bioanalytical technique. Typical fused-silica capillary used were in the order of 49 to 75 microns internal diameter (ID) and 150 to 200 microns outside diameter (OD).

4.6 Modes of CE separation

There are many mode of separation used CE analyses in studying complex biomolecules. Among these, the five most commonly encountered modes of operation include; capillary isoelectric focusing (CIEF), capillary gel electrophoresis (CGE), capillary zone electrophoresis (CZE) and micellar electrokinetic capillary chromatography (MEKC). The study involving the monooxygenase enzyme only involved MEKC and CZE techniques however, due to inconsistencies CZE was chosen as the primary separation technique, nonetheless the MEKC technique will be discussed in details.

Table 4.1 CE technique based on the type of sample to be analyzed.

Small ions	**Small molecules**	**peptides**	**proteins**	**Oligonucleotides**	**DNA**
CZE	MECC	CZE	CZE	CGE	CGE
ITP	CZE	CGE	CGE	MECC	
	ITP	IEF	IEF		
		ITP	ITP		
		MECC			

4.7 Capillary zone electrophoresis (CZE)

CZE is the simplest mode of capillary electrophoresis and is also the most commonly used technique in bioanalyses. This technique involves the direct filling of the capillary solely with the mobile phase run buffer. The primary principle to CZE is solutes moves with different mobility in sample zone. This differential movement of the analytes is based on a charge-to-mass

ratio with small highly charged species eluting first, while the small highly negatively changed one eluting last. Unlike many of the other popular used electrophoresis techniques, the run buffer remains homogenous and constant field strength is maintained throughout the entire length of the capillary.

Once the sample is injected and a direct current or voltage is applied, the components of the sample are separated into discrete zones or separation bands. The net charge of each individual analyte is usually pH dependent hence, selectivity can be easily achieved by varying the pH of buffer or/ and mixing additives, such as surfactants. The pH dependence and its effect on selectivity dictate that the running buffer pH be maintained constant during the entire separation process.

4.8 Micellar electrokinetic capillary chromatography (MEKC)

MEKC is another form of electrophoresis technique that is commonly used in bioanalyses for separating analytes such as antibodies, proteins and nucleic acids. MEKC is most often performed when separation of small charged or uncharged molecules is required. This method involves the use of a micelle-forming surfactant solution that creates a separation mode that resembles a conventional liquid chromatography (LC) with the unique benefits of the capillary electrophoresis. Unlike classical CZE that only separates charged analytes, MEKC can also separate uncharged species by the formation of the molecular encapsulating micelles that are usually either negatively or positively charged. At a critical micelle concentration, individual surfactants aggregate to form the micellar structures which follow the same or opposite direction of EOF. Because EOF is faster than micelle migration in neutral or basic solution, the apparent direction

of micelle migration is same as that of EOF; towards the detector. During electroosmosis, the micelle migrate similarly, it has hydrophobic and/or electrostatic interactions with solutes, as in the stationary phase in chromatography, and then the nonionic solutes can be separated by the interaction with micelle.

There are four main types of surfactants used in MEKC. There are cationic, anionic, zwitterionic and nonionic surfactants used for bioanalyses. While the choice of surfactant is typically discretionary, the chemical and physical nature of the analytes is an important factor when any mobile phase additive is considered. Table 4.2 list some commons surfactants used in MEKC and the associated critical micelle concentrations (CMC)

Table 4.2 Technique based on the type of sample to be analyzed.

Surfactant	Type	CMC	Aggregation no.
SDS	Anionic	8.1×10^{-3}	62
CTAB	Cationic	9.2×10^{-4}	170
Brij-35	Nonionic	1.0×10^{-4}	40
Sulfobetaine	Zwitterionic	3.3×10^{-3}	55

SDS – sodium dodecyl sulfate, CTAB – cetyltrimethylammonium bromide, Brij-35 – polyoxyethylene-23-lauryl ether, sulfobetaine – *N, N*-dimethylammonium-3-propane-1-sulfonic acid

4.9 Type of detection techniques in capillary electrophoresis

There are many different detection modes that are used in the modern capillary electrophoresis instruments. While most of the CE detection modes are based around very contrasting operational principles, each is developed with the advantage of speed and high separation efficiency. In comparison to conventional liquid chromatography, CE is exhibits the ability for both on-column and off-column detection such as UV-Vis absorption, chemilluminescence, fluorescence, refractive index, mass spectrometry and so forth. However, due to the small detection window of the capillary and small volume of sample injected, the technique requires highly sensitive detection systems. More sensitive detection modes like electrochemical detection (ECD) and inductively coupled plasma atomic emission (ICP-AE) become more tedious and time consuming and thus the use of the more costly ultra-microelectrodes must be employed. This is because the high voltage applied to create the separation can easily affect the on column detection.

Because of the inherent limitations of the on-column detection, more CE analyses are being conducted using off-column detection instead. This mode of detection however may lead to band broadening which is attributed to laminar flow inside the capillary during the analysis. Despite the detection method used, each exhibits its own unique advantages and limitations. Here, we will further discuss fluorescence detection and its benefits in developing new bioanalytical assays. A brief description of available detectors is also presented in table 4.3.

.

4.9.1 Fluorescence detection CE

Fluorescence detection is becoming increasing popular in CE and LC for bioanalyses. This detection mode is well documented in literature for its convenience, low cost, flexibility and avail-

ability[1, 13-21]. Traditional fluorescence detection is known to utilize conventional deuterium or xenon lamps as light sources but more instruments are incorporating laser induced excitation. It is clear that the deuterium or xenon lamps provide a more stable light signal over a wide spectrum range however the use of lasers greatly improves sensitivity and detectability. This enhanced sensitivity is due in part to the fact that since the fluorescence is measured against zero background signal[13, 16, 21] thus enabling an increased signal-to-noise ratio. But more importantly, lasers can be easily incorporated into the CE system by light-controlled feedback or by doubling of diode lasers, which in turns remarkably increases sensitivity. Besides, the use of a NIR laser and the ability to focus the light into a small volume inside the capillary to excite the analyte creates higher than normal efficiency and reduces the light scattering effects of the capillary walls.

The most commonly encountered on-column NIR laser induced Fluorescence CZE (NIR-LIF-CZE) detection setup incorporates a stable high intensity NIR laser diode (or dye laser) with little to no tenability in wavelength. It also includes microscope objectives, focusing mirrors and a photomultiplier tube (PMT) capable of detecting in the Vis-NIR range. As shown in figure 4.3, the Beckman Coulter Co. designed device is equipped with collinear rather than an orthogonal geometry with an optical filter and an ellipsoidal mirror. In the scheme, a combined notch and band pass optical filter pair is inserted in an axial excitation beam and placed at 180^{0} to the capillary and PMT. Even though the detector is in-line to the source, the combination of the notch and bandpass filter setup allows for detection levels in the order of femto molar with the suitable NIR fluorophores. This detection setup provides the ultimate detection limits and sensitivity for complex biochemical process that would rather be affected by strong background noise if another detection technique was utilized.

Table 4.3 Outline of list of Capillary electrophoresis detection technique.

Detection Method	Mass detection limit (grams)	Concentration detection limit (moles)	Advantages/ Limitations
		Spectroscopic detection methods	
UV-Visible Absorbance	$10^{-13} – 10^{-15}$	$10^{-5} – 10^{-6}$	• Universal technique • Multi-wavelength detection possible • Diode array detector can provide spectral information on analytes
Fluorescence	$10^{-15} – 10^{-18}$	$10^{-7} – 10^{-9}$	• Very sensitive • May require derivitisation • Xenon source can be costly •
Laser Induced Fluorescence (LIF)	$10^{-18} – 10^{-21}$	$10^{-14} – 10^{-16}$	• Extremely sensitive • May require derivitisation • Laser source usually inexpensive
Mass Spectrometry (MS)	$10^{-16} – 10^{-17}$	$10^{-8} – 10^{-9}$	• Sensitive • Capable of providing structural information
Indirect UV and Fluorescence	10 – 100 times less than direct method		• Universal • Lower sensitivity than direct methods • May be affected by electrolyte matrix effect
		Non-spectroscopic detection methods	
Amperometry	$10^{-18} – 10^{-19}$	$10^{-10} – 10^{-11}$	• Very sensitive • Selective but useful only for electroactive analytes • Requires special electronics and capillary modifications
Conductivity	$10^{-15} – 10^{-16}$	$10^{-7} – 10^{-8}$	• Universal • Requires special electronics and capillary modification

4.10 Summary

The use of capillary electrophoresis to study the interaction of complex biomolecules has proven quite successful in investigating new binding modalities involving fluorescent dyes and molecules such as protein, nucleic acids and enzymes. Unlike many other bioassays such as high performance liquid chromatography and slab gel electrophoresis, the technique has become well established in both analysis and purification of biopolymers irrespective of the type of analytes being analyzed. The merits of the technique include simplicity and high purity where purification is required. Major limitations experienced with other popular techniques such as labor intensiveness, long analysis time, poor efficiency, automation and problems with detector type are easily overcome by the versatility of the technique and the ease of both method and instrumentation adjustments with little adverse effect on performance.

There are numerous operation modes and separation mechanisms in CE analyses. Key among these mechanisms is the CZE. The main advantage of CZE is the fact that same uniform equipment is applied regardless of the type of samples analyzed. Also, the possibility to substitute the standard Arc lamp source used for absorbance studies with the more sensitive laser diode for fluorescence detection makes CZE more versatile and capable of detecting a wider variety of biopolymers for lower LOD and LOQ values. In addition, other photophysical benefits can be realized when the laser source includes NIR laser diodes creating the more powerful near infrared laser induced fluorescence capillary zone electrophoresis (NIR-LIF-CZE). This coupled effect of NIR spectroscopy and LIF has made the technique more robust, sensitive and efficient for bioanalyses at the sub-nano molar concentration levels. These factors have allowed the NIR-LIF-

CZE to be assessed as a suitable bioanalytical technique to study enzyme catalysis involving water soluble Vis-NIR active substrates.

4.11 References

1. T. Fukushima, N. Usui, T. Santa and K. Imai, *Journal of Pharmaceutical and Biomedical Analysis*, 2003, **30**, 1655-1687.
2. I. E. Valko, H. Siren and M. L. Riekkola, *Journal of Microcolumn Separations*, 1999, **11**, 199-208.
3. C. L. A. Berli, M. V. Piaggio and J. A. Deiber, *Electrophoresis*, 2003, **24**, 1587-1595.
4. C. J. Evenhuis, R. M. Guijt, M. Macka, P. J. Marriott and P. R. Haddad, *Electrophoresis*, 2006, **27**, 672-676.
5. J. H. Flanagan, C. V. Owens, S. E. Romero, E. Waddell, S. H. Kahn, R. P. Hammer and S. A. Soper, *Analytical Chemistry*, 1998, **70**, 2676-2684.
6. C. A. Keely, T. Vandegoor and D. McManigill, *Analytical Chemistry*, 1994, **66**, 4236-4242.
7. B. Potocek, B. Gas, E. Kenndler and M. Stedry, *Journal of Chromatography A*, 1995, **709**, 51-62.
8. Z. Q. Wu, X. D. Cao, L. Chen, J. R. Zhang, X. H. Xia, Q. Fang and H. Y. Chen, *Electrophoresis*, 2010, **31**, 3665-3674.
9. J. Sowell, K. A. Agnew-Heard, J. C. Mason, C. Mama, L. Strekowski and G. Patonay, *Journal of Chromatography B*, 2001, **755**, 91-99.
10. W. Y. Yan, A. L. Sloat, S. Yagi, H. Nakazumi and C. L. Colyer, *Electrophoresis*, 2006, **27**, 1347-1354.

11. N. Nuchtavorn, P. Smejkal, M. C. Breadmore, R. M. Guijt, P. Doble, F. Bek, F. Foret, L. Suntornsuk and M. Macka, *Journal of Chromatography A*, 2013, **1286**, 216-221.

12. Y. Y. Xu, X. Y. Niu, Y. L. Dong, H. G. Zhang, X. Li, H. L. Chen and X. G. Chen, *Journal of Chromatography A*, 2013, **1284**, 180-187.

13. P. L. Chang, K. H. Lee, C. C. Hu and H. T. Chang, *Electrophoresis*, 2007, **28**, 1092-1099.

14. T. C. Chiu, W. C. Tu and H. T. Chang, *Electrophoresis*, 2008, **29**, 433-440.

15. P. Y. Diao, H. Y. Yuan, F. Huo, L. F. Chen, D. Xiao, M. C. Paau and M. M. F. Choi, *Talanta*, 2011, **85**, 1279-1284.

16. C. Huhn, L. R. Ruhaak, J. Mannhardt, M. Wuhrer, C. Neususs, A. M. Deelder and H. Meyer, *Electrophoresis*, 2012, **33**, 563-566.

17. S. Mallampati, A. Van Aerschot, J. Hoogmartens and A. Van Schepdael, *Electrophoresis*, 2007, **28**, 3948-3956.

18. T. Revermann, S. Gotz and U. Karst, *Electrophoresis*, 2007, **28**, 1154-1160.

19. Y. Z. Xu, S. Chen, X. J. Feng, W. Du, O. M. Luo and B. F. Liu, *Electrophoresis*, 2008, **29**, 734-739.

20. X. P. Yang, F. Huo, H. Y. Yuan, B. Zhang, D. Xiao and M. M. F. Choi, *Electrophoresis*, 2011, **32**, 268-274.

21. X. P. Yang, H. Y. Yuan, C. L. Wang, S. L. Zha, D. Xiao and M. M. F. Choi, *Electrophoresis*, 2007, **28**, 3105-3114.

5 INVESTIGATING THE CATALYTIC ACTIVITY OF ALKANESULFONATE MONOOXYGENASE USING NEAR INFRARED DYES BASED CAPILLARY ZONE ELECTROPHORESIS BIOASSAY

5.1 Introduction

Among the most popular methods of detecting bacteria species are those that involve cultures grown on differential agar media followed by culture and colony counting assays, like polymerase chain reaction (PCR)[1-3]. While these techniques are quite useful, they exhibit a myriad of limitations and are often times considered labor intensive, time consuming and are solely for *in vivo* detection. Vis-NIR spectroscopic enzymatic detection promises a rigorous *in vitro* detection with the advantage of portability, speed, sensitivity and possibility of 'on-the-spot' detection. In addition, while conventional methods are designed to provide qualitative results, spectroscopic bioanalytical assay can also provide precise analytical data to quantitate the enzyme activity of alkanesulfonate monooxygenase that is an indication of organism viability.

5.1.1 E. coli and sulfate assimilation

Sulfur is known to play a vital role in the growth and proliferation of most bacterial organisms. While many bacteria species possess the ability to utilize inorganic sulfur for the production of sulfur-containing metabolites, the accessibility of inorganic sulfur aerobic soil remains a challenge for these organisms. In absence cysteine or under sulfate-starvation conditions, the organism expresses two operons whose products are capable of enabling the assimilation of sulfur from other sulfur containing compounds mainly taurines and aliphatic alkanesulfonates. The *E*. coli organism utilizes a two-component alkanesulfonate monooxygenase system to synthesize either taurine dioxygenase or alkanesulfonate monooxygenase proteins which enables the uptake of sulfur from the alternate sources[4-7]. In the sulfate assimilation reaction, the monooxygenases enzyme uses flavin as a substrate instead of a bound prosthetic group[6, 7] . Thus, this results in the catalytic oxygenolytic cleavage of *1*-substituted alkanesulfonates in the presence dioxygen and

$FMNH_2$, hereby producing a sulfite, which is then assimilated into the sulfur-containing compounds, along with the formation of the corresponding aldehyde. Among the most popular bacteria types that express this alkane monooxygenase enzyme are the *Escherichia* coli species. *E*. coli, as they are commonly called is a type of bacteria commonly found in the intestinal tracts of humans and many other warm-blooded animals. Because of its rather wide distribution, it is often considered as an indicator organism and is quite specific for water pollution and a reliably reflects fecal contamination[8]. Different strains of *E*. coli are known to be involved in many types of gastrointestinal diseases such as diarrhea and even more serious illnesses like inflammations and urinary tract infections and peritonitis in immune-suppressed patients[9]. Consequently, *E*. coli contamination has always considered a great potential health risk, thus tremendous efforts are being made by different research laboratories to develop new and reliable detection techniques for key enzymes that are involved in growth and proliferation of these microorganisms[1-3, 10-15].

Recent studies by Eichhorn *et al.* demonstrated that that *E*. coli derivatives K-12[16] and B[17] strains can utilized alkanesulfonate side chains which will be attached to fluorescence dyes as sulfur sources for normal organism growth. This was further supported in data presented by Urianickelsen *et al.* involving the PAO1 *E*. coli strains [16, 18]. In addition, more work is underway to test these biochemical pathways in fecal isolate *E. coli* organisms [16]. As mentioned earlier, these fluorescent compounds possessing negatively charged *N*-indoline alkanesulfate moieties inherently dissolve in polar solvents and exhibit sharp absorption and emission peaks. However, enzymatic cleavage of the sulfate group results in aggregate formation and subsequent diminished fluorescence. However, when exposed to key binding proteins in the order of 20 to 70 kilo Daltons dyes again exhibit strong absorbance and emission.

The sulfonate assimilation processes by these sulfur fixing enzymes can cleave the charged sulfonate group thus improving bio-conjugation to proteins. The protein-ligand interaction of the dyes will reduce the aggregation tendencies in aqueous media and improve the absorbance and fluorescence properties. This technique satisfies a key bioanalytical approach for studying the expression of the $FMNH_2$-dependent alkanesulfonate monooxygenase (SsUD) enzyme in *E*. coli organisms[6]. As mentioned previously, in polar buffer solvents the alkyl sulfonate substituted dye exhibit strong Vis-NIR emission which diminishes once enzyme catalysis is achieved and the corresponding aldehyde is formed. From the early characterization of the sulfonated test substrates, this reduction and re-enhancement of the emission signal as determined by CZE underscores the usefulness of the technique as a bioassay for both *in vitro* qualitative and quantitative enzyme detection.

5.2 Methods and Procedure

5.2.1 Instrumentation

Capillary Zone Electrophoresis measurements were performed with a Beckman Coulter 5510 P/ACE instrument equipped with a 34 sample holder water cooled auto sampler (Brea, CA). The device is equipped with a NIR 635 diode laser and a visible 488 nm Xenon laser. The LIF detector was equipped with a Hamamatsu R2368 photomultiplier tube (PMT). At excitation of 635 nm, a 810 nm bandpass filter was utilized for emission signal while at excitation of 488 nm, a 520 nm bandpass and a 488 nm notch filter were used on the emission side of the detector.

5.2.2 Riboflavin photo-reduction

FMN, glucose oxidase, potassium phosphate (mono and dibasic anhydrous) and EDTA were obtained from Sigma Aldrich (St. Louis, MO). 500 μL of an oxygen free solution of FMN was prepared in an evacuated anaerobic glove box followed by equilibration with an ultrahigh purity nitrogen gas. As proposed by Zhan *et al., u*nder the anaerobic conditions, an oxygen scrubbing system comprising of 50 μL of glucose (20 mM) and 50 μL excess glucose oxidase (20 mM) were added to removed trace amounts of dioxygen. A stand alone prepared EDTA (100 50 μL, 10 Mm) was then added[19, 20]. While still under anaerobic conditions within the glove box, the reaction flask was exposed to a strong visible 250 watts Sylvania lamp source for 72 hrs. After photo-reduction, the reduced FMN was utilized for enzyme catalysis as needed under anaerobic conditions. The solution was diluted to final concentration by standardized phosphate buffer solution (10 mM, pH 7.4). All solutions are kept in the dark at 4 ^{0}C until use.

5.2.3 Preparation of substrates for enzyme catalysis

Once photo-reduction was achieved, excess amount of the reduced flavin (2 equiv.) were added to a reaction mixture containing 10 equivalents of the sulfonated dye substrate and kept at 4 ^{0}C until catalysis by adding the appropriate varied equivalents of the SsUD enzyme component.

5.2.4 Preparation of capillary

Prior to each batch of analysis, the polyacrylamide coated capillary was prepared by washing with two sodium hydroxide solutions each for a period of 60 minutes. First it was washed with a 1.0 M and then a 0.1 M solution of the base. The capillary was then rinsed with the running buffer/ electrolyte also for 60 minutes and finally with double de-ionized water for

60 minutes as well. In between analyses, the capillary walls were re-generated with 5 minutes consecutive rinses with both sodium hydroxide solutions in the same order as previously, then with the buffer and finally with water, both for 10 minutes. The entire wash and re-generation cycles were performed pneumatically while all sample injections were done by means of electro-kinetic injection as to maintain stable lamina flow patterns during separation.

5.2.5 LIF-NIR CZE Analysis of the catalytic process

The CZE analyses were performed applying a high DC voltage (5 to 25 kV) across a thin poly-acrylamide capillary (49 to 75 microns ID and varied length to achieve best peak efficiency) using a phosphate buffer (10 mM, pH 7.4) as the running electrolyte/ buffer. The sample was injected electro kinetically for 3 seconds and capillary was maintained at 24 ^{0}C by internal cooling. The SsUD enzyme was added and left to equilibrate at room temperature prior to injection under anaerobic conditions. Once injected samples were discarded and new samples prepared for repeat analyses.

5.3 Results & Discussion

5.3.1 Alkanesulfonate monooxygenase and desulfonation of fluorophores

Previous reports by Eichhorn. *et al.*, revealed that numerous of *E.* coli strains; B, BL21(DE3), C, SG60,SG61, ECOR30 and ECOR31, exhibit the alkanesulfonate monooxygenase enzyme capable of utilizing alkanesulfonates as sulfur sources for growth and proliferation [5]. Here in our labs, we instead propose the use of the isolated commercially available alkanesulfonate monooxygenase enzyme from these microorganisms to perform the sulfonate

assimilation *in vitro*. Previously, data obtained from the dye characterization studies revealed that the NIR fluorescent compounds bearing charged moieties such as the sulfonate group exhibit strong fluorescent properties in aqueous solvents. A NIR-based spectrochemical technique is developed to monitor the degradative effects of the desulfonating enzymes; reducing the sulfonated *N*-indoline aliphatic sidechains of the fluorophores to the corresponding aldehyde with a virtual loss of the strong fluorescent signal associated with these classes of dyes when dissolved in polar solvents. Alkanesulfonate monooxygenase exist as a two-component enzyme system consisting of a reductive SsUD and an oxidative SsUE component.

The reductase enzyme associated with these types of two-component system catalyzes the *in vivo* reduction of flavin with reducing equivalents provided by a pyridine nucleotide. The reductase component exhibits great specificity for either flavin mononucleotide (FMN) or the dinucleotide equivalence (FAD), and that specificity is quite observed in the monooxygenase enzyme. Research have shown that the SsUD that have been characterized either have a flavin tightly bound with a signature spectrum for oxidized flavin, or the flavin may play the the role of a substrate during catalysis. The SsuE enzyme however, does not utilize flavin as a substrate, and there was no flavin bound to the enzyme when purified [5, 6, 21]. Interestingly, SsUE also has a 1000-fold higher affinity for the oxidized form of FMN substrate over the reduced product [19, 21-24]. These results indicate that SsuE has a clear preference not only for FMN, but more so for the oxidized form of the flavin. However, while the SsUE demonstrated great prospects for *in vitro* catalysis, to date there is no reported data to confirm *in vivo* substrate transformation using the SsUD. For this reason, any *in vitro* application of alkanesulfonate monooxygenase must first involve the reduction of the FMN to the reduced form.

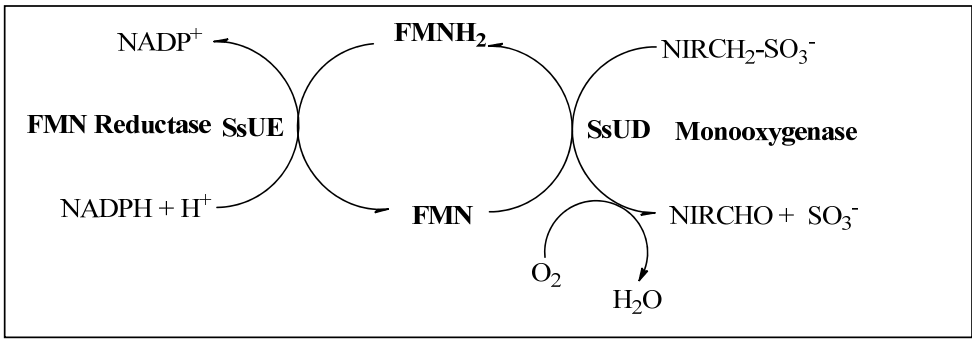

Scheme 5.1 The *in vivo* catalytic conversion of NIR sulfonated substrate to the aldehyde derivative. Because of the complex catalytic properties of this flavin dependent two component enzyme (SsUE/ SsUD), the reductive component does not occur *in vitro*, thus the riboflavin (FMN) must be first reduced $FMNH_2$ before catalysis can occur.

Similar to a modified method reported by Eichorn *et al.*, enzymatic activity is then initiated by the addition of $FMNH_2$ to the reaction mixture containing alkanesulfonate monooxygenase and the *n*-butylsulfonate substituted dye in standard phosphate buffer. The Vis-NIR absorbance and fluorescence of the mixture is utilized to monitor the catalytic activity of the enzyme. It is expected that the more hydrophobic dye species formed will self-aggregation in polar media.[5, 7, 25]. Once enzyme catalysis is achieved, it is then confirmed by the interaction of the newly formed hydrophobic dye with serum albumin through protein-ligand hydrophobic interactions. Ideally, and from the photophysical data presented in table 3.2, these dye-albumin interactions are characterized by binding affinities that are several orders greater than that of the enzyme-dye affinity[26], if the dye does interact with the enzyme subsequent to catalysis.

Dye-albumin interaction finally serves to confirm that the enzyme catalysis occurs followed by the bio-conjugation of the aggregated dye (the product of catalysis) and the serum albumin. Since the preliminary albumin binding studies we recognize that *n*-butyl substituted dyes

exhibited the strongest binding affinity, the assay is developed with this particular type of fluorophore in mind.

Further to the changes in absorbance and fluorescence associated with the sulfur assimilation, now that it is confirmed that these fluorescent molecules interact strongly with serum albumin, it is of potential interest to assess the technique using capillary electrophoresis. Using absorbance and fluorescence detection Capillary Zone Electrophoresis (CZE), the free dye will exhibit a specific electroosmotic mobility. Upon cleavage of the indoline alkanesulfonate group this mobility changes depending on factors such as the charge/size ratio of the ligand and pH of the running buffer. In addition, the dye-protein conjugate also migrate at a different mobility, enabling simultaneous detection of the different dyes species in solution. Having, developed a precise CZE procedure to detect the different forms of the dye, it will further serve to formulate the quantitative basis of this method for monitoring the enzymatic reaction that would otherwise proven difficult to study using standard analytical procedures.

5.3.2 FMN photo-reduction

The light dependent absorption behavior of Flavin in phosphate buffer solution (pH 7.4) was performed with the addition of 10 mM EDTA under anaerobic conditions inside an oxygen free glove box. As shown in Figure 5.2 and scheme 5.1 the brightly colored FMN decolorized over a period of 72 hrs at an excitation of 350 – 440 nm under the strong light source.

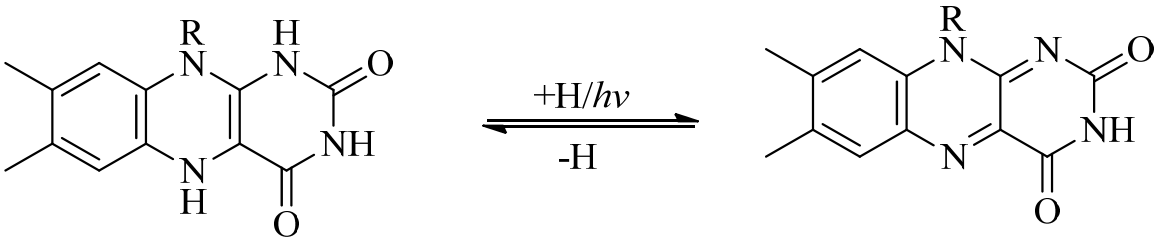

Scheme 5.2 Photo-reduction of the riboflavin mononucleotide (FMN)using EDTA in the presence of a glucose/ glucose-oxygenase scavenging system.

At the start of the reaction, the FMN exhibited strong absorbance in the 455 nm band which was then gradually reduced to nil as the sample was further exposed for oxygen scavenging glucose oxygenase/ glucose system in the EDTA electron rich environment as shown in figure 5.2.

Figure 5.1 Photo-reduction of Riboflavin mononucleotide (FMN) using EDTA in the presence of a glucose/ glucose oxygenase oxygen scavenging system.

After successfully reducing the FMN, air bubbled through the reaction mixture (3 cm^3 during 30 s) resulted in negligible rise in absorbance, confirming the degradative effect of the oxygen scavenging system. However, when the air was bubbled to a portion of the reduced flavin in the absence of the light, there was a slight increase in absorbance which mimics the reducing nature of the *in vivo* reductive half-reaction involving SsUE and thus further demonstrated that the overall photo-reduction is a reversible reaction pathway.

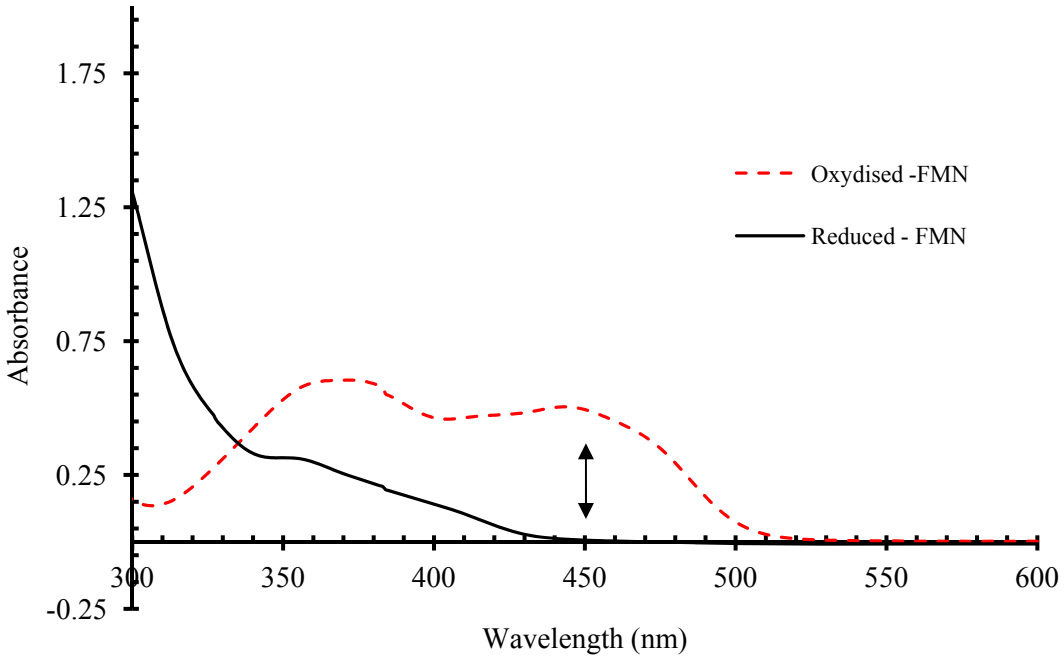

Figure 5.2 Absorbance spectra showing the photo-reduction of FMN using EDTA in the presence of a glucose/ glucose-oxygenase oxygen scavenging system. The main absorbance band at 455 nm disappears.

Similar to the *in vivo* redox capabilities of the SsUE oxidative component of the enzyme, exposure of the flavin to visible light results in the excitation of the FMN_{ox}, from the singlet ground-state to a singlet excited state according to the equation 5.1.

$$FMN_{ox} + h\nu \longrightarrow FMN_{ox}^{*} \qquad \textit{equation 5.1}$$

It is believed that a portion of the singlet excited molecules inadvertently experienced relaxation to the triplet state by singlet–triplet intersystem crossing in the process FMN_{ox}^{*} to the ^{3}Flox. The triplet-state lifetime of FMN is reported to be about 11 microseconds. This reduction reaction FMN_{ox}^{*} is thought to occur from the triplet state. It is likely that the full flavin reduction

proceeds via flavin–semiquinone formation according to equation 5.2 followed by and fast flavin semiquinone disproportionation.

$$FMN_{ox} + H \longrightarrow FMN_{H_2} \qquad \textit{equation 5.2}$$

At just above neutral pH, the neutral hydroquinone form becomes anionic; equation 5.3,

$$FMN_{H_2} + OH^- \longrightarrow FMN_H + H_2O \qquad \textit{equation 5.3}$$

5.3.3 Desulfonation product Analyses using Capillary Zone Electrophoresis (CZE) with Heptamethine dye

One unique fundamental advantage of this CZE technique is the capability for detection at the nano-molar level for *in vitro* studies as demonstrated by the test results. As shown in Figure 5.3, at a concentration of 20.0×10^{-9}Molar, the pure sulfonated dye was readily detected using the LIF detection at 810 nm. This peak remained constant as the concentration was increased five-fold to 100.0 nanao molar with a retention time (t_R) of 27.34 min. *(peak shown in black)*. Addition of the pure reduced form of the FMN resulted in an similar peak with constant elution time demonstrating the dye is stable in the presence of the flavin and does not from form any undesired adduct at low flavin concentration *(peak shown in red)* after mixing and equilibration for 10 min. Once the oxidizing enzyme component was added up to 50 equivalents and analyzed, the peak remained at 27.31 min. *(peak shown in blue)* which further indicates that at 810 nm there is little to know spectral interference from the flavin thus enabling lower detection limits and im-

proved effectiveness of this detection technique. After numerous consecutive analyses, the retention time yielded an average value of 27.37 min. with a standard deviation of only ± 0.034.

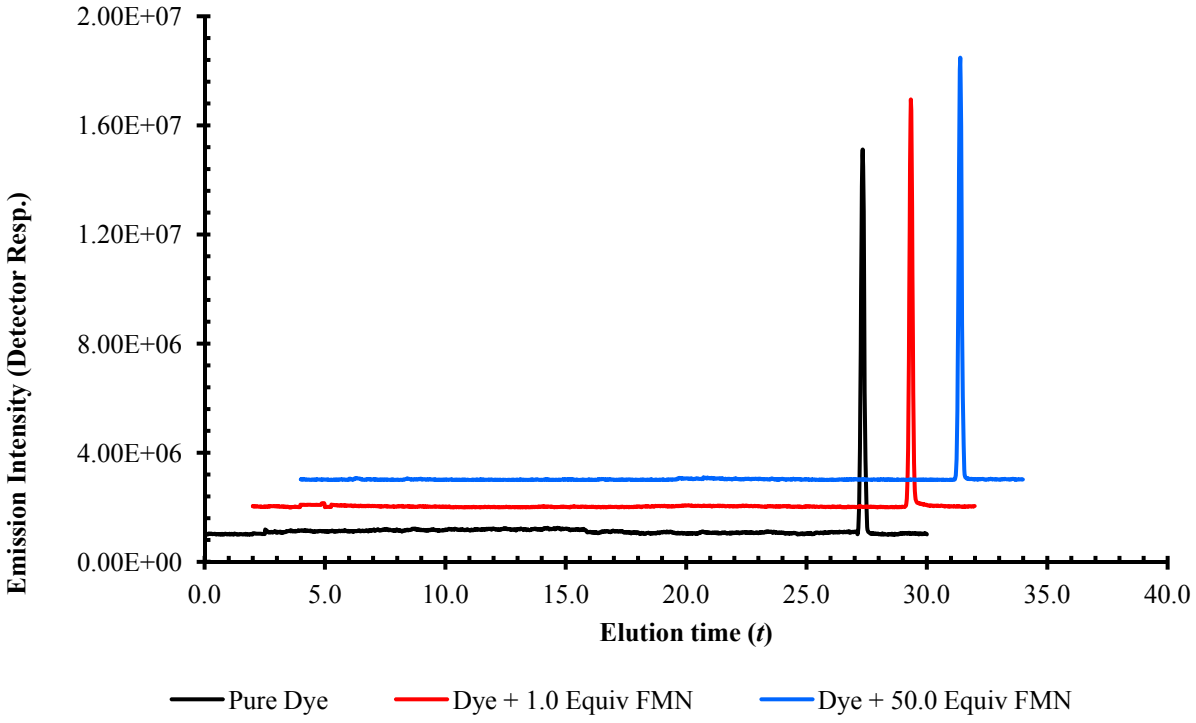

Figure 5.3 LIF-CZE analyses of the heptamethine dye-FMN mixture before for the addition of the SsUD. Separation was achieved with a 63 cm long, 49 micron ID polyacrylamide coated capillary, 5 kV separation potential and 20 mM phosphate buffer-saline (pH 7.4). FMN concentration ranged from 0 to 50 equivalents.

Once the dye is successfully detected in the 810 nm detection window and displayed reasonable stability in the presence of excess flavin, the next step of the technique development involved the monitoring of the oxidative catalytic process using the SsUD enzyme component. As

shown in figure 5.3, the dye exhibited a retention time of just over 27 min. which could affect practical application of the technique as fast and reliable method. Thus further steps were conceptualized to adjust key separation parameters in order to achieve reliable separation, improved detectability in the chosen detection window but most importantly to achieve a more rapid analysis. Subsequent to each change made to the reaction mixture, the oxidative enzyme component was added to the reaction mixture to monitor the catalytic conversion of the substrate to the bis-aldehyde product.

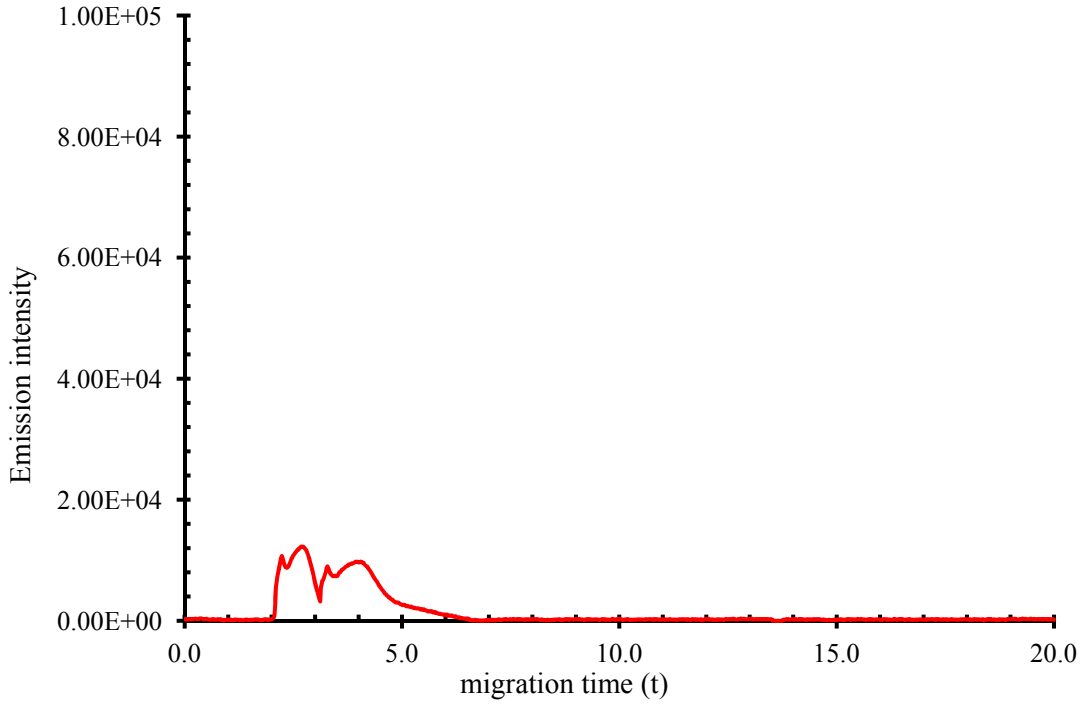

Figure 5.4 The initial separation conditions revealed that the technique requires further optimization efficient and reliable separation and detection the pure dye. Variation to the capillary size, length, buffer concentration and separation voltage were conducted until the optimum conditions were determined; Trial 1. The analyses was performed using 63 cm, 75 micron ID polyacrylamide coated capillary and the sulfonated dye eluted with a characteristic broad peak over a three minutes period.

Contrary to the initial analyses, the first approach to optimizing the separation technique was to eliminate the NaCl from the phosphate buffer saline (PBS) running buffer solution. Preliminary results showed that the NaCl suppresses the electroosmotic force (EOF) and also leads to lengthy retention times and consequentially increases the separation current above 120 micro-ampere (μA)which is the upper limit of the CE instrument for effective separation. With the lowering operating current the technique made possible the use larger 74 micron ID capillary with and yielded more rapid separation. However, as depicted in figure 5.4, with the shorter retention time less distinct peaks were observed and the resolution was poor. As outlined in table 5.1 after many successive analyses it was determined that the best separation conditions could be achieved with instead the 49 micron ID polyacrylamide coated glass capillary at 20 kV using a 20×10^{-3} molar saline free buffer. These results were further illustrated in figure 5.5.

Table 5.1 The showing the separation conditions used to yield optimum separation and detection of the catalytic product produced from the conversion of the heptamethine sulfonated substrate to the di-aldehyde.

Trials	Capillary ID (Microns)	Separation Potential (kV)	Buffer Concentration ($\times 10^{-6}$ M)
1	74	20.0	10
2	49	7.50	5
3	74	10.0	15
4	74	20.0	10
5	74	20.0	15
6	**74**	**20.0**	**20**
7	74	20.0	25

According to the results presented in table 5.1 previously reported data, it is clearly demonstrated that the enzyme is capable of converting the sulfonated NIR probe to its carbonyl derivative. Once the SsUD enzyme was added in the presence of the reaction mixture of reduced FMN and the substrate followed by a 5 minute reaction equilibration period three distinct peaks were observed in the electropherogram. As the technique is optimized with the most effective, separation potential, capillary size and buffer concentration, what appeared to be a single large broad poorly resolved peak later became a well defined symmetrical and two other less resolved peaks. This indicates that there are at least three separated species which includes the starting material or bi-sulfonated heptamethine substrate.

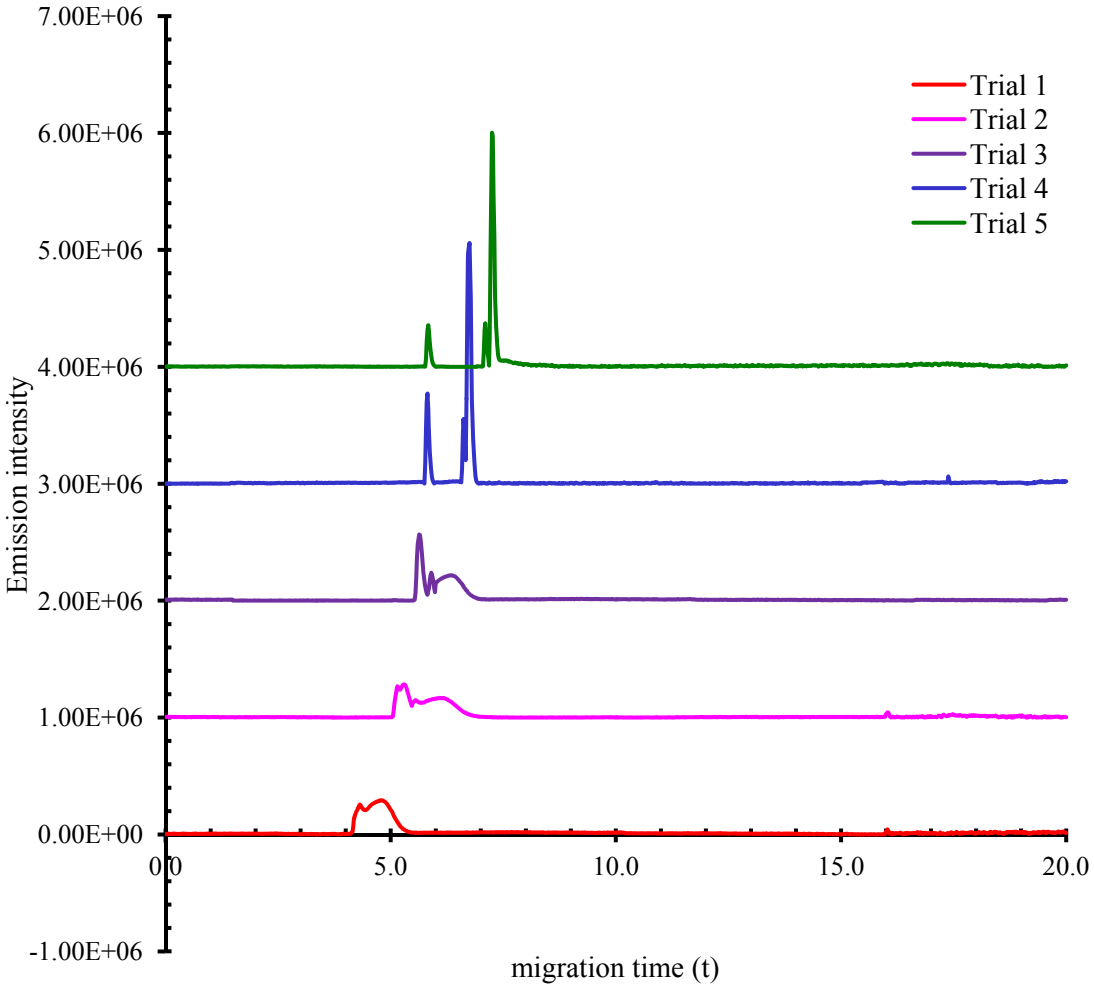

Figure 5.5 The initial separation conditions revealed that the technique requires further optimization efficient and reliable separation and detection the pure dye. Variation to the capillary size, length, buffer concentration and separation voltage were conducted until the optimum conditions were determined; Trial 1. The analyses was performed using 63 cm, 75 micron ID polyacrylamide coated capillary and the sulfonated dye eluted with a characteristic broad peak over a three minutes period

It is believed that the di-sulfonated substrate undergoes an enzymatic double desulfonation reaction to yield two distinct products. As demonstrated in scheme 5.4, this substrate first undergoes a single desulfonation reaction to yield **II** with an elution time of 7.10 min.

almost similar to the 7.25 min. elution time obtained for the least retained substrate **I**. Owing to the presence of the second sulfonate moiety, the compound is further cleaved to yield the corresponding bis-aldehyde **III**. Hence. yielding the final product with a net positive charge and displayed greater electrophoretic mobility. This resulted a reduced elution time of just 5.83 min.

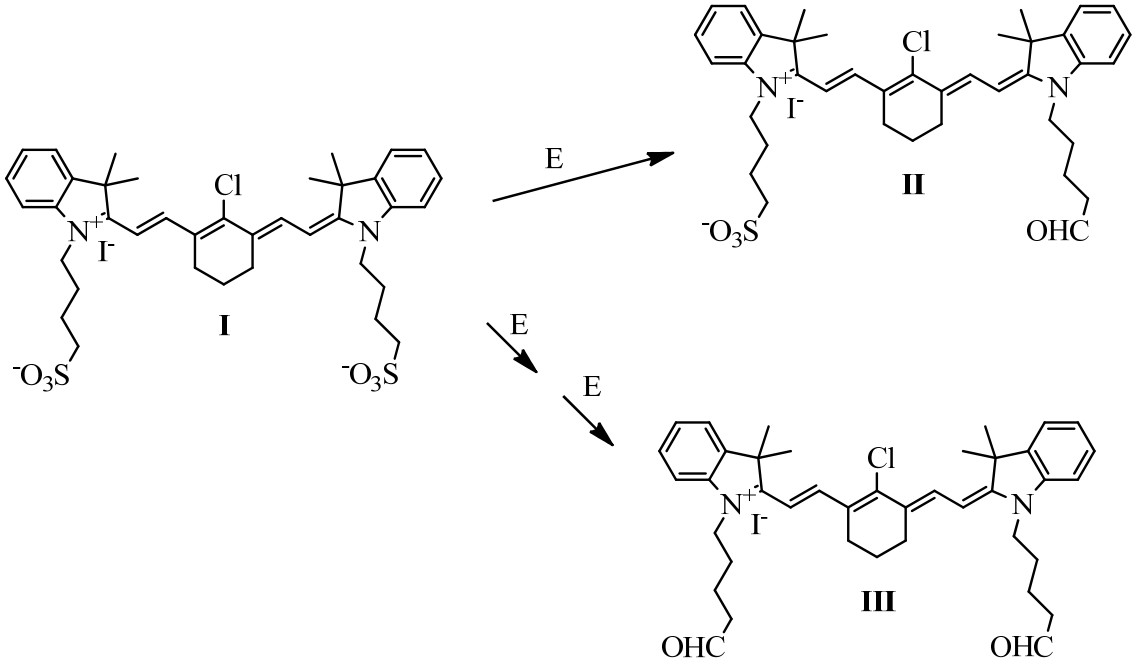

Scheme 5.3 Proposed catalytic oxidative conversion of the heptamethine dye to the corresponding mono and di-aldehyde derivatives.

As reported by Ellis *et al.*, this desulfonation can take one of two or both possible proposed mechanism. While limited information is available on the nature of the flavin peroxide, the catalysis is believed to have occurred through a C4a-hydroperoxyflavin (Fl-OOH) or the more oxygenating C4a-peroxyflavin ($Fl\text{-}OO^-$) intermediate [20, 21, 27]as shown in scheme 5.5.

In the hydroperoxyflavin (Fl-OOH) pathway, the C4a-hydroperoxyflavin adduct is formed by reacting the reduced flavin with dioxygen followed by the abstraction of an active site proton from the C1 carbon of the alkanesulfonate substrates. This in turns generates a nucleophilic carbanion intermediate (Fig. 4A-II and III) which then attacks the hydroperoxyflavin. Once the hydroperoxyflavin in formed it reacts with the carbanion to generate an unstable 1-hydroxyalkanesulfonate which decomposes to the corresponding aldehyde and sulfite (Scheme 5.5A-IV and V). [20, 21]

Unlike the former, the C4a-peroxyflavin pathway involves the formation of a peroxyflavin intermediate (Scheme 5.5B-II) which attacks the sulfur atom of the organosulfonate substrate to generate a peroxyflavin-organosulfonate adduct (Scheme 5.5B-II and III). Rearrangement of the peroxyflavin-organosulfonate adduct results in the formation of a sulfite along with a peroxyalkane intermediate (Scheme 5.5B-IV). Abstraction of C1 proton of the alkyl chin by an active-site base will subsequently result in the heterolytic cleavage of the oxygen-oxygen bond of the alkane-flavin adduct to form the aldehyde product and the C4a-hydroxyflavin (Scheme 5.5B-IV and V).

While both techniques are quite dissimilar, each mechanism involves the common dioxygen activation to form the oxygenating C4a-(hydro) peroxyflavin. The exact mechanism is determined by the ease of protonation of the distal oxygen, which is highly dependent on the active site microenvironment[20]. Nonetheless regardless of the specific mechanism, desulfonation of the sulfur bound substrate can be achieved by the catalytic process of the alkanesulfonate momooxygenase enzyme.

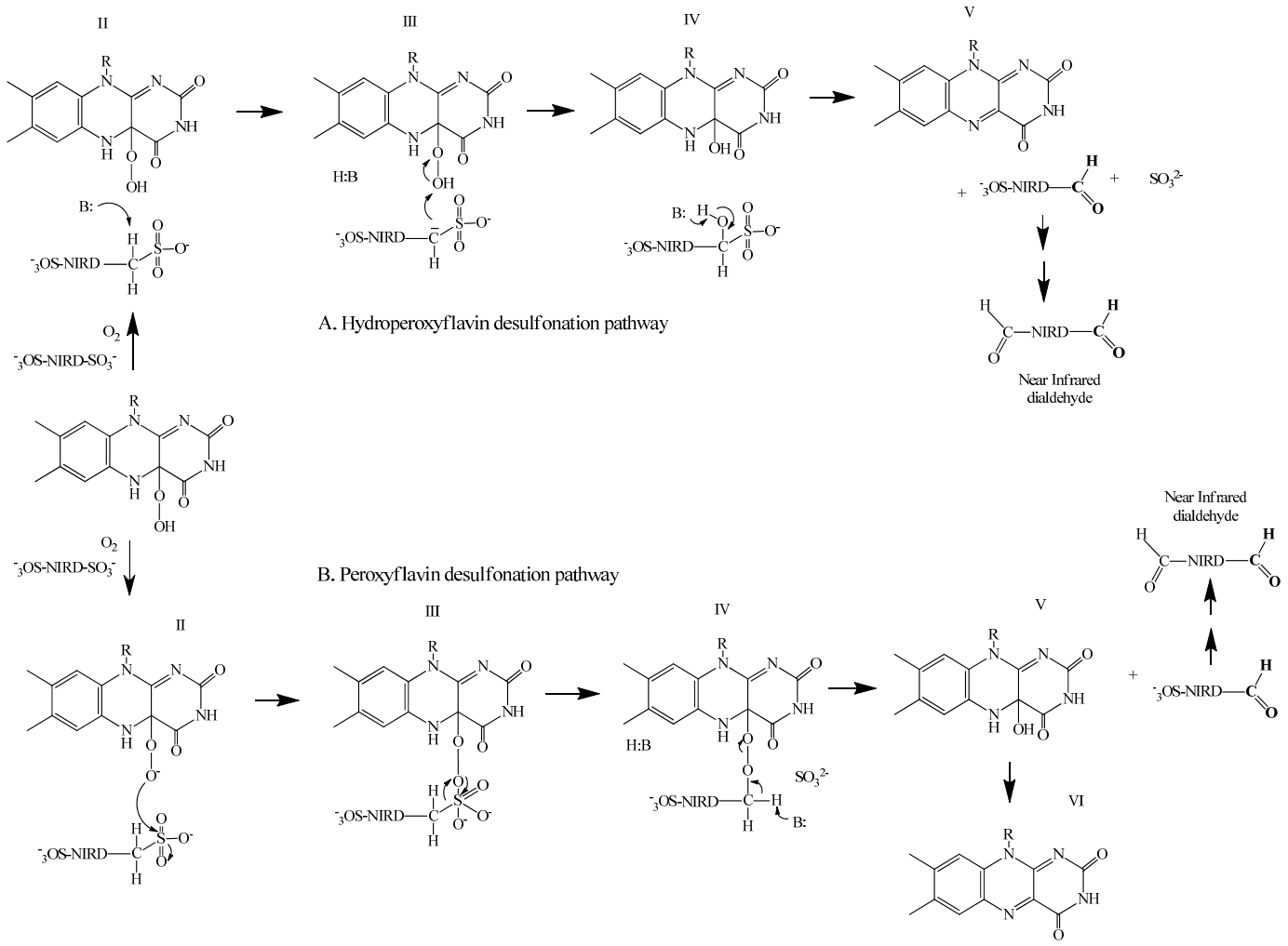

Scheme 5.4 Proposed mechanisms for desulfonation of alkeanesulfonate by SsuD to the corresponding Near Infrared (NIR) dialdehyde (OHC-NIRD-CHO). Pathway A represents the C4a-hydroperoxyflavin intermediate mechanism and pathway B represents the C4a-peroxyflavin intermediate mechanism. The desulfonation occurs simultaneously at both terminals of the NIR dye.

As shown in figure 5.5, regardless of the exact desulfonation mechanism, either the C4a-hydroperoxyflavin (Fl-OOH) or the more oxygenating C4a-peroxyflavin ($Fl\text{-}OO^-$), it is rather difficult to separate the mono aldehyde intermediate **II** from the initial substrate **I** and thus validate the technique. While this result is not uncommon, it is expected that compound **II** is neutral at pH 7.4 in the phosphate buffer once the first aldehyde group is formed and compound **I** having two alkyl sulfonate groups and a single positive charge to the heterocyclic chromophoric region of the molecule, there is an overall single negative charge. This in turn should allow the two compounds to migrate at considerable different migration mobility through the capillary but instead the two compounds displayed almost similar migration patterns. This is due in part to the high hydrophobic nature of these cyanine dyes thus both molecules migration with the EOF resulting poor peak resolution. Besides, owing to the fact that any changes to the capillary walls or buffer composition could potentially affect the EOF, separation based on purely EOF mobility can be easily affected by sample composition which could limit the robustness of the technique and its applicability to a wide range of different buffer media. This could also render the technique less attractive for further development towards *in vivo* or live microorganism detection capabilities.

5.3.4 Trimethine NIR dye detection technique

Having developed the enzyme detection technique based on the use of a di-alkyl sulfonate heptamethine dye the next step was to determine the effect of the alkyl length on the overall specificity and efficacy of the technique. In order to do so, the Henary research group took the approach to design substrates with single alkyl sulfonate group (**IV**) in an effort to prevent the formation a neutral single catalyzed dye species (compound **II**) which potentially over-

laps with the migration time of the substrate or even migrate similarly to the final di-aldehyde product, based on the buffer pH and capillary wall conditions among other factors. Also attempts to design the single alkyl sulfonate were unsuccessful due to the complex procedure of synthesizing this particular type of substrate. In addition, after determining that the maximum enzymatic cleavage was achieved with the butyl sulfonate derivative, variation to the alkyl chain length was attempted but proven futile and other heptamethine substrates were not further assessed. For these reasons the new trimethine cyanine dye substrates displaying similar solvatochromic and spectral properties were introduce.

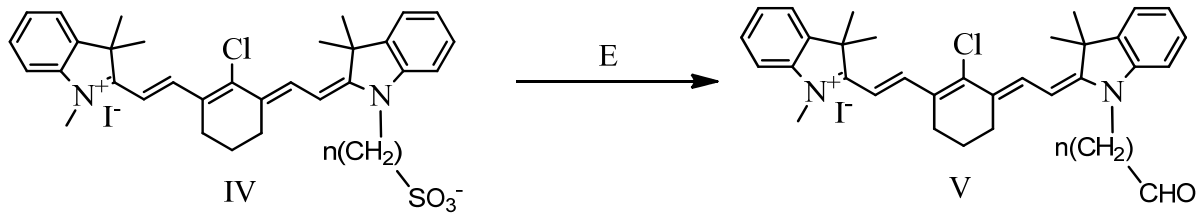

n = 3; **IV-A**
n = 4; **IV-B**

Scheme 5.5 Proposed mechanisms for desulfonation of the single alkyl sulfonate heptamethine dye by SsUD to the corresponding aldehyde.

Unlike the heptamethine dyes that absorb above 750 nm with strong absorbance and emission properties, the trimethine counterparts are less absorbing and emit just outside the NIR range and in the visible region below 600 nm. The lower molar absorptivity and absorbance maximum observed with these new dye substrates resulted in lower detection limits of the enzyme from times 10^{-10} to 10^{-7} molar. This was further exacerbated by the laser source and PMT detector used for these dyes. Nonetheless, the synthetic pathway was rather less complex thus allowing the preparation of both the propyl sulfonate and its butyl counterpart. As shown in figure 5.6 the butyl sulfonate dye exhibited strong emission properties as evident by the pure dye electrophoretic peak under standard test conditions.

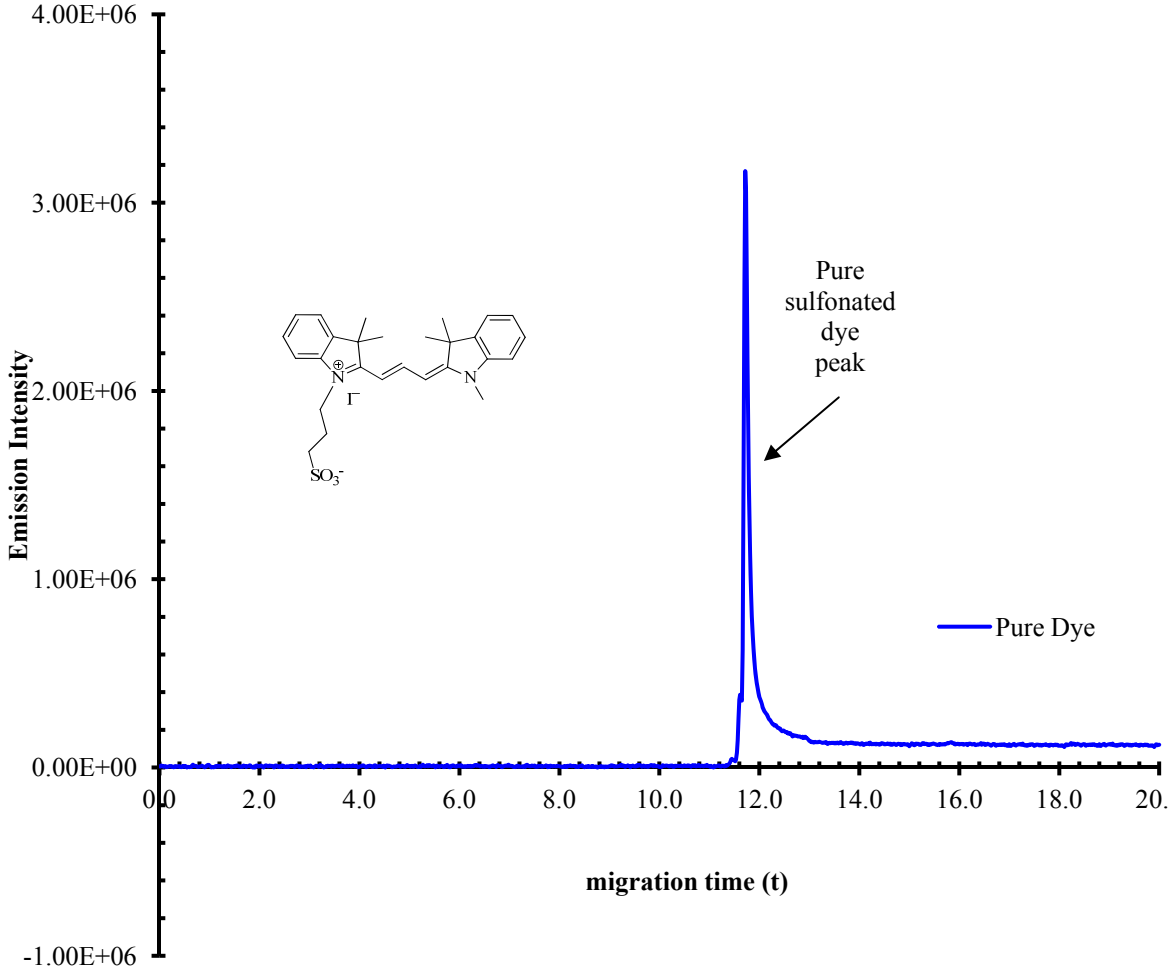

Figure 5.6 - Initial C-3 analyses dye using 63 cm, 74 micron ID capillary resulted in tremendous amount of tailing and poor baseline resolution due to effects of EDTA in the FMN reduction process. Increased buffer concentration had virtually no effect of the peak symmetry. The pure dye eluted at 11.73 min using 10kV for a total analysis time of 20 min. Dye concentration of 2 micro molar, separation performed in phosphate buffer (saline free), 15.0 mM at pH7.4.

However the separation profile was characterized by tremendous peak inconsistencies and poor peak symmetry resulting from strong peak tailing.

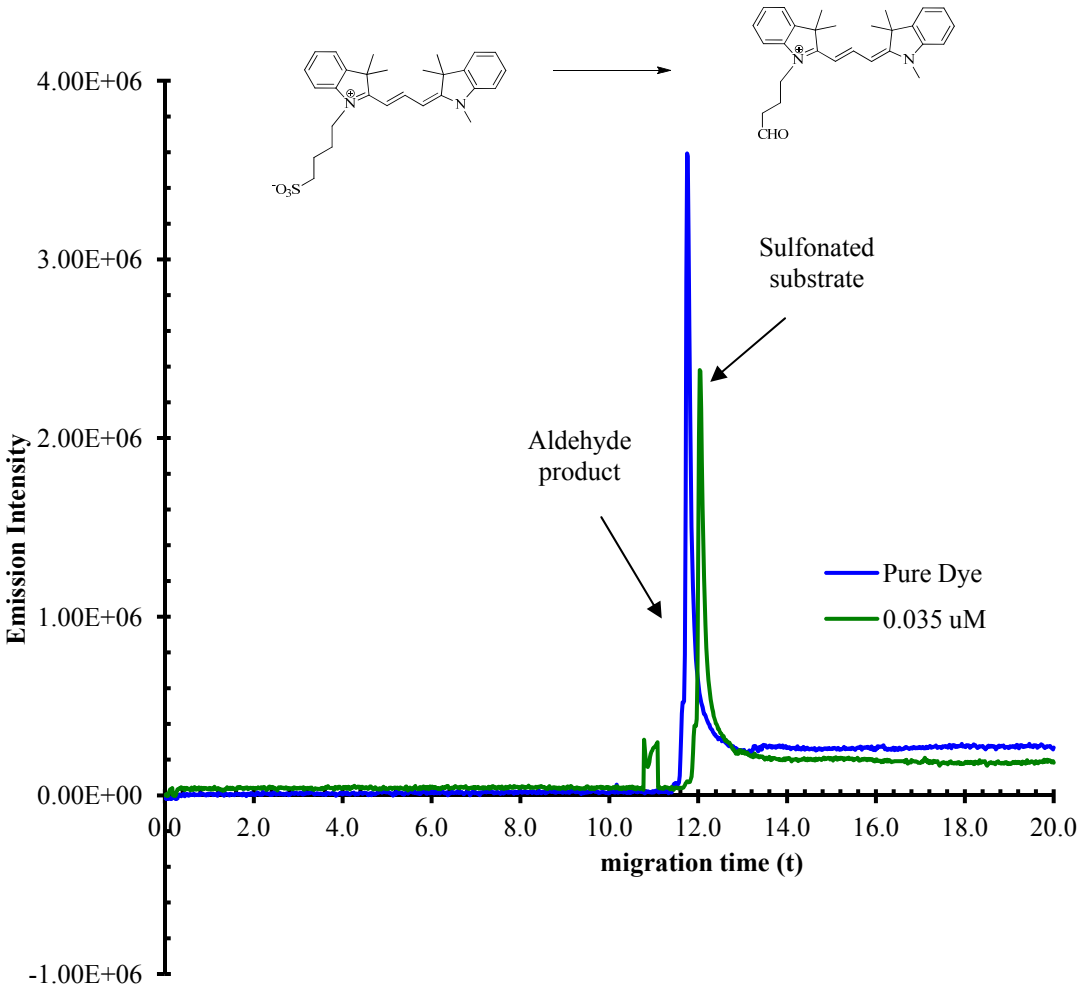

Figure 5.7 - Similarly to the propyl sulfonate substituted NIR substrate, the butyl dye eluted at about 11.70 min. The pure dye also eluted at about 11.73 min using 15kV for a total analysis time of 20 min. Dye concentration of 2 micro molar, separation performed in phosphate buffer (saline free), 15.0 mM at pH 7.4. $FMNH_2$ is used as the oxidant to facilitate the oxidative enzymatic cleavage of the sulfonate group to yield the corresponding aldehyde. Peak inconsistency and poor base line resolution was also evident in the enzymatic oxidative desulfonation process of the butyl derivative.

Similar elution patterns were observed once the sulfonated dye substrate was exposed to the reduced flavin and the enzyme component for catalysis. A second peak appearing at an elution time 10.83 min. depicted the catalyzed portion of the dye, while the original peak at 11.73 min indicated that of the pure dye of which the majority remained in the uncatalyzed sulfonated

form and less than 10 % had been enzymatically transformed to the aldehyde. In addition, the aspect of peak tailing was further investigated and assessed by applying different separation stabilizers. It was observed that a 5% addition of ethanol was suitable for stabilizing the mobile phase thus reducing the peak tailing. However, this resulted in an increased current gain on the CE instrument to values exceeding 120 microampere; the upper limit of the instrument as compared to up to 45 microamperes recorded without stabilization. This increased potential is believed to disrupt the EOF charged bi-layer at the capillary walls thus reducing the electrophoretic and electroosmotic forces, in turn reducing the efficiency of the separation technique along with other key parameters of method development. The increased current is also considered detrimental to the overall instrument performance and limits the lifespan of the device. This current gain limitation is overcome by lowering the separation voltage from 10kV to just about 5kV, increasing the capillary length to 83 cm and reducing the buffer concentration to $2.5.0\times10^{-3}$ Molar; effectively limiting the ionic strength of the buffer. As depicted in figure 5.8, this further optimization of the separation parameters resulted in increased elution time of up to 22.4 and 23.00 min. for the propyl and butyl sulfonate derivative respectively with virtually no recurrence of the peak tailing. Instead of the usual 74 micron, the 49 micron capillary was re-introduced, because without sufficient cooling the increased plug flow of liquid through the capillary could potentially create Joule heating and ruin the internal capillary walls. The new elution times were then confirmed by applying a Rhodamine 6G internal standard. Also, shown in figure 5.8 is elution peaks of both the enzyme catalyzed dye and the internal standard. One general limitation of CZE techniques is the tendency to create poor peak repeatability with successive analyses on the same capillary stationary phase. Over time the bi-layer positively charged capillary walls become less effective in maintaining a constant EOF thus contributing to poor repeatability and limited peak

consistency. As demonstrated with the Rhodamine 6G at buffer pH 7.4, internal standards are usually chosen that are non-polar and migrate with the EOF, any changes made to the stationary phase could have negative effect on the outcome of the technique especially with regards to re-peatability. There were virtually minimum changes to the stationary phase as illustrated by the high precision obtained by the technique among successive analyses.

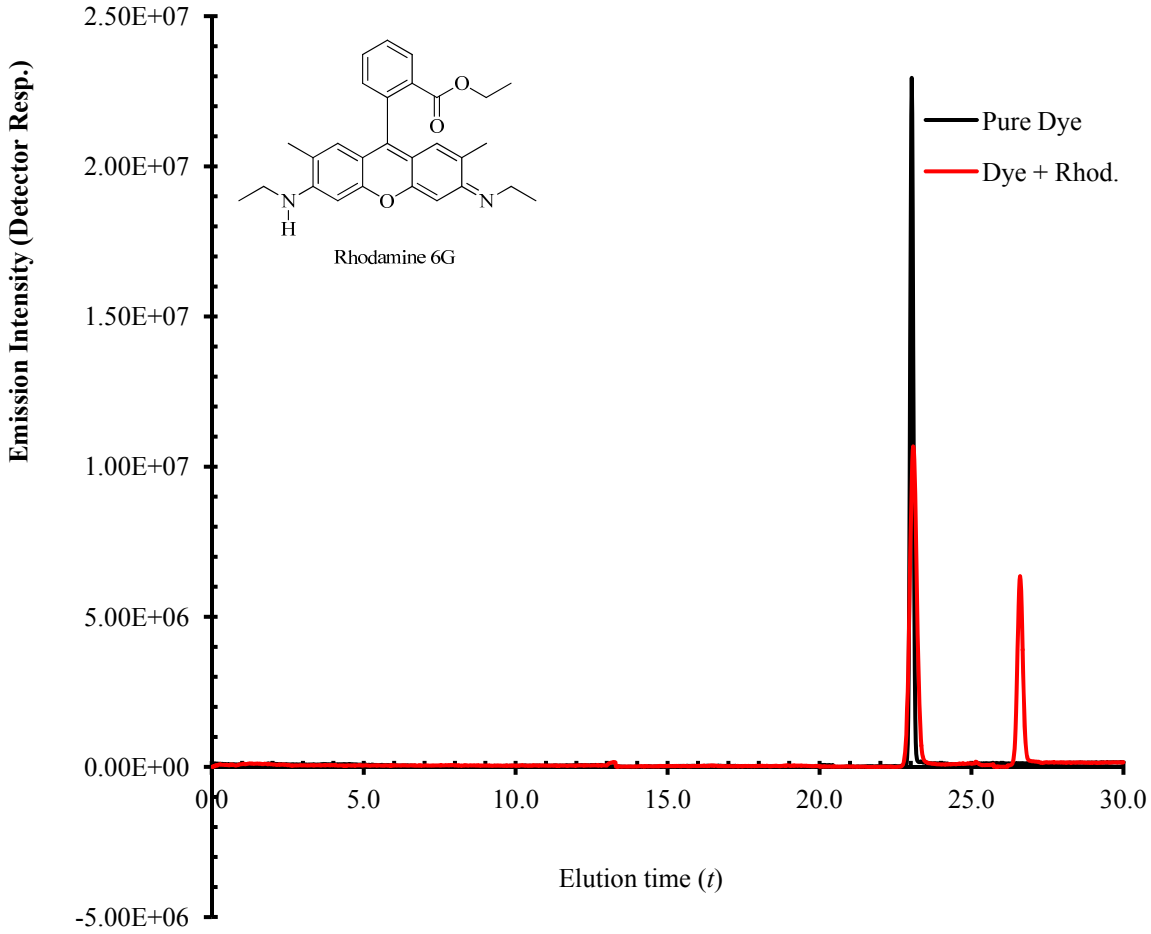

Figure 5.8 Analyzing the asymmetrical trimethine dyes, the technique was optimized and an 83 cm capillary of 49 micron ID along with a saline free phosphate buffer solution (2.5 mM, pH 7.4) and 5.0kV were most suitable to achieve relatively effective CZE analysis. Using the longer capillary, the pure dye eluted at 23.00 min (22.4 min. for the *n* = 3 NIR counterpart) using for a total analysis time of 30 min. Dye concentration was kept constant at 10.0 *u*M. The sulfur free standard (Rhodamine 6G) was used to monitor any possible peak drift and eluted it at 26.4 min. Methanol was added to the reaction as a reaction stabilizer.

Having fully optimized the separation method to analyze the unsymmetrical alkyl sulfonated substrate it was imperative to assess the effect of enzyme composition and the overall quantitative usefulness. As shown in figure 5.9, an increase in enzyme concentration from 0 to 0.070×10^{-6} molar resulted in a concomitant increase in peak height of the catalyzed portion of the dye. In fact, a detailed study of the data revealed that no enzyme catalysis was observed until the concentration of the SsUD enzyme component exceeded a concentration 0.035×10^{-6} molar. This indicated the limit of detection (*LOD*) of the technique under the current test conditions. These results have the potential could be useful for future studies if the method should be further assessed for other *in vitro* investigations involving live bacterial micro-organisms. This was also illustrated in figure 5.10, which involved increased SsUD up to concentration of 2.10×10^{-6} molar. Beyond this enzyme concentration there was no discernible increase in peak height without potential peak shift or peak broadening, thus depicting the upper limit of the method under the current test conditions.

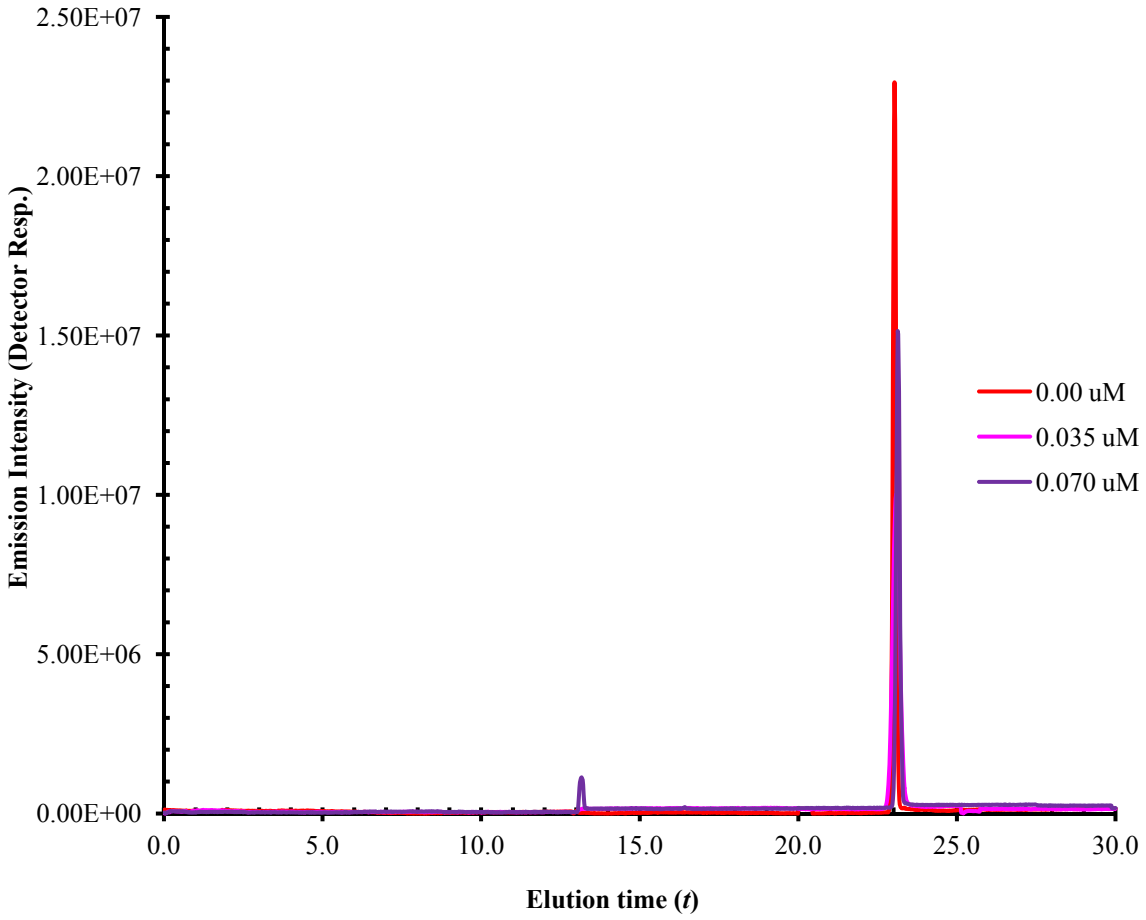

Figure 5.9 Once the enzyme component (SsUD) was added to the reaction mixture of reduced FMN and alkyl substituted sulfonated dye (substrate) and left to equilibrate for five minutes the second peak appeared, corresponding to the conversion of the sulfonate group to the corresponding aldehyde appears (12.9 min. for the *n* =˙ 3 and 13.2 min. for the *n* =˙ 4 dyes). By increasing the amount of SsUD the peak area increased as well. However, no product peak was noticeable until the SsUD concentration exceeded 0.035 *u*M at constant excess dye concentration of 10.0 *u*M.

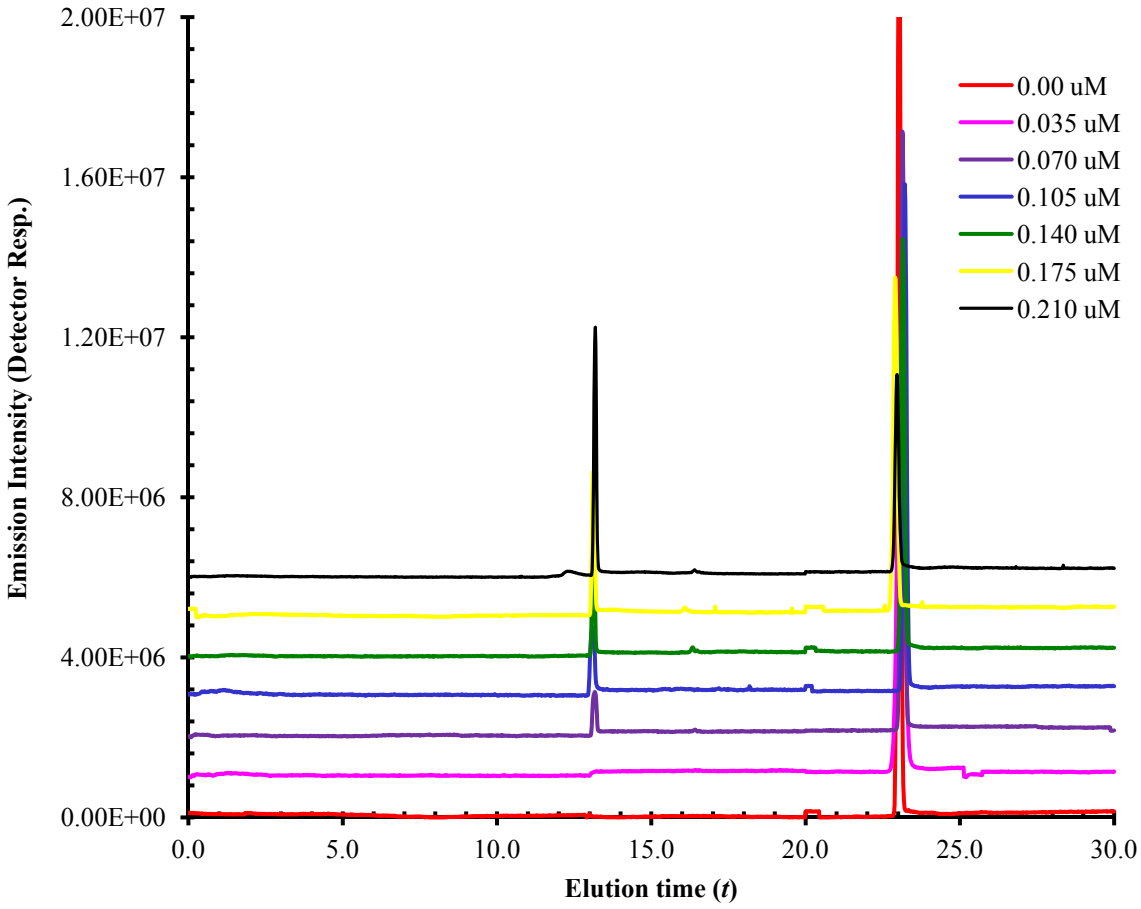

Figure 5.10 Further exposure of the dye to the enzyme under the same reaction conditions resulted in more enzymatic conversion as illustrated by the continued increase corresponding aldehyde (product) peak (12.9 min. for the *n* = 3 and 13.2 min. for the *n* = 4 dye).

5.3.5 Quantitation using the newly developed NIR-based enzyme detection technique

Like any new bioanalytical assay, the ability to quantitate has been one of the main aspects of this newly developed technique. As shown in figure 5.9 and 5.10, there is no clear correlation of proportionality between the increase in enzyme concentration and emission signal from the enzyme catalyzed species. The data collected revealed that there was poor linearity between the enzyme concentration and the change in emission. It is evident that as the SsUD concentration is increase, the enzyme does not necessarily linearly pattern with the excess substrate available. Form this it is inferred that the enzyme catalysis does not necessarily follow a simple first order mechanism as expected for these enzyme catalysis processes. Instead it could be inferred that the mechanism may more be one that is characterized by proximity or cooperative kinetics. This renders the overall spectroscopic method less reliable as a technique of quantification and thus required further optimization. Figure 5.11A and B revealed that as the enzyme concentration was varied at constant dye concentration, the overall emission curves were non-linear for both the propyl sulfonate (**R^2 = 0.950**)and the four carbon butyl sulfonate derivative (**R^2 = 0.970**).

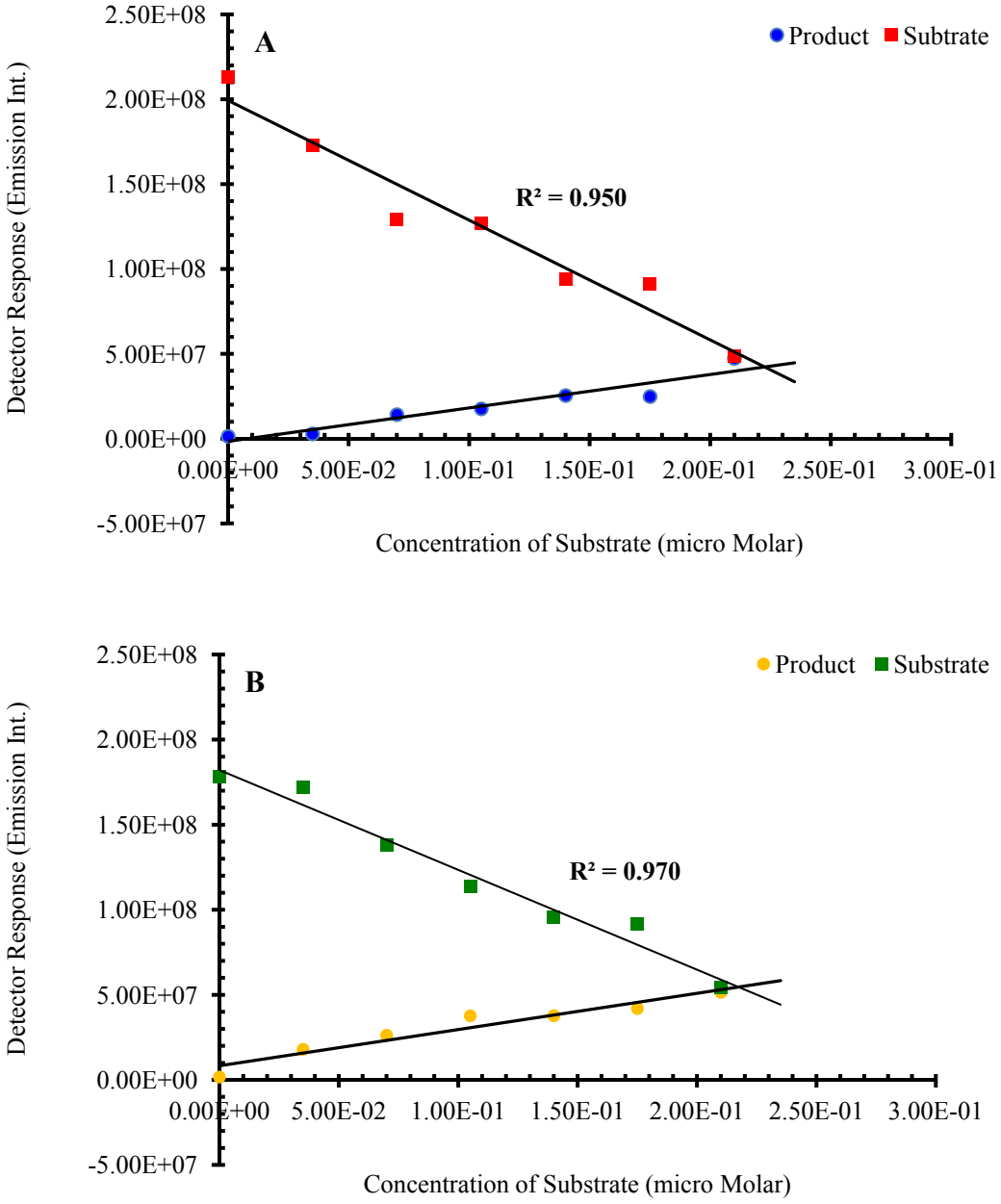

Figure 5.11 (A and B) After studying the desulfonation process with the trimethine dyes, it was evident that the change in integrated peak area of the aldehyde product is not quite linear with the change in enzyme concentration as expected. This makes it rather complex to determine other key interaction parameters such as association constants and enzyme turnover number. Also, quantitation becomes rather difficult with the current experiment conditions.

5.3.6 Quantitation at constant dye concentration

To investigate the quantitative applicability of the newly developed technique a different approach was applied to study the desulfonation properties of the NIR based substrate with the enzyme. Unlike the previously applied interaction, this binding mode involved maintaining a constant enzyme concentration with variation to the dye. As shown in figures 5.12 A and B, having chosen a suitable enzyme concentration of 2.05×10^{-6} Molar from the previous studies, changing the dye concentration from 0 to 14.0×10^{-6} Molar yielded a more linear plot of R^2 value of 0.992 for the propyl sulfonate but a less than ideal regression of 0.903 for the butyl derivative instead. Even though this new approach did not produce considerable greater improvement to the regression plot of the enzyme activity as a function of available substrate, the need to maintain constant enzyme concentration cannot be overstated. This approach makes available the opportunity the ability to investigate other key pharmacokinetic parameters such as enzyme efficiency, rate of catalysis and turnover numbers.

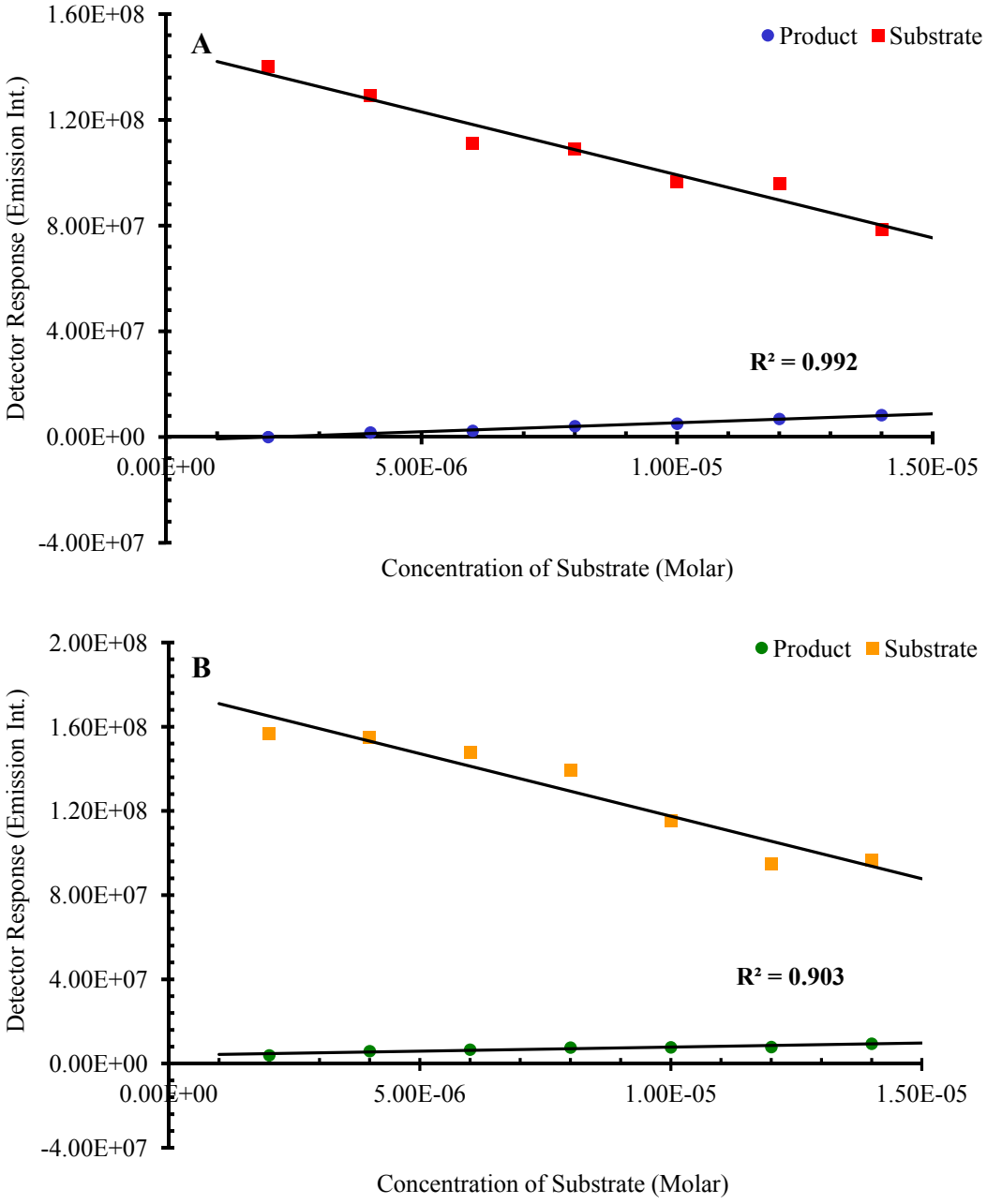

Figure 5.12 (A and B) Re-evaluating the enzyme catalyzed reaction with fixed SsUD concentration and varied dye yielded a relatively straight linear curve. The enzyme concentration was kept constant at 2.05×10^{-6} molar while varying the dye from 2.0 to 14.0×10^{-6} molar. The linearity of the curve made it simplified to determine other key interaction parameters such as association constants and enzyme turnover number that may not have been possible without a linear plot. This reveals that the enzyme concentration must be kept constant during the catalysis in order the yield the best quantitative results.

The hyperchromic shift in the integrated emission peak of the enzyme catalyzed species provided key analytical information on the overall binding parameters of the enzyme interaction with the alkyl substituted sulfonated substrate. However, once the sulfonate group is transformed into the corresponding aldehyde, the once well solubilizing dye became less hydrophilic and thus self-aggregates in the polar buffer solvent. For this reason, changes in peak size cannot directly or linearly be correlated to rate or extent of enzyme catalysis but rather a more complex solvatochromic behavior of the dye must be considered. Interestingly, reduction in emission signal of the aldehyde product attributed to this unique dye behavior was further evident with the introduction of serum albumin; a key dye binding carrier protein. At optimum dye and enzyme concentrations of 10.00×10^{-6} and 2.05×10^{-6} Molar respectively, introduction of serum albumin resulted in a concomitant reduction in the integrated peak area of the aldehyde peak with elution times of 12.88 and 13.18 min. for the substituted propyl and butyl aldehyde respectively. Similarly, a new peak appeared at 24.55 min. for the proypl (24.75 min. for the butyl) derivative and exhibited an increased peak area with increased albumin form 1.0 to 6.0 $\times10^{-6}$ Molar as demonstrated in figure 5.13 A and B. This newly appeared electrophoretic peak confirms the interaction of the highly hydrophobic aldehyde product of enzyme catalysis with the carrier protein. In addition, as was expected, the binding patterns yielded relatively linear plots useful to determine other binding parameters such as the binding affinities and binding stoichiometry.

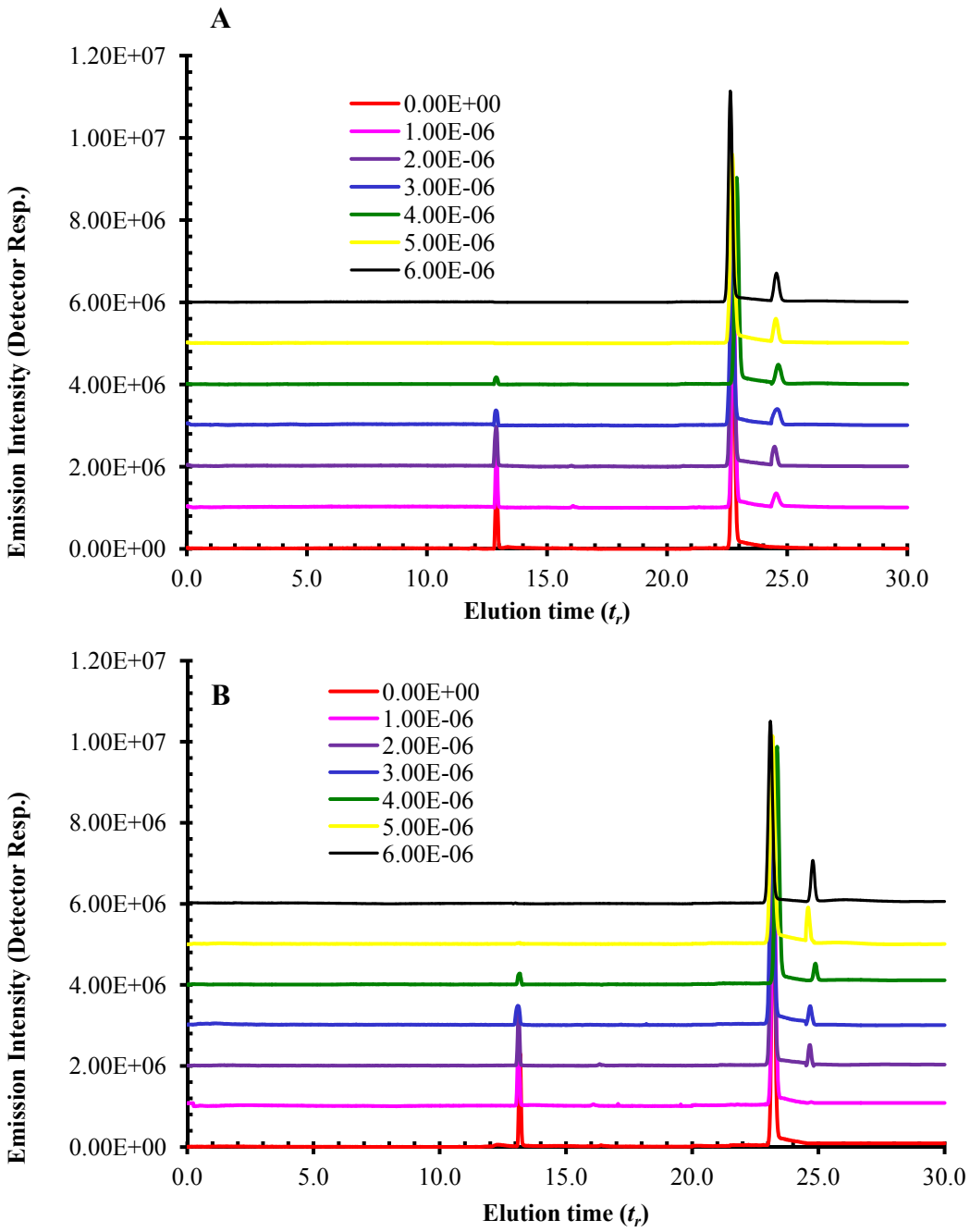

Figure 5.13 (A and B) The cyanine dye substrate does not interact with serum albumin as it does with the monooxygenase through enzyme catalysis. However, once the aldehyde species are formed the dye become more hydrophobic and is capable of interacting with the hydrophobic binding pockets of the albumin resulting in a third peak on the electropherogram.

5.3.7 Association constant determination

Prior studies revealed that these uncatalyzed cyanine dyes bearing the highly polar sulfonate moiety are virtually uncreative with serum albumin and the similar more hydrophobic forms react in a 1:1 stoichiometry with the said protein. Assuming once the substrate is converted to the aldehyde, this latter hydrophobic form of the dye in excess interacts completely with the limited albumin as demonstrated in the results. Beyond 6.00×10^{-6} Molar albumin concentration there was no further discernible increase in the protein-dye conjugate peak. At this point it is believed that equilibrium is reached. In accordance with the Scatchard Plot, the concentrations (activities) of the different reaction species are measured to determine the affinity constant (K_s). A double reciprocal plot of $1/\Delta F$ versus the reciprocal of HSA concentration yielded a linear relationship that intersects the ordinate (*y-axis*). The affinity constant was calculated by dividing the intercept by the slope of the line as shown in figure 14 and 15. Thus, the Scatchard plots yielded similar affinity constants for both trimethine derivatives. For the C-3 alkyl compound the value determined was $\mathbf{3.99\times10^4 \pm 0.44 \times10^4\ M^{-1}}$ and a value of $\mathbf{4.21\times10^4 \pm 0.37\times10^4}$ M^{-1} for the C-4 derivative. Interaction with the albumin provided an indirect indication that increasing the alkyl chain length from a propyl to a butyl had virtually no effect on the catalytic capability of the enzyme to bio-transform the sulfonated cyanine dye to the corresponding aldehyde, this is based on the assumption that both forms of the aldehyde forms of the dye interact similarly with serum albumin.

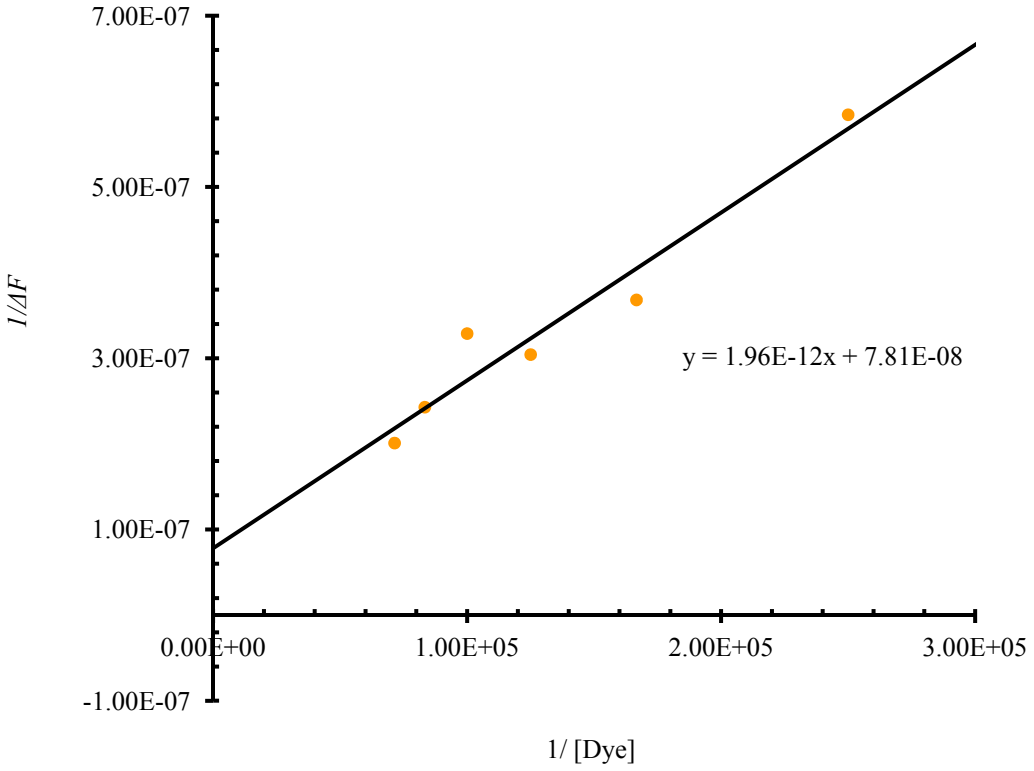

Figure 5.14 Double reciprocal plot Scatchard plot of the propyl cyanine dye derivative that formed the corresponding aldehyde. A plot of $1/\Delta F$ versus the reciprocal of HSA concentration yield a linear relationship that intersects the ordinate (*y-axis)*.

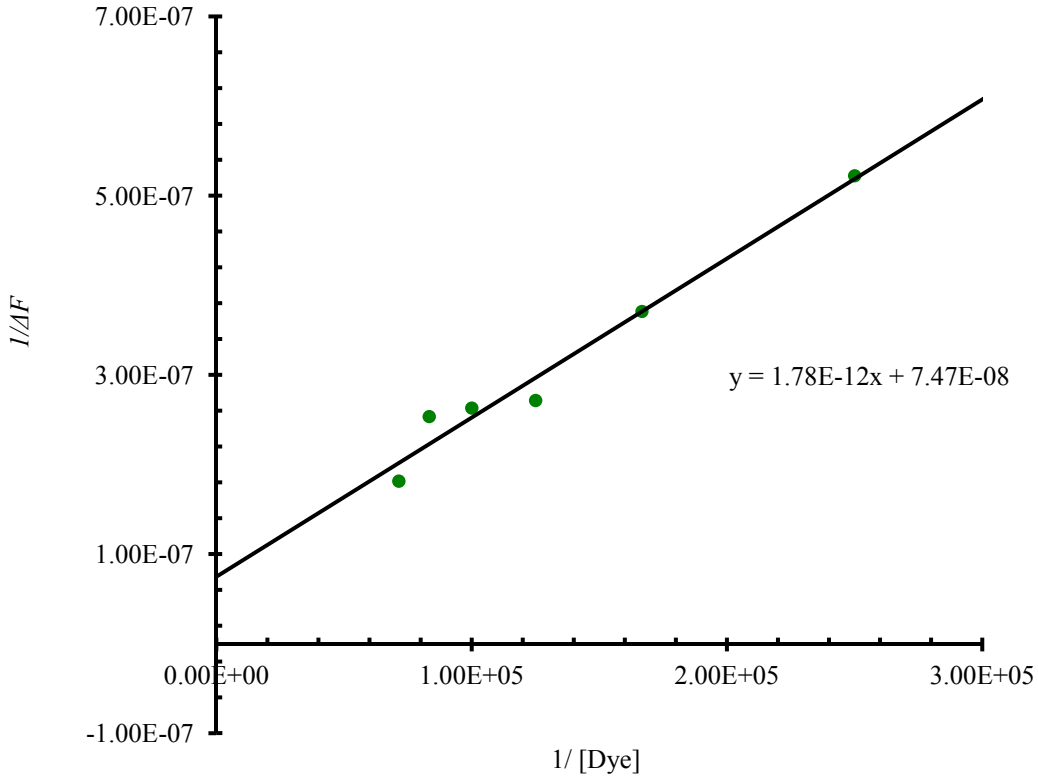

Figure 5.15 Double reciprocal plot Scatchard plot of the butyl cyanine dye derivative that formed the corresponding aldehyde. A plot of $1/\Delta F$ versus the reciprocal of HSA concentration yield a linear relationship that intersects the ordinate (*y-axis)*.

5.3.8 Method Validation

In accordance with the International Conference on Harmonization (ICH)[28-34], method validation confirmed that the current analytical procedure is suitable for its intended purpose. Results obtained from method validation studies were useful in assessing the quality, reliability and consistency of overall analytical technique. In this context six fundamental areas of validation were examined; specificity, detection limit and quantitation limit, linearity, accuracy and precision, Range and finally, robustness of technique.

5.3.8.1 Specificity

Specificity of the LIF-CZE based chromatographic technique is the ability to detect and quantify the desired analyte response in the presence of all potential sample components, in active reagents and other matrix. In this new method several factors were adjusted to achieve optimized separation and detection of the enzyme catalyzed NIR product, these include; buffer composition, buffer pH, capillary wall composition, excitation and detection wavelengths. During the electrophoresis analyses **AL-36**; a NIR dye (shown in figure 5.16) similar to the propyl sulfonate derivative was added to the reaction mixture. Under the standard oxidative test conditions only one peak was observed with a without the introduction of the monooxygenase. This demonstrates that in the presence of other similar fluorophore the enzyme exhibited exclusive catalytic properties solely for the alkyl sulfonated substrate. Once the latter was added, the usual second peak owing to sulfonate conversion to aldehyde appeared. This further confirms that the monooxygenase is substrate specific and will only catalyze substrates that are alkyl substituted.

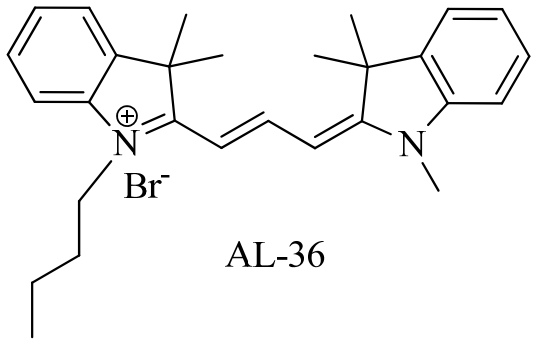

Figure 5.16 (A and B) NIR dye used to test the specificity of the monooxygenase technique to detect the process of desulfonation. Under the desired test conditions, no enzyme catalysis was observed with this substrate analog.

5.3.8.2 Detection limit and quantitation limit

The limit of detection (*LOD*) of an analytical technique determines the lowest analytical concentration at which an analyte(s) could be detected for qualitative purposes. Like any other technique various factors must be considered when the *LOD* is to be determined. In this procedure key among the factors considered was peak height which was calculated at two to three times the noise level (signal-to-noise). Analysis of the heptamethine bi-sulfonated substrate yielded values at the sub-nano molar levels. In fact, at 0.05×10^{-9} molar dye concentration there was obvious indication of enzyme catalysis as evident in the formation of an aldehyde peak once the sulfonated moiety had been converted to the corresponding aldehyde. However, this value was significantly changed when the unsymmetrical trimethine derivatives were introduced. At concentrations below 0.05×10^{-6} molar no discernible sign of enzyme catalysis was observed, as also determined by the appearance of the second electrophoresis peak. At this point the signal-to-

noise ratio decreased to less than 0.27. Enzymatic conversion only became noticeable once dye concentration reached or exceeded average value of 0.087×10^{-6} with excess enzyme. Similar patterns were observed when the limits of Quantitation (*LOQ*) were studied. The lowest concentrations at which quantitation was determined for the symmetrical heptamethine substrate was 0.14×10^{-9} molar, while the values for the trimethine propyl and butyl were 0.37 and 0.40×10^{-6} respectively. Below these dye concentrations standard calibration curves became non-linear which made accurate concentration determination virtually impractical. This of course was highly dependent on the light source as compared to other excitation methods such as the arch lamp which could yield very different results. Also, the detector used along with the emission properties of each class of dye, played an important role in *LOD* and *LOQ* values obtained.

5.3.8.3 Linearity

Linearity describes the ability to of the procedure generate a proportional response of the analyte is to a change concentration within a specific range. The linearity study was designed and conducted appropriately for the intended analysis which includes the use of NIR/ Vis cyanine based fluorophores. This allowed us choose the most appropriate range of the both dye and enzyme concentrations thus optimizing the technique as a new and comprehensive bioassay. From the preliminary studies of the dyes, it was revealed that these compounds are affected by photodegradation and other factors that may limit their photophysical usefulness. In addition, these fluorescent probes exhibit high solvatochromic behavioral patterns, thus limiting their use to specific types of solvent media. For these reasons the most appropriate concentration ranges were determined as assessed using the Beer's Law. As shown in figure 5.17, linearity study was performed by preparing standard solutions at five different concentration levels from 50 to 150%

of the target analyte concentration for each type of fluorophore. As outlined in the ICH guidelines, minimum a of five concentration levels is required to adequately assess the linearity of the technique, which is then demonstrated via least−square regression. The data in the graph is considered acceptable as determined the correlation coefficients which were in the order of 0.999 for the trimethine but slight lower at 0.997 for the heptamethine. Also, an extension of the Beer's Law requires that the *y-intercept* be close to zero or at most be a less than few percent of the overall response, and that was the case of all three classes of sulfonated substrate.

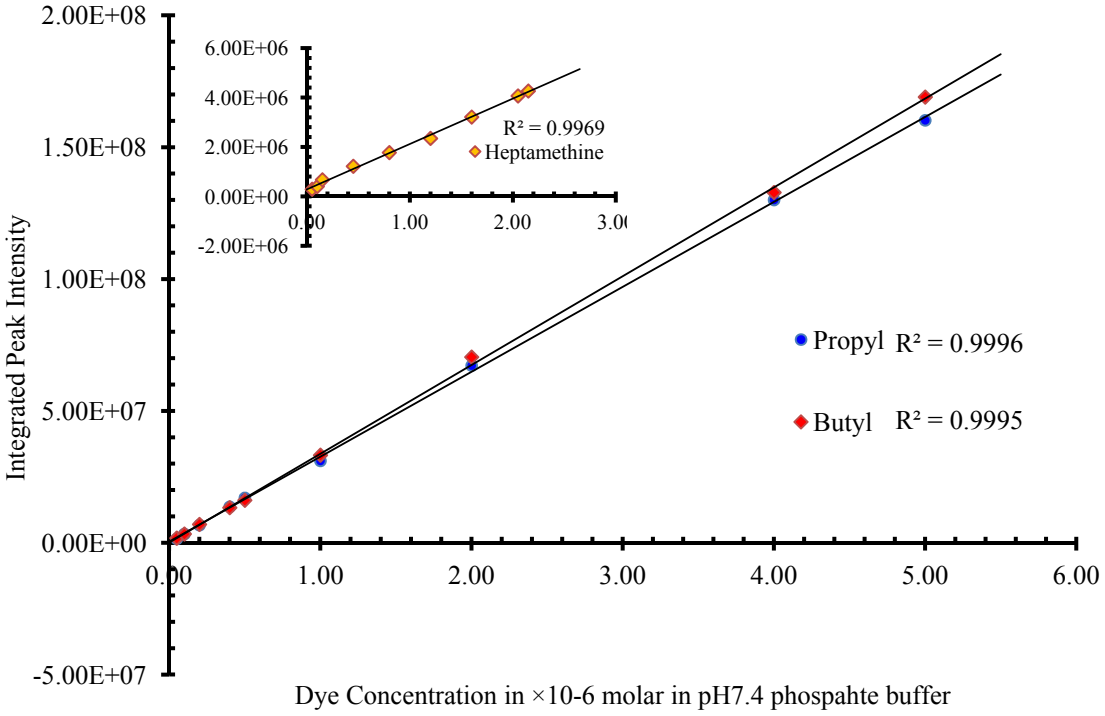

Figure 5.17 Calibration curve of the two classes of cyanine dyes (inset; symmetric heptamethine) illustrating each linear range of detection. The trimethine derivatives yielded linear range vales of 0.09 to 3.25×10^{-6} molar while the heptamethine yielded 0.05 to 2.15 ×10^{-6}. Linear range was determined in 5.00 ×10^{-3} molar saline-free phosphate buffer, pH 7.4.

5.3.8.4 Accuracy and precision

Achieving accurate results was of tremendous importance to the success of this new bioanalytical assay that investigates the monooxygenase ability to enzymatically transform the fluorescent probes. To accurately assess and quantitate the enzyme's catalytic ability this newly bioassay technique was developed through careful sample analyses and handling of test compounds and standard. Accuracy could easily be compromised by either human error or by systematic errors resulting from test instrumentation and other test hardware. Throughout the development of the technique great care was taken to ensure the preservation of data integrity at all levels and elimination of most systematic errors. However the complete avoidance of error was virtually impractical thus minimal human error was inevitable.

Similar to the accuracy, the technique is also characterized by significant precision or repeatability of the results. Form the data observed, the test method demonstrated sufficient repeatability as the analyses are performed repeatedly in using the same equipment over a a time period of thirty days.

5.3.8.5 Range

The range of an analytical technique is a precise linear interval for the test method. It measures the distance between the upper and lower concentration levels (including these levels) within which linear and accurate results can be obtained with any deviation to the Beer's Law. In order to achieve precise, accurate and linear data from the newly developed bioanalytical method target concentrations were determined with linear ranges as a multiple of the target. For the sym-

metrical heptamethine the range was determined to be 0.05 to 2.15 × 10^{-9} molar. For both trimethine, the values were 0.09 to 3.25 × 10^{-6} molar.

5.3.8.6 Robustness

The robustness was used to assess the ability of the technique to remain unaffected by performing relatively small adjustments to the analytical method. Based on the studies some of the main areas that were changed were buffer, strength, separation voltage, capillary size, pH and detection wavelength. Overall, these technique modifications had virtually no effect on the overall outcome of the method except for effects such as change in elution time, elution order and of the analytical species. The two most severe modification that could potentially ruin the robustness of the technique are; **1)** temperature fluctuation during the separation CE process and **2)** the presence of saline in the separation buffer.

Changes to these two parameters were found to have profound effect on the outcome of the experiment. Temperature control is a common problem with most electrophoresis separation procedure and in this particular technique beyond ambient room temperature there was reduced enzyme catalysis even at optimum conditions.

Saline plays a vital role in maintaining the native three dimensional structures in many biological specimens like the enzyme and the serum albumin. However, when introduced at even small quantities thus limit the ability to observe the enzyme catalysis. It also resulted in other problems such as poor peak separation and peak overlap due to reduce analyte mobility through EOF suppression. Overall the technique was considered very robust for the intended purpose.

5.4 Summary

The results obtained from the enzyme catalysis of the di-sulfonated heptamethine dye revealed that under the test conditions, in the presence of reduced flavin, SsUD was capable of converting the alkyl sulfonate moiety into the corresponding bis-aldehyde through a two stage desulfonation process. In the first stage a single desulfonation is achieved resulting in the formation neutrally charged mono-aldehyde species which migrates with the EOF under the influence of a strong electrophoretic force. However, further exposure to the oxidative enzyme along with excess riboflavin leads to the transformation of the mono-aldehyde to the corresponding bis-aldehyde.

It is believed that this oxidative catalytic transformation is achieved by one of two pathways. The process occurred either by a C4a-hydroperoxyflavin (Fl-OOH) or by the formation of a more oxygenating C4a-peroxyflavin ($Fl\text{-}OO^{-}$) intermediate resulting in the neutral bis-aldehyde species. Although the separation conditions are designed to provide optimum separation and peak identification, changes to the electroosmotic double layer established on capillary walls have lead to poor peak resolution and peak identification. In addition, owing to the fact that a symmetrical NIR bis-sulfonated dye is rather complex to synthesize a more simplified approach was taken to utilize the less synthetically complex unsymmetrical trimethine derivatives. Unlike the heptamethine dyes, the unsymmetrical trimethine yielded solely one catalyzed product peak and the second peak was due to the uncatalyzed dye substrate. For this reason identification of the product peak became mode definitive given the propensity for the capillary wall double layer to break down after repetitive analyses and affecting the EOF and thus the over elution peak pattern.

Like any standard chromatographic of electrophoresis procedure, the newly developed NIR-dye enzyme coupled bioassay yielded both qualitative and quantitative data on investigating the oxidative desulfonation process of the cyanine substrate. Besides the expected appearance of a second peak in the electropherogram with the introduction of the enzyme component, the concomitant increase in the peak intensity and peak area at constant enzyme concentration confirms that the technique is quite useful as method of quantitation with the potential for *in vivo* utilization. The results also demonstrated that a change in the length of the alkyl sulfonate had virtually no effect on the enzyme catalytic capability with the assumption that any change in the enzyme activity would become discernible from the change to the emission properties before and after catalysis. As reported in previous results, the increased hydrophobic properties of the aldehyde product of enzyme catalysis exhibited strong affinity for the hydrophobic binding domains for the serum albumin, a unique property not displayed by the more polar sulfonated form of the dye. Applying the Scatchard analysis with the double plot, yielded an affinity constant of $\mathbf{3.99\times10^4 \pm 0.44 \times10^4\ M^{-1}}$for the trimethine C-3 alkyl compound and for $\mathbf{4.21\times10^4 \pm 0.\ 37\times10^4}$ M^{-1} for the C-4 derivative. This product-albumin binding relationship further provided an indirect insight into the enzyme catalysis of the monooxygenase and further serves a template for *in vitro* detection and quantitation of the enzyme. Considering that the enzyme is in excess, the linear proportionality between observed peak area and the change in the concentration of the monoaldehyde product of catalysis enables the possibilities of estimating the enzyme efficiency and other key enzymatic kinetic parameters to further validate the overall usefulness of the technique.

5.5 Reference

1. D. H. Lee, J. E. Bae, J. H. Lee, J. S. Shin and I. S. Kim, *Journal of Microbiology and Biotechnology*, 2010, **20**, 1463-1470.
2. J. M. Simpson and D. V. Lim, *Biosensors & Bioelectronics*, 2005, **21**, 881-887.
3. R. Sting and M. Stermann, *Deutsche Tierarztliche Wochenschrift*, 2008, **115**, 231-238.
4. E. Eichhorn, J. R. vanderPloeg, M. A. Kertesz and T. Leisinger, *Journal of Biological Chemistry*, 1997, **272**, 23031-23036.
5. E. Eichhorn, J. R. van der Ploeg and T. Leisinger, *Journal of Biological Chemistry*, 1999, **274**, 26639-26646.
6. E. Eichhorn and T. Leisinger, *Fems Microbiology Letters*, 2001, **205**, 271-275.
7. J. R. van der Ploeg, E. Eichhorn and T. Leisinger, *Archives of Microbiology*, 2001, **176**, 1-8.
8. A. S. Mittelmann, E. Z. Ron and J. Rishpon, *Analytical Chemistry*, 2002, **74**, 903-907.
9. K. Y. Gfeller, N. Nugaeva and M. Hegner, *Applied and Environmental Microbiology*, 2005, **71**, 2626-2631.
10. J. V. Costa, I. A. Nunes and L. Franca, *Boletim Do Centro De Pesquisa De Processamento De Alimentos*, 2011, **29**, 117-128.
11. P. M. Fratamico and L. K. Bagi, *Journal of Industrial Microbiology & Biotechnology*, 2001, **27**, 129-134.
12. N. N. Mishra, B. Filanoski, M. Fellegy, E. Cameron, S. K. Rastogi, W. C. Maki and G. Maki, *Ultra-Sensitive Electrochemical Detection of E. coli Using Nano-Porous Alumina Membrane*, 2008.
13. J. Ye, Y. Liu and Y. Li, *Transactions of the Asae*, 2002, **45**, 473-478.

14. Z. X. Zhang, F. Zhang and Y. Liu, *Acta Chimica Sinica*, 2012, **70**, 2251-2256.

15. L. X. Zhou, D. G. He, X. X. He, H. Shi, K. M. Wang and J. E. Cao, *Chemical Journal of Chinese Universities-Chinese*, 2011, **32**, 2274-2279.

16. M. R. Urianickelsen, E. R. Leadbetter and W. Godchaux, *Journal of General Microbiology*, 1993, **139**, 203-208.

17. M. A. Kertesz, K. Schmidt-Larbig and T. Wuest, *Journal of Bacteriology*, 1999, **181**, 1464-1473.

18. M. R. Urianickelsen, E. R. Leadbetter and W. Godchaux, *Archives of Microbiology*, 1994, **161**, 434-438.

19. X. Z. Zhan, R. Carpenter and H. Ellis, *Abstracts of Papers of the American Chemical Society*, 2007, **234**.

20. H. R. Ellis, *Bioorganic Chemistry*, 2011, **39**, 178-184.

21. B. L. Gao and H. R. Ellis, *Biochemical and Biophysical Research Communications*, 2005, **331**, 1137-1145.

22. R. A. Carpenter, X. Z. Zhan and H. R. Ellis, *Abstracts of Papers of the American Chemical Society*, 2007, **234**.

23. R. A. Carpenter, X. Z. Zhan and H. R. Ellis, *Biochimica Et Biophysica Acta-Proteins and Proteomics*, 2010, **1804**, 97-105.

24. X. Zhan, R. A. Carpenter and H. R. Ellis, *Biochemistry*, 2008, **47**, 2221-2230.

25. E. Eichhorn, J. R. Van der Ploeg and T. Leisinger, *Journal of Bacteriology*, 2000, **182**, 2687-2695.

26. G. Beckford, E. Owens, M. Henary and G. Patonay, *Talanta*, 2012, **92**, 45-52.

27. B. L. Gao and H. R. Ellis, *Biochimica Et Biophysica Acta-Proteins and Proteomics*, 2007, **1774**, 359-367.

28. B. L. Barton, *Drug Information Journal*, 1998, **32**, 1143-1147.

29. M. S. Christian, *International Journal of Toxicology*, 1997, **16**, 659-668.

30. L. P. Icart, O. J. T. Gemeil, J. Cevallos, F. T. Barbosa, L. B. Martinez and H. Sancho-Garnier, *Drug Information Journal*, 2002, **36**, 743-750.

31. C. McCarthy, *Drug Information Journal*, 2001, **35**, 369-376.

32. G. A. Shabir, *Journal of Chromatography A*, 2003, **987**, 57-66.

33. K. Vorauer-Uhl, A. Wagner and H. Katinger, *European Journal of Pharmaceutics and Biopharmaceutics*, 2002, **54**, 83-87.

34. P. J. Whitehouse, *Alzheimer Disease & Associated Disorders*, 2000, **14**, S119-S122.